NTNU
Norwegian University of
Science and Technology

Statistical Validation of Rigid Body Rocking Response Models Against Experimental and Numerical Data

Mathias Strand

Civil and Environmental Engineering
Submission date: February 2017
Supervisor: Jochen Kohler, KT
Co-supervisor: Prof. Dr. Bozidar Stojadinovic, ETH Zürich
Dr. Michalis Vassiliou, ETH Zürich
Mr. Jonas Bachmann, ETH Zürich

Norwegian University of Science and Technology
Department of Structural Engineering

Eidgenössische Technische Hochschule Zürich
Swiss Federal Institute of Technology Zurich

NTNU – Trondheim
Norwegian University of
Science and Technology

Statistical Validation of Rigid Body Rocking Response Models Against Experimental and Numerical Data

Mathias Strand

February 2017

MASTER THESIS

Norwegian University of Science and Technology

Faculty of Engineering

Department of Structural Engineering

Supervisor	Prof. Dr. Jochen Köhler	NTNU
Supervisor	Prof. Dr. Bozidar Stojadinovic	ETHZ
Advisor	Dr. Michalis Vassiliou	ETHZ
Advisor	Mr. Jonas Bachmann	ETHZ

Preface

Before you lies the thesis "Statistical Validation of Rigid Body Rocking Response Models Against Experimental and Numerical Data", which marks the end of a long and challenging education. It has been written to finish the Master of Science degree in Civil and Environmental Engineering at Norwegian University of Science and Technology (NTNU). The research and writing have been performed entirely at Swiss Federal Institute of Technology Zürich (ETHZ) in the period September 2016 to January 2017.

This project was initiated by supervisor Prof. Dr. Stojadinovic, who granted me the possibility to do the master thesis work at his Chair of Structural Dynamics and Earthquake Engineering at ETHZ. Rocking motion was a totally new topic for me, but advisors Dr. Vassiliou and Mr. Bachmann have patiently answered all my questions and shared their deep knowledge of this interesting and challenging phenomenon. I am deeply grateful for your guidance and support during the process. Dr. Broccardo at ETHZ has been to treasured support by helping me understand how the artificial ground motions are generated and by supplying the software implementation. The research has been difficult, but at the same time rewarding. By extensive analysis of both numerical and laboratory results I have been able to answer the problem statement.

I would like to thank Prof. Dr. Köhler at NTNU for establishing the connection with Stojadinovic and making this exchange period in Switzerland possible.

I hope you enjoy the reading!

Zürich, January 30, 2017

Mathias Strand

Abstract

Slender, free-standing structures subjected to ground motions, may substantially decrease the seismic moment and shear at the base by uplifting and rocking motion. However, the rocking motion response is sensitive to all parameters, and slight differences in the parameters, can lead to significant changes in the time history.

The aim of this study is to explore whether the rocking response could be predicted by a statistical approach. *Could the maximum response and the probability of overturning of a rigid rocking oscillator subjected to an ensemble of ground motions with same statistical properties be predicted in terms of average quantities?*

Two recorded ground motions are used as a basis for generation of two ensembles of 100 statistically similar ground motions. The rocking motion of the oscillator subjected to the ensembles, are tested experimentally on a shaking table to three different prototype scales. Thus 600 laboratory tests establish an experimental basis for statistical comparison with numerical predictions.

Conclusions There is observed an apparent correlation between the statistical distribution of maximum rocking response for the numerical and laboratory results. Based on a limited number of 100 predictions, the maximum response of a rigid rocking oscillator could be well estimated by mean and median values for the two smallest prototype scales. The largest scale shows larger relative errors on the predicted means, but the values are numerically small and prone to be dominated by physical and numerical disturbance.

The effect of a slight parameter change that is unpredictable on the individual level, is shown to be more predictable on the distribution of maximum response. These findings support the view that maximum rocking response could be predicted in a statistical manner.

Contrastingly, the obtained prediction of overturning is shown to be uncertain and highly sensitive to small changes in coefficient of restitution or accelerations. Based on a limited number of 100 predictions, the probability of overturning is not well estimated. The results that are observed, call in to question whether the probability of overturning could be predicted with the limited number of 100 tests. The estimates on overturning could presumably be improved by increasing the number of test or by studying overturning with more than one variable.

Sammendrag

Slanke, frittstående konstruksjoner utsatt for bakkebevegelser, kan vesentlig redusere seismisk moment og skjærkraft på bunnen av konstruksjonen ved oppløft og påfølgende vuggebevegelse. Imidlertid er vuggeresponsen svært følsom for alle parametere som bestemmer den, og små forskjeller i parameterne, kan føre til betydelige endringer i tidshistorien.

Målet med denne studien er å undersøke om vuggeresponsen kan bli forutsagt ved en statistisk tilnærming. *Kan maksimal respons og sannsynligheten for velting av en stiv vugge-oscillator utsatt for en gruppe av bakkebevegelser med samme statistiske egenskaper, forutsies med gjennomsnittlige verdier?*

To målte bakkebevegelser benyttes som grunnlag for generering av to grupper av 100 statistisk lignende bakkebevegelser. Vuggeresponsen til oscillatoren utsatt for bakkebevegelser, er testet eksperimentelt på et ristebord ved tre forskjellige prototypeskalaer. Dermed danner 600 laboratorietester et eksperimentelt grunnlag for statistisk sammenligning med numeriske forutsigelser.

Konklusjon Det er observert en tydelig sammenheng mellom den statistiske fordelingen av maksimal vuggerespons for de numeriske og eksperimentelle resultatene. Basert på et begrenset antall på 100 prediksjoner, kan den maksimale responsen av en stiv vugge-oscillator bli godt anslått av gjennomsnitts- og medianverdier for de to minste prototypeskalaene. Den største skalaen utviser større relative feil på de predikerte resultatene, men verdiene er numerisk små og mer utsatt for å bli dominert av fysisk og numerisk forstyrrelse.

Effekten av en liten parameterendring som er uforutsigbar på individnivå, er vist å være mer forutsigbar når fordelingen av maksimal respons blir vurdert. Disse funnene støtter det syn at maksimal vuggerespons kan forutsies på en statistisk måte.

På den annen side har den oppnådde prediksjon av velting vist seg å være usikker og svært følsom for små endringer i dempingsparameteret eller akselerasjoner. Basert på et begrenset antall på 100 prediksjoner, er sannsynligheten for velting ikke godt estimert. Resultatene som blir observert, setter spørsmålstegn ved om sannsynligheten for velting kan forutsies med et begrenset antall av 100 tester. Estimatene for velting kan antagelig bli forbedret ved å øke antallet tester eller ved å studere veltefenomenet med mer enn en variabel.

Contents

List of Figures

List of Tables

Part I

Introduction and Background

Chapter 1

Introduction

1.1 Background

Rocking motion of rigid columns is a technique that might be used for seismic isolation of large bridges. Slender, free-standing structures subjected to ground motion shaking, may substantially decrease the seismic moment and shear at the base by uplifting and rocking motion. The rocking motion response is however sensitive to all parameters, and the existing models are not able to predict the entire time history with sufficient accuracy. The idea of this project is to explore the chaotic nature of rocking motion with a statistical approach. In the end, earthquake engineering is performed on statistical quantities based on an ensemble of ground motions with same earthquake hazard.

The goal of this project is to determine whether the maximum response could be predicted in a statistical manner. 600 laboratory tests are performed as an experimental basis for statistical comparison with numerical predictions.

Example of Sensitive Response Figure 1.1 shows in the upper plot the laboratory rocking response of a rigid column that overturns. The two lower plots show the predicted numerical response to the measured accelerations from the laboratory. The only difference in the predictions is a slight change of the damping parameter by 0.7 %. Nevertheless the maximum predicted responses differ with 62 % and they do not overturn, which the experimental response that should be predicted does.

The existing numerical models for rocking motion are evidently not able to predict the entire time history with sufficient accuracy. This project is initiated to explore whether we

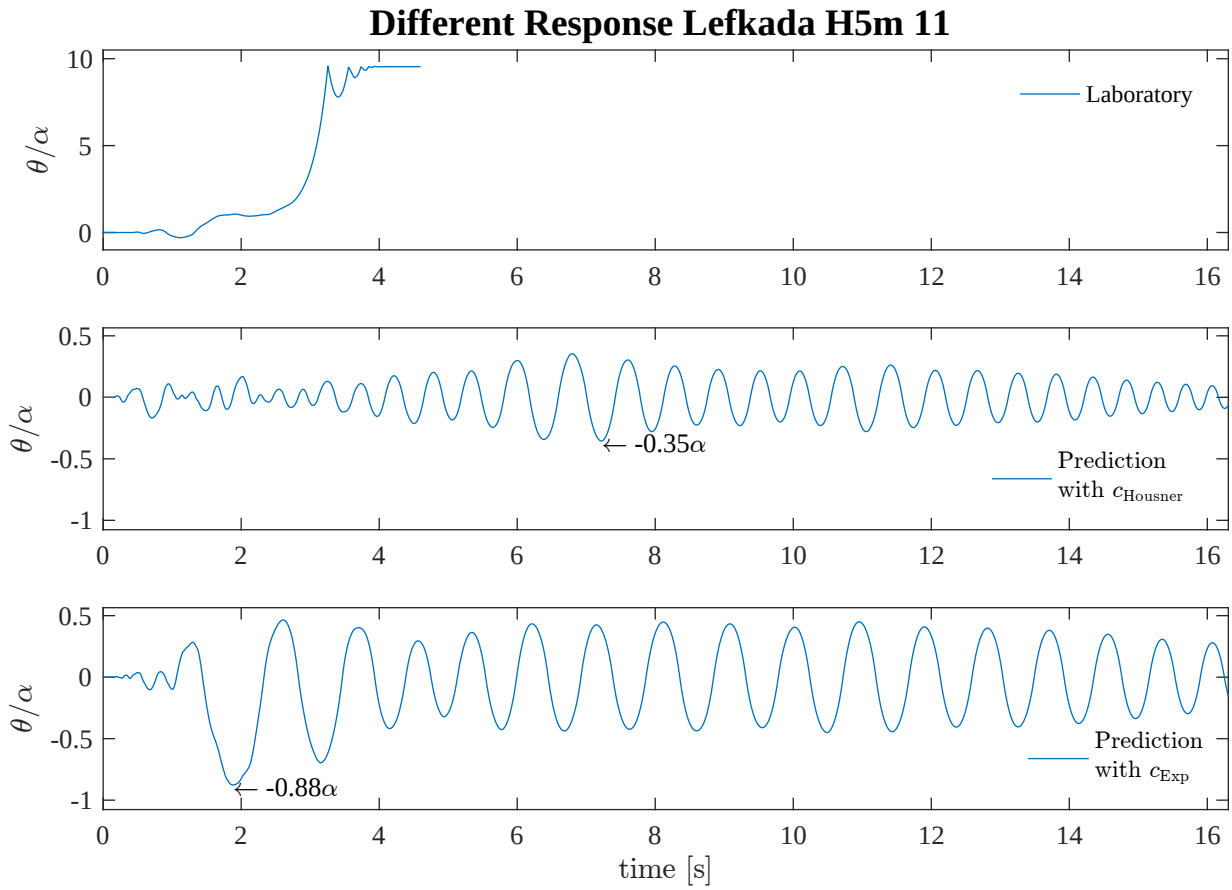

Figure 1.1: Different rocking response. Top: overturning in laboratory. Middle and bottom: predicted sustained rocking motion with slightly different damping parameters c_{Housner} and c_{Exp}. For rocking angles θ larger than the critical angle α, i.e. $|\theta/\alpha| \geq 1$, the motion becomes unstable and the column overturns in most cases.

are able to predict the maximum response in a statistical manner. If a rigid block is subjected to an ensemble of statistically similar ground motions, will we able to predict the maximum rocking response and the probability of overturning in an average sense?

1.2 Objectives

The main goal of this project is to explore whether the response of a rigid rocking oscillator to an ensemble of ground motions with the same statistical properties can be predicted by the numerical model in terms of average quantities. The two quantities

- average maximum rotation angle for those specimens that did not overturn
- probability of overturning

should be obtained by experimental tests and numerical predictions and finally compared. The two sub-questions that should be answered in this thesis are thus:

- *Could the mean of maximum rocking response of a rigid rocking oscillator be predicted when subjected to an ensemble of ground motions with similar statistical properties?* The maximum rocking response is here meant as the maximum absolute rotation angle for those specimens that do not overturn.
- *Could the probability of overturning of a rigid rocking oscillator be predicted when subjected to an ensemble of ground motions with similar statistical properties?*

Research Design The research is performed in the following four main steps:

1. Generate artificial ground motions that are suitable for producing shaking table motions. The ground motions are generated as two sets of 100 statistically similar motions, which thereafter are time scaled to model three different prototypes. The ground motions should be chosen such that a considerable amount of the the test do not overturn. Thus preliminary numerical predictions should be made.
2. Test the rocking response of a rigid rocking oscillator experimentally on the shaking table. The rocking response and the actual accelerations of the shaking table should be measured. The 600 measured acceleration signals of the shaking table are used as input for the numerical predictions.
3. Post process the measured signals to obtain laboratory values for the rocking response. Perform numerical predictions of the rocking response based on the measured accelerations.
4. Perform statistical analysis of the laboratory and numerical results and compare the findings.

1.3 Limitations

The limitations of the project are as follows:

- The main limitation of the project is the shaking table. First of all, the table is not able to represent the ground motions accurately. The numerical rocking predictions based on input accelerations are thus not expected to be comparable with the experimental rocking response. Secondly, the table has limits for maximum displacement and velocities of the input signal. Due to these limitations the input accelerations must be chosen with care, and the actual accelerations of the shaking table must be measured.
- The rocking oscillator is assumed to be rigid and rotate in only one direction. Thus the

problem is modeled as a single degree of freedom system, where the rocking angle is the only variable. This variable is continuous and limited by the boundary conditions: no rocking and overturning.

- The overturning phenomenon is quantified by a discrete variable with only two outcomes: overturning or not overturning.
- The problem is limited to explore the response of a rigid rocking oscillator to an ensemble of ground motions with same statistical properties. If the statistical properties of the ensemble are not the same, then each rocking response represents different processes and will not necessarily be comparable.
- Each ensemble of ground motion consists of 100 artificial ground motions. Thus the accuracy of the average quantities is bound by the limited size of the set of results.
- The numerical results are limited by the accuracy of acceleration measurements and optical measurements of the experimental rocking motion.

1.4 Structure of the Report

The rest of the report is organized as follows:

Chapter 2 gives an introduction to the relevant theory of rocking motion, generation of ground motions and prototype scaling.

Part II Method

Chapter 3 describes the generated ground motions, choice of prototype scales and initial assessments before the experimental tests.

Chapter 4 describes how the properties of the test specimen, shaking table and the measurement equipment. Further are the setup of the laboratory and the experiments described.

Chapter 5 presents how the measured results are post processed in order to obtain physical quantities that could be analyzed and compared.

Chapter 6 defines and explains statistical variables, terms and visualization methods that are used to compare the results.

Part III Results

Chapter 7 verifies that the measured accelerations share the same statistical properties in time and frequency domain.

Chapter 8 presents the results from the laboratory and the numerical prediction with tables,

plots and comments.

Chapter 9 discusses the results in order to answer the problem statement. The conclusions are presented.

Chapter 10 summarizes the project and the main conclusions.

Appendix

Appendix A shows all box plots for the results grouped by the ground motion.

Appendix B shows cumulative distribution function (CDF) plots including response from simulated accelerations.

Appendix C presents CDF plots of the response with varying slenderness of the rigid block.

Most of the figures are implemented as vector graphics, which enables zooming with accuracy if details of figures need to be investigated. All references to figures, tables, equations, sections and bibliography are clickable links. Consequently this report is best read digitally.

Chapter 2

Theoretical Background

2.1 Rocking Response of Rigid Block

The theory of rocking response of rigid blocks will be presented based on descriptions by Housner [6], Makris [7], Makris and Konstantinidis [8], Zhang and Makris [11]. The equations and assumptions that are stated, establish the basis for the numerical rigid body rocking response model to be validated.

2.1.1 Response to Quasistatic Loads

Consider a free-standing rigid block with semidiagonal $R = \sqrt{b^2 + h^2}$, slenderness $b/h = \tan(\alpha)$ and slenderness angle α as shown in figure 2.1. In the quasistatic situation we are considering a slowly increasing ground acceleration $\ddot{u}_g$ at the base of the block. The block will uplift when the seismic demand $m\ddot{u}_g h$ reaches the seismic resistance mgb. The static moment equilibrium about point O gives

$$m\ddot{u}_g h = mgb \qquad \text{or} \qquad \ddot{u}_g = g\frac{b}{h} = g\tan\alpha \tag{2.1}$$

The uplift criterion for the block is

$$\ddot{u}_g \geq g\frac{b}{h} = g\tan\alpha \tag{2.2}$$

The moment rotation diagram is presented in figure 2.2. Until the seismic resistance moment M reaches its maximum at $\pm mgR\sin(\alpha)$, the stiffness is infinite. After uplift has occurred, the block experiences a positive rotation $\theta(t)$. Due to the assumption that the base

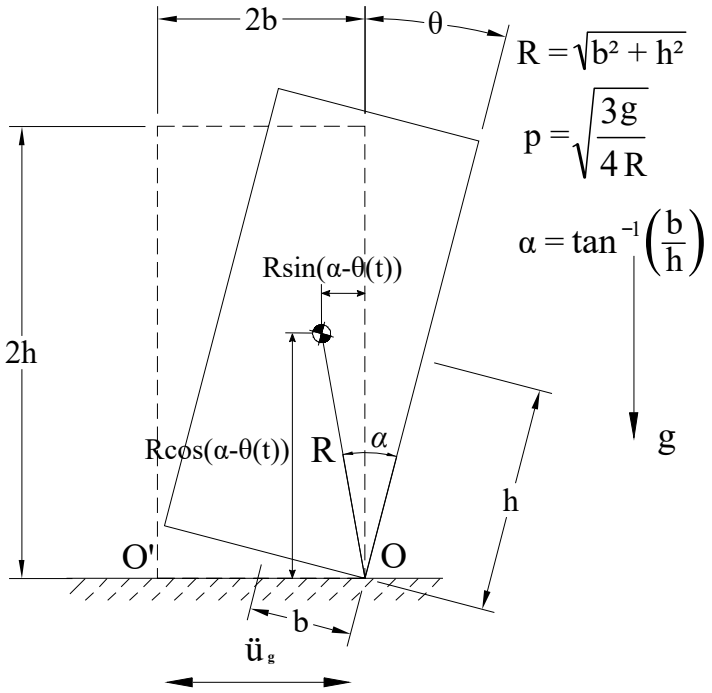

Figure 2.1: Geometric characteristics of rigid block with height $H = 2h$ and width $B = 2b$ rotating with positive angle θ about point O due to the ground motion $\ddot{u}_g$. *Based on figure from [8].*

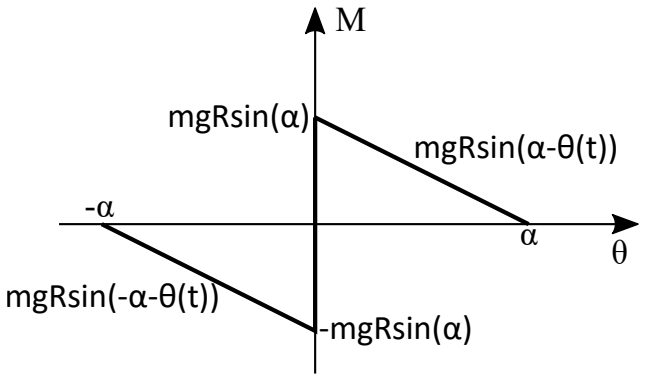

Figure 2.2: Moment rotation diagram of rigid block. The block has infinite stiffness until the seismic resistance moment M reaches its maximum at $\pm mgR\sin(\alpha)$. Thereafter the block uplifts, the stiffness is negative, and the seismic resistance moment M decreases until it becomes zero at $\theta = \pm\alpha$. The rocking motion is notably sensitive for angles in the range close to α.

acceleration is quasistatic, the inertia moment due to rotational acceleration is negligible, $\ddot{\theta}(t) \approx 0$. Now the seismic demand is $m\ddot{u}_g R\cos(\alpha-\theta(t))$ and the seismic resistance is merely $mgR\sin(\alpha-\theta(t))$. For $\theta > 0$ the seismic resistance of the block after uplift is $g\tan(\alpha-\theta(t)) < g\tan(\alpha)$. The seismic resistance moment M decreases with increased rocking angle, hence the stiffness is negative.

Under quasistatic loading conditions we can draw two conclusions. Firstly once the block has uplifted, it will also overturn. Secondly the stability of the block is only dependent on the slenderness $\tan\alpha$ and is independent of the size R.

2.1.2 Response to Dynamic Loads

When considering earthquake loads, $\ddot{u}_g$ is not quasistatic, rather time varying. After uplift the block will experience rotational acceleration $\ddot{\theta}(t) \neq 0$. Dynamic moment equilibrium gives

$$-m\ddot{u}_g(t)R\cos(\alpha-\theta(t)) = I_O\ddot{\theta}(t) + mgR\sin(\alpha-\theta(t)), \qquad \theta > 0 \tag{2.3}$$

where I_O is the rotational moment of inertia about the pivot point O at the base. This quantity is proportional to the square of the size parameter R. For rectangular blocks where the mass is evenly distributed, $I_O = \frac{4}{3}mR^2$ and equation 2.3 simplifies to

$$-\ddot{u}_g(t)R\cos(\alpha-\theta(t)) = \frac{4}{3}R^2\ddot{\theta}(t) + gR\sin(\alpha-\theta(t)), \qquad \theta > 0 \tag{2.4}$$

The implications of equation 2.4 are remarkable, as stated by Housner [6]. The seismic demand is proportional to R whereas the seismic resistance is proportional to R^2. This means that regardless of how intense the ground motion $\ddot{u}_g$ or how slender the block is, the second power of R can ensure stability of the block. This scale effect explains why the larger of two geometrically equal blocks, i.e. same slenderness angle α, can survive the excitation that will overturn the smaller block.

According to the time history of the fluctuating ground motion, the ground acceleration could either act in the same or the opposite direction of the restoring force at each time instant. Consequently, under dynamic loads an uplifted block will not necessarily overturn, which is the case under quasistatic loads. Moreover, we might also experience rocking angles larger than the critical angle α without overturning.

Due to the negative stiffness of the rocking block there exists no resonance frequency.

Hence, the block neither amplifies nor resonates due to any frequency content in ground motions, which is a great advantage in rocking isolation applications, Makris [7].

2.1.3 Equation of Motion

For negative rotations $\theta(t) < 0$, the equation of motion of a rocking block is

$$-m\ddot{u}_g(t)R\cos(-\alpha-\theta(t)) = I_O\ddot{\theta}(t) + mgR\sin(-\alpha-\theta(t)), \qquad \theta < 0 \tag{2.5}$$

Equation 2.3 and 2.5 can be expressed in the general and compact form

$$\ddot{\theta}(t) = -p^2\left[\sin\left[\alpha\,\mathrm{sgn}\left[\theta(t)\right]-\theta(t)\right] + \frac{\ddot{u}_g}{g}\cos\left[\alpha\,\mathrm{sgn}\left[\theta(t)\right]-\theta(t)\right]\right] \tag{2.6}$$

where $p = \sqrt{mRg/I_O}$ is the frequency parameter of the block and is an expression of its size R. sgn$[\theta(t)]$ is the signum function that returns +1 for positive values of $\theta(t)$ and -1 for negative values for $\theta(t)$. Equation 2.6 is used in the numerical rigid body rocking response model to be validated.

2.1.4 Rotational Inertia of Inhomogeneous Block

For a rigid block with evenly distributed mass, the rotational inertia could easily be calculated by integration. For other blocks, e.g. blocks with hollow cross sections, the calculations are more cumbersome. In rocking motion the rotational inertia, I_O, about the pivot point O, is of interest. In the following, the geometrical center of the block is assumed to coincide with the mass center C. A factor λ given by

$$\lambda = \frac{I_C}{mR^2} \tag{2.7}$$

expresses the ratio between I_C, the rotational inertia about C, and mR^2 where m is the mass of the block and R is the distance between O and C. The rotational inertia of a block I_O about point O, is then given by

$$I_O = I_S + I_C = mR^2 + \lambda CR^2 = (1+\lambda)mR^2 \tag{2.8}$$

where I_S is the added rotational inertia according to Steiner's theorem. For a rigid block with evenly distributed mass $\lambda = 1/3$. λ could be interpreted as a measure of the inertia distribution around the mass center. If the main part of the mass exists far from the mass center, compared to evenly distributed mass, the λ-value is greater than $1/3$. Thus for hollow cross sections $\lambda > 1/3$. The factor λ could be determined by calculations as well as by experiments.

The frequency parameter $p(\lambda)$ dependent on the the inertia factor, could then be calculated as

$$p(\lambda) = \sqrt{\frac{g}{(\lambda+1)R}} \tag{2.9}$$

2.1.5 Coefficient of Restitution

When a specimen exhibits oscillatory rocking motion, energy is only lost during impact, which is when the angle of rotation reverses, Housner [6], Makris [7]. Once during each half-cycle there would be an increment decrease in kinetic energy. The coefficient of restitution c equals the ratio of kinetic energy before and after the impact and is given as

$$c = \left(\frac{\dot{\theta}_2}{\dot{\theta}_1}\right)^2 \tag{2.10}$$

where $\dot{\theta}_1$ and $\dot{\theta}_2$ are the angular velocities before and after impact respectively. If the impact is assumed to be inelastic, the moment of momentum about the tilting point O is conserved, and equation 2.10 is further developed into

$$c = \left(1 - \frac{3}{2}\sin^2\alpha\right)^2 \tag{2.11}$$

for rigid blocks with evenly distributed mass, Housner [6]. For general blocks where the geometrical center coincides with the mass center, equation 2.11 is expressed as

$$c = \left(1 - \frac{\frac{1}{2}\sin^2\alpha}{\frac{1}{4}(1+\lambda)}\right)^2 \tag{2.12}$$

Equation 2.12 is used in the numerical response calculations when an experimental value is not given. Equations 2.11 and 2.12 are equal for $\lambda = 1/3$.

2.2 Generation of Artificial Ground Motions

The goal of the process described in this section is to fit a stochastic model to a single recorded target ground motion. The fitted model is further utilized to generate artificial ground motions with similar frequency content and energy distribution as the target ground motion.

The theoretical background for generation of artificial ground motions using frequency domain discretization as applied in this project, is briefly summarized here. The theory is based on the work of Broccardo and Der Kiureghian [3], which is an extension of the work of Rezaeian and Der Kiureghian [9] into frequency domain. For further details and derivations, see their work.

2.2.1 Frequency Domain Discretization

A spectral representation of a zero-mean stationary stochastic process could be discretized as a canonical random Fourier series

$$X(t) = \sum_{k=1}^{K} \sigma_k \left[u_k \cos(\omega_k t) + \bar{u}_k \sin(\omega_k t) \right] \tag{2.13}$$

where the variance of the process is described by $\sigma_k^2 = 2\Phi(\omega_k)\Delta\omega$. $\Phi(\omega_k)$ is the power spectral density (PSD) of $X(t)$ for frequency ω_k, and K is the number of frequency increments. u_k and $\bar{u}_k$ are standard normal variables, thus making the process Gaussian. The process described by equation 2.13 is stationary in both time and frequency domain, and must consequently be further developed to describe the nonstationarities of ground motions.

2.2.2 Spectral and Temporal Nonstationarity of Ground Motions

Earthquake ground motions have nonstationary characteristics both in time and frequency domain. The temporal nonstationarity arises from the transient nature of the earthquake. The intensity of a typical ground motion is increasing from zero to a nearly constant intensity during a strong shaking phase. Thereafter the intensity decreases to zero with a total duration of 20-60 seconds. The spectral nonstationarity arises from the evolving nature of the seismic waves arriving at the site. The first few seconds are typically dominated by high-frequency P waves. These are followed by moderate-frequency S waves, which tend to dominate the strong shaking phase. Thereafter the ground motion is dominated by low-frequency

surface waves. The total ground motions is a mixture of these waves with a dominant frequency that tends to lower values with time, Rezaeian and Der Kiureghian [9].

Spectral Nonstationarity The spectral nonstationarity is obtained by letting the power spectral density be varying with time, that is defining an evolutionary power spectral density (EPSD). The discretized EPSD of a nonstationary colored noise process can be written as $\Phi(\omega_k) = \Phi_f(\omega_k|\theta(t))\Phi_0$, where $\Phi_f(\omega_k|\theta(t))$ is a parametrized filter with time varying parameters $\theta(t)$, and Φ_0 is the white noise spectral density. The EPSD is normalized such that the process is temporally stationary with unit variance. In this way the variance of the process $X(t)$ is controlled by time modulating function $q(t)$ only.

The parametrized filter $\Phi_f(\omega_k|\theta(t))$ can be compared with a damped single degree of freedom oscillator with time varying parameters $\theta(t) = [\omega_g(t), \zeta_g(t), \omega_f, \zeta_f]$. The time varying frequency $\omega_g(t)$ controls the predominant frequency, and the time varying damping ratio $\zeta_g(t)$ controls the bandwidth of the process. The fixed model parameters ω_f and ζ_f ensures that the process is twice integrable such that the ground velocity and displacement processes have finite variances.

Temporal Nonstationarity The time varying intensity of the process is controlled by the non-parametric time modulating function $q(t)$. $q(t)$ is determined such that the expected Arias intensity $I_a(t)$ of the process is fitted to the Arias intensity of the target ground motion. Arias intensity is defined as

$$I_a(t) = \left(\frac{\pi}{2g}\right) E\left[\int_0^t X^2(\tau)\,d\tau\right] = \left(\frac{\pi}{2g}\right) E\left[\int_0^t q^2(\tau)\,d\tau\right] \tag{2.14}$$

2.2.3 Probabilistic Model

A fully nonstationary process with N time steps and K frequency steps could be described in its discretized form as

$$X[n] = \sum_{k=1}^{K} \sigma[n,k]\,\{u[k]\cos[n,k] + \bar{u}[k]\sin[n,k]\} \tag{2.15}$$

where $\sigma^2[n,k] = q^2[n]2\Phi[n,k]\Delta\omega$, $\Phi[n,k] = \Phi(\omega_k|\theta(t_n))$, $\cos[n,k] = \cos(\omega_k t_n)$ and $\sin[n,k] = \sin(\omega_k t_n)$. The main and important difference from equation 2.13 is that the variance given by $\sigma^2[n,k]$ varies with time and frequency.

Estimation of Model Parameters The model is estimated based on a target ground motion acceleration $\ddot{u}_g(t)$. The empirical EPSD of $\ddot{u}_g(t)$ is calculated using short-time Thomson's multiple-window spectrum estimation (TMWSE) as explained by Conte and Peng [5].

In this study the modulating function $q(t)$ is a non-parametric function. This is obtained by a kernel smoothing of the cumulative energy density. The kernel is a Hanning window of size 5 s. The justification for a cumulative non-parametric function can be found in Broccardo and Dabaghi [2]. Here shortly, it is reported that the non-parametric cumulative function represents a significant improvement of the fitting; moreover, it relates directly the model to the engineering quantities $t_{5-95} = t_{95} - t_5$, t_{45} and t_{75}, which are of great interest in engineering application. These quantities state the time t_n for reaching n % of the Arias energy as determined by the relation

$$I_a(t_n) = \frac{n}{100} I_a(T) \tag{2.16}$$

where T is the total duration of the earthquake. t_{5-95} could be interpreted as the duration of the strong shaking phase.

Thereafter the empirical EPSD is fitted to a Kanai Tajimi PSD one main frequency parametric function. Finally the parameters of the earthquake ground model are estimated such that the analytical EPSD best fits, in a least-squares sense, the EPSD of the target ground motion.

Simulation of Ground Motions An artificial acceleration signal $X(t)$ is generated by equation 2.15 and the determined model parameters. However, integration of the signal may exhibit non-zero velocity residuals, which is not physically realizable for ground motions. To satisfy this requirement, a high-pass filter in form of a critically damped oscillator is applied as described by Rezaeian and Der Kiureghian [9]. Due to the high damping of the filter, the acceleration, velocity and displacement residuals of the resulting process will rapidly vanish, thus leading to zero or small displacement residuals even though the target motion might exhibit finite end displacements.

2.2.4 Similarities Between Target and Artificial Ground Motions

The main similarities between the target and artificial ground motions are the time-varying characteristics of

- Intensity
- Predominant frequency
- Bandwidth

All together the target and artificial ground motions could be regarded as realizations of the same stochastic ground motion that has the characteristics of the site and earthquake that produced the target signal, Rezaeian and Der Kiureghian [9].

2.3 Prototype Scaling of Ground Motion Signals

In order to experimentally test the rocking response of rigid blocks with equal slenderness, but different prototype sizes, the ground motions could be scaled in time domain. Through dimensionless analysis it can be shown that the time scale of the ground motion to experimental scale can be increased or decreased in order to describe an equivalent motion for a smaller or larger prototype block respectively.

Consider a ground acceleration pulse $\ddot{u}_g$ with peak acceleration a_p and peak frequency ω_p. From equation 2.6 we can see that the rocking response $\theta(t)$ of a rigid block to the ground acceleration pulse is given as a function of five variables

$$\theta(t) = f(p, \alpha, g, a_p, \omega_p) \tag{2.17}$$

The six variables $\theta = []$, $p = [T]^{-1}$, $\alpha = []$, $g = [L][T]^{-2}$, $a_p = [L][T]^{-2}$, $\omega_p = [T]^{-1}$ are represented by the two dimensions length $[L]$ and time $[T]$.

2.3.1 Vaschy-Buckingham Π-theorem

The Vaschy-Buckingham Π-theorem of dimensional analysis Makris [7] states that the number of dimensionless products p with which the problem can be completely described, is equal to the number of variables n minus number of reference dimensions k. Applying the theorem on equation 2.17, the number of variables may be reduced. In our case equation

2.17 may be described by $p = n - k = 6 - 2 = 4$ dimensionless variables

$$\begin{aligned} \Pi_\theta &= \theta \\ \Pi_\omega &= \frac{\omega_p}{p} = \omega_p \sqrt{\frac{4R}{3g}} \\ \Pi_\alpha &= \tan(\alpha) \\ \Pi_g &= \frac{a_p}{g} \end{aligned} \tag{2.18}$$

as

$$\theta(t) = \phi(\frac{\omega_p}{p}, \tan(\alpha), \frac{a_p}{g}) \tag{2.19}$$

2.3.2 Time Scaling

Consider a rigid, homogeneous block to experimental scale with slenderness angle α and semidiagonal $R_{\text{experimental}}$. It is of interest to experimentally determine the rocking response $\theta(t)$ of a prototype block to a given ground motion. The prototype has the same slenderness angle α, but different semidiagonal $R_{\text{prototype}}$. By scaling the time vector of the ground motion, the response could be tested to the experimental scale.

As long as the values of the dimensionless variables Π_ω, Π_α and Π_g remain constant, equation 2.19 holds and represents the rocking angle $\theta(t)$ according to the input variables. Since g in Π_g is a natural constant and Π_α is represented by one variable α, these variables determining Π_α and Π_g could not be changed without changing the values of the dimensionless variables. Π_ω is on the other hand given by two independent variables ω_p and $p = \sqrt{\frac{3g}{4R}}$, and could thus be scaled by the same factor.

If we require that Π_ω be equal for the experimental and the prototype scale, we have

$$\begin{aligned} \Pi_{\omega,\text{experimental}} &= \Pi_{\omega,\text{prototype}} \\ \omega_{p,\text{experimental}} \sqrt{\frac{4R_{\text{experimental}}}{3g}} &= \omega_{p,\text{prototype}} \sqrt{\frac{4R_{\text{prototype}}}{3g}} \\ \omega_{p,\text{experimental}} \sqrt{R_{\text{experimental}}} &= \omega_{p,\text{prototype}} \sqrt{R_{\text{prototype}}} \\ \omega_{p,\text{experimental}} &= \omega_{p,\text{prototype}} \sqrt{\frac{R_{\text{prototype}}}{R_{\text{experimental}}}} \end{aligned} \tag{2.20}$$

If we have a larger prototype to be tested to a smaller experimental scale, $R_{\text{experimental}} < R_{\text{prototype}}$, we see from equation 2.20 that the experimental peak frequency must be increased

by a factor $\sqrt{\frac{R_{\text{prototype}}}{R_{\text{experimental}}}}$.

In general a ground motion signal consist of different frequencies. Since frequency ω and period T are reciprocal quantities, i.e. $\omega = \pi / T$, an increase in frequency leads to a decrease in period by the same factor. Hence, to scale the frequency content of the ground motion signal, the time scale could be changed accordingly. The actual ground motion to be tested is discretized using a prototype time scale with a constant time step $dt_{\text{prototype}}$. The time vector in experimental scale is calculated with time step

$$dt_{\text{experimental}} = dt_{\text{prototype}} \sqrt{\frac{R_{\text{experimental}}}{R_{\text{prototype}}}} \tag{2.21}$$

We see that when a larger prototype is tested to a smaller experimental scale, $R_{\text{experimental}} < R_{\text{prototype}}$, the experimental time scale is reduced by the factor $\sqrt{\frac{R_{\text{experimental}}}{R_{\text{prototype}}}}$.

Part II

Method

Chapter 3

Initial Calculations and Assessments

In the preparation period for the laboratory experiments 2×100 artificial ground motions were produced based on the earthquakes El Centro and Lefkada respectively. The rocking response to different time scales was tested numerically in order to choose scaling factors that will produce results with statistical significance. Additionally must the scaling factor be chosen such that the shaking table was able to reproduce the signal appropriately.

3.1 Generation of Artificial Ground Motions

The artificial ground motions utilized in this project are generated with a MATLAB script developed by Dr. Marco Broccardo at ETHZ. The script generates artificial ground motions according to the descriptions in section 2.2.

Throughout the work in this project the Zürich value for the gravitational constant $g = 9.807\ \mathrm{m/s^2}$ is chosen.

3.1.1 El Centro Simulations

The original El Centro ground motion is shown in figure 3.1 together with the mean values of the simulations. The original signal record is given as acceleration time history with peak acceleration 0.3141 g, time step 0.02 seconds and a duration of 49.62 seconds. The velocity and displacement are integrated numerically. The mean values of the simulations show values near zero, as expected for Gaussian variables.

In figure 3.2 the 100 simulations are shown. By comparing the accelerations in the two figures, it can be seen that the intensities has a similar distribution. As seen in table 3.1, the

peak values for acceleration, velocity and displacement are compared for the original signal and the mean of the simulations. The acceleration and velocity mean values are higher for the simulations, and all standard deviations are small compared to the means. The peak displacement for the original is not baseline corrected and is thus higher than the mean value of the simulations, which are limited by the high-pass filter.

Figure 3.4 shows the cumulative energy distribution of 100 simulations, the mean of the simulations and the original signal. As seen from figure 3.4 and table 3.2, the energy distribution of the simulations fit well to that of the original. The mean of the simulations has a strong shaking phase with duration $t_{5-95} = 24.50$ s as compared to $t_{5-95} = 24.10$ s for the original. The shape of the curves are similar, and for all signals there is almost no increase in cumulative energy for $t > 25.70$ s. The cumulative energy $E(t)$ is calculated as

$$\frac{\pi}{2g} I_a(t) = \int_0^t X^2(\tau) d\tau \tag{3.1}$$

where $I_a(t)$ is the Arias intensity as given in equation 2.14.

The upper plot of figure 3.3 show the time modulation function $q(t)$ compared to the absolute value of original $|\ddot{u}_{g,0}|$ and mean absolute value of simulated $\overline{|\ddot{u}_g|}$ accelerations. $q(t)$ and $\overline{|\ddot{u}_g|}$ fit well as expected, since the simulations are time modulated with this function. The original signal could be interpreted as one realization of the underlying stochastic ground motion, of which $q(t)$ is describing the time varying intensity. As seen in the lower plot of figure 3.3, $q(t)$ and $-q(t)$ are enveloping the original ground motion acceleration in a smoothed sense.

Figure 3.5 show the the smoothed and time modulated evolutionary PSD that is generated based on the original El Centro ground motion. This EPSD is assumed to represent the non-stationary characteristics of the underlying stochastic ground motion in both time and frequency domain.

Table 3.1: Comparison of peak values for El Centro. Original values compared with mean μ and standard deviation σ of the 100 simulations.

		$\ddot{u}_{g,p}$ [g]	$\dot{u}_{g,p}$ [mm/s]	$u_{g,p}$ [mm]
Original		0.314	408.3	515.7
Simulations	μ	0.354	498.2	441.5
	σ	0.00219	6.59	12.93

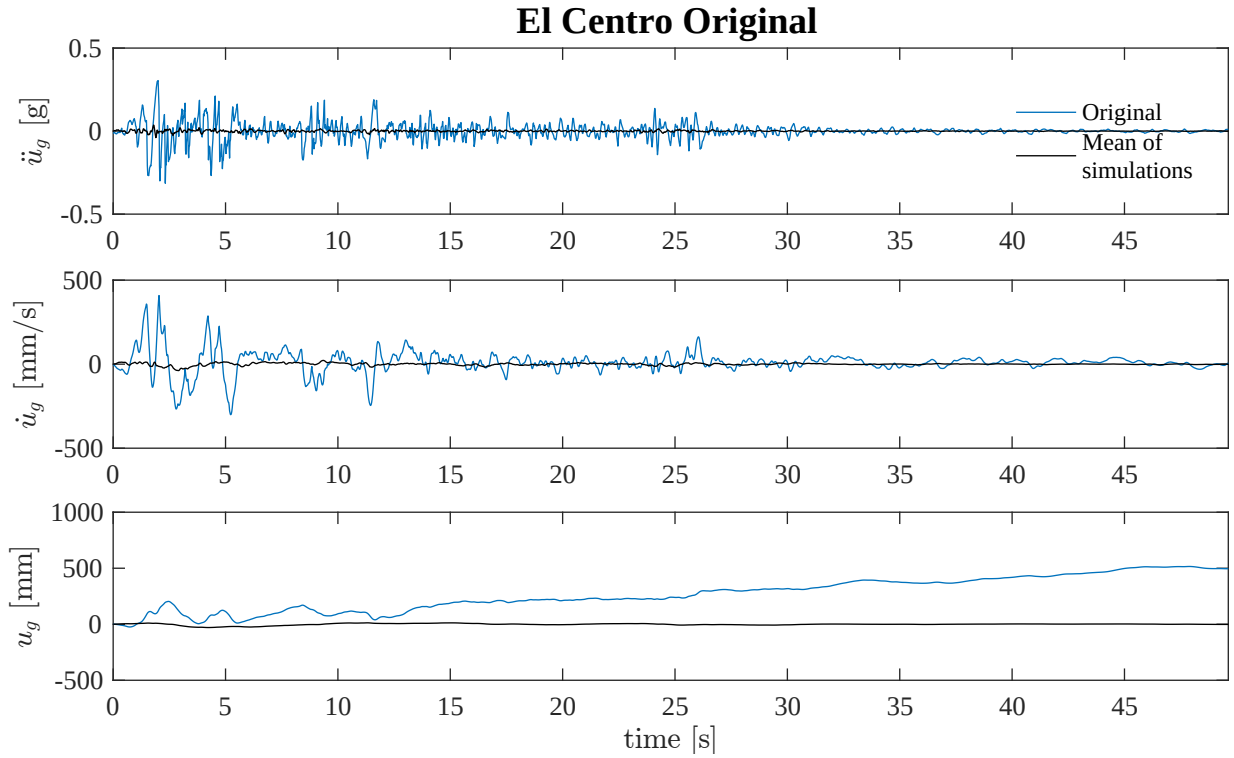

Figure 3.1: Original acceleration, velocity and displacement history for El Centro. The simulations have a near-zero mean in all plots.

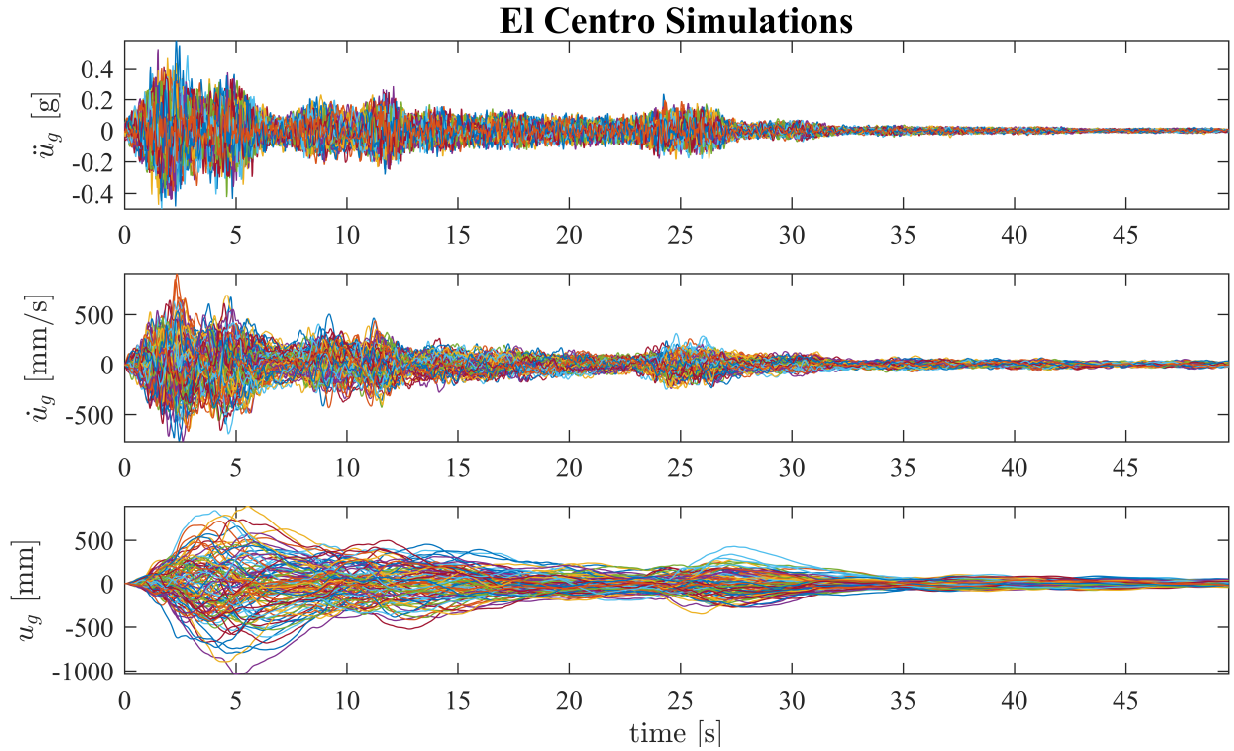

Figure 3.2: 100 simulated acceleration, velocity and displacement histories for El Centro compared with mean of simulations.

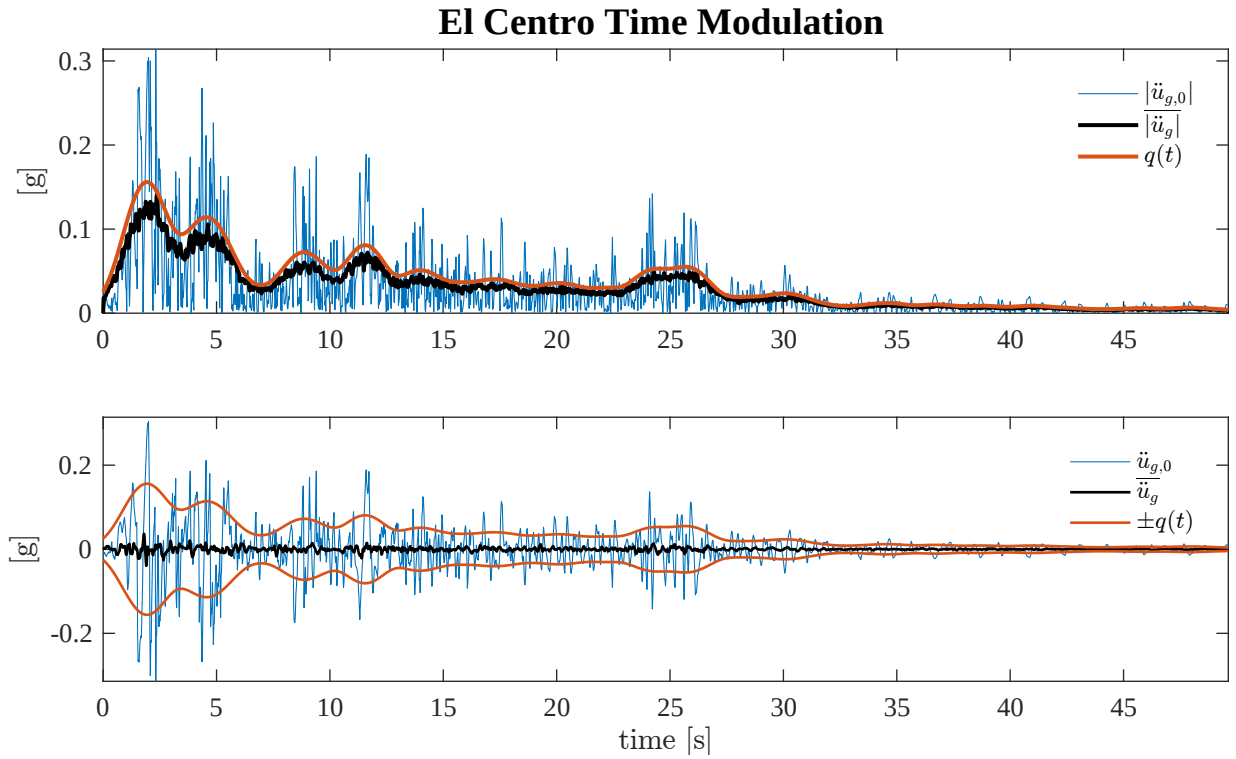

Figure 3.3: The original accelerations $\ddot{u}_{g,0}$ and mean value of simulated $\overline{\ddot{u}_g}$ accelerations compared to time modulation function $q(t)$. Upper figure show absolute values, lower figure actual values. The absolute mean values of the simulations fit well to the time modulation function $q(t)$.

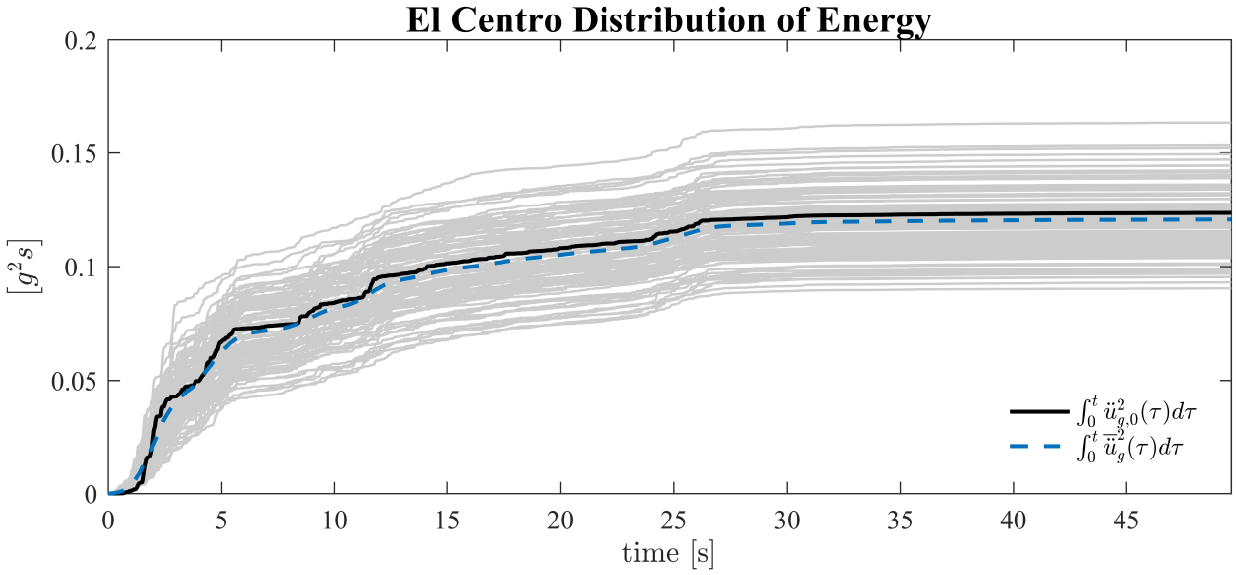

Figure 3.4: Cumulative distribution of energy of 100 simulations compared with original acceleration $\ddot{u}_{g,0}$ and mean of simulations $\overline{|\ddot{u}_g|}$. The mean of the simulations is well fitted to the original ground motion.

Table 3.2: Comparison of time for energy accumulation for El Centro. Values for original accelerations and mean of simulations. The time measures are well fitted.

	t_5 [s]	t_{45} [s]	t_{75} [s]	t_{95} [s]	t_{95-5} [s]
Original	1.54	4.36	11.70	25.64	24.10
Simulations	1.20	4.38	12.00	25.70	24.50

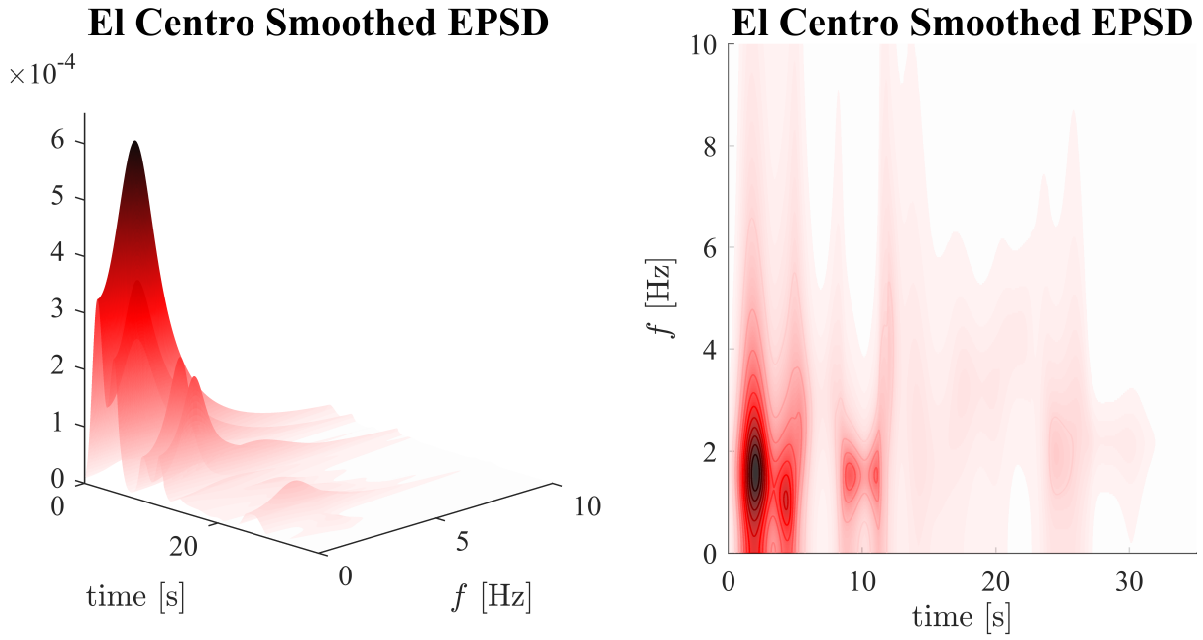

Figure 3.5: Smoothed and time modulated evolutionary power spectral density for original El Centro ground motion. Highest value of EPSD for $t = 2.04$ s and $f = 1.5667$ Hz. The EPSD shows the variation of the stochastic model in time and frequency domain.

3.1.2 Lefkada Simulations

The original Lefkada ground motion and the mean values of the simulations are shown in figure 3.6. The original signal record is given as acceleration time history with peak acceleration 0.4473 g, time step 0.01 seconds and a duration of 46.82 seconds. The velocity and displacement are integrated numerically. As observed for El Centro the mean values of the simulations are near zero, and there is a finite displacement residual in the original signal because it is not baseline corrected. The peak values for the original signal and the mean of the simulations are presented in table 3.3.

As observed by comparing table 3.4 and figure 3.8 and 3.9, the distribution of energy is well fitted for Lefkada in the same manner as discussed for El Centro. The shape of the curves in figure 3.9 are similar, and for all signals there is almost no increase in cumulative energy for $t > 12.34$ s. The mean of the simulations has a strong shaking phase with duration $D_{5-95} = 10.63$.

When Lefkada is compared to El Centro, it is observed that Lefkada has a shorter and more distinct strong shaking phase, 12.34 s compared to 24.60 s (mean of simulations), and a higher measure of cumulative energy.

Figure 3.10 show the smoothed and time modulated evolutionary PSD that is generated based on the original Lefkada ground motion. This EPSD is assumed to represent the non-stationary characteristics of the underlying stochastic ground motion.

Table 3.3: Comparison of peak values for Lefkada. Original values compared with mean μ and standard deviation σ of the 100 simulations.

		$\ddot{u}_{g,p}$ [g]	$\dot{u}_{g,p}$ [mm/s]	$u_{g,p}$ [mm]
Original		0.447	344.9	137.6
Simulation	μ	0.554	511.2	274.7
	σ	0.00259	4.48	3.60

Table 3.4: Comparison of time for energy accumulation for Lefkada. Values for original accelerations and mean of simulations. The time measures are well fitted.

	t_5 [s]	t_{45} [s]	t_{75} [s]	t_{95} [s]	t_{95-5} [s]
Original	1.73	5.05	7.02	12.21	10.48
Simulations	1.71	5.17	7.22	12.34	10.63

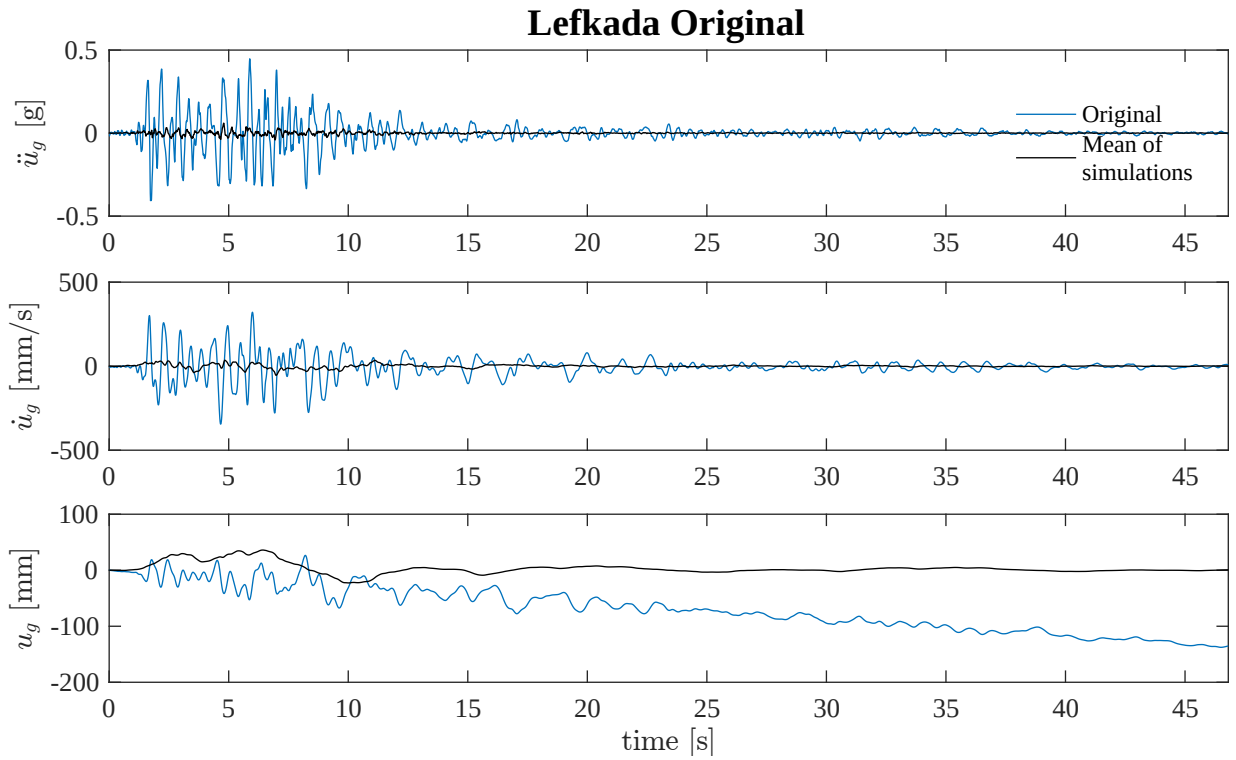

Figure 3.6: Original acceleration, velocity and displacement history for Lefkada compared with mean of simulations.

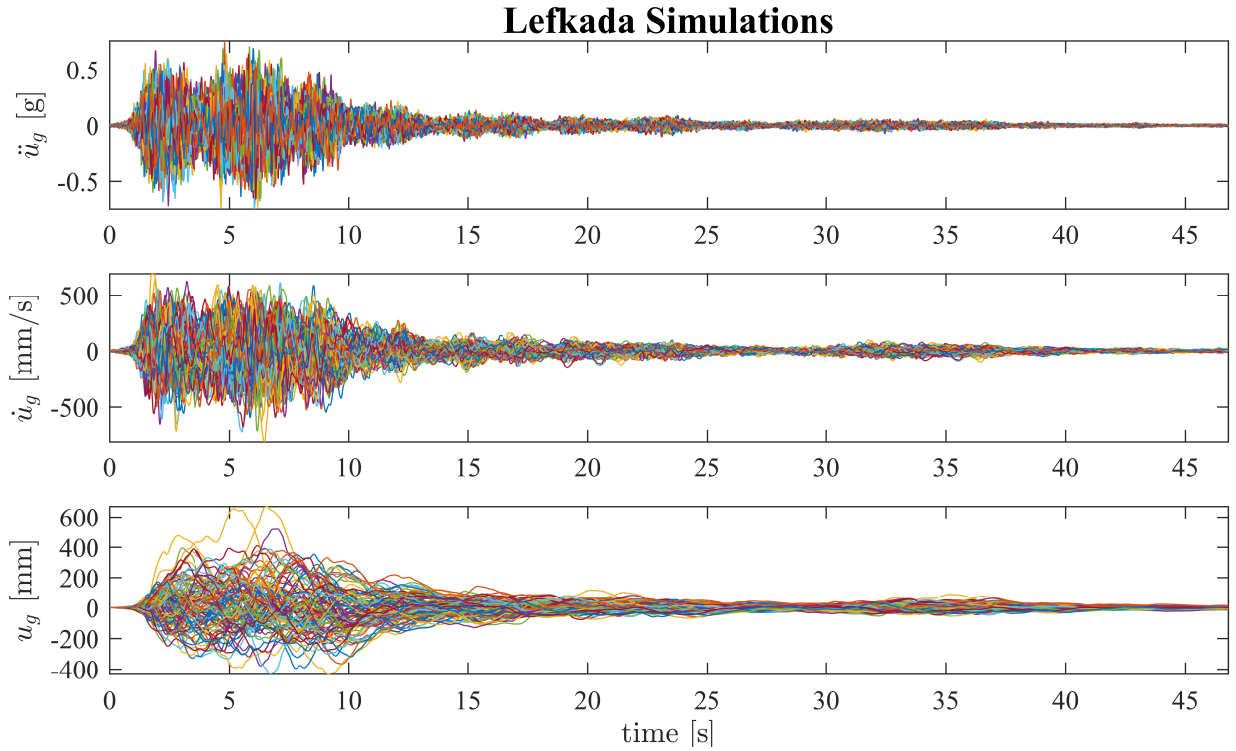

Figure 3.7: 100 simulated acceleration, velocity and displacement histories for Lefkada. The simulations have a near-zero mean in all plots.

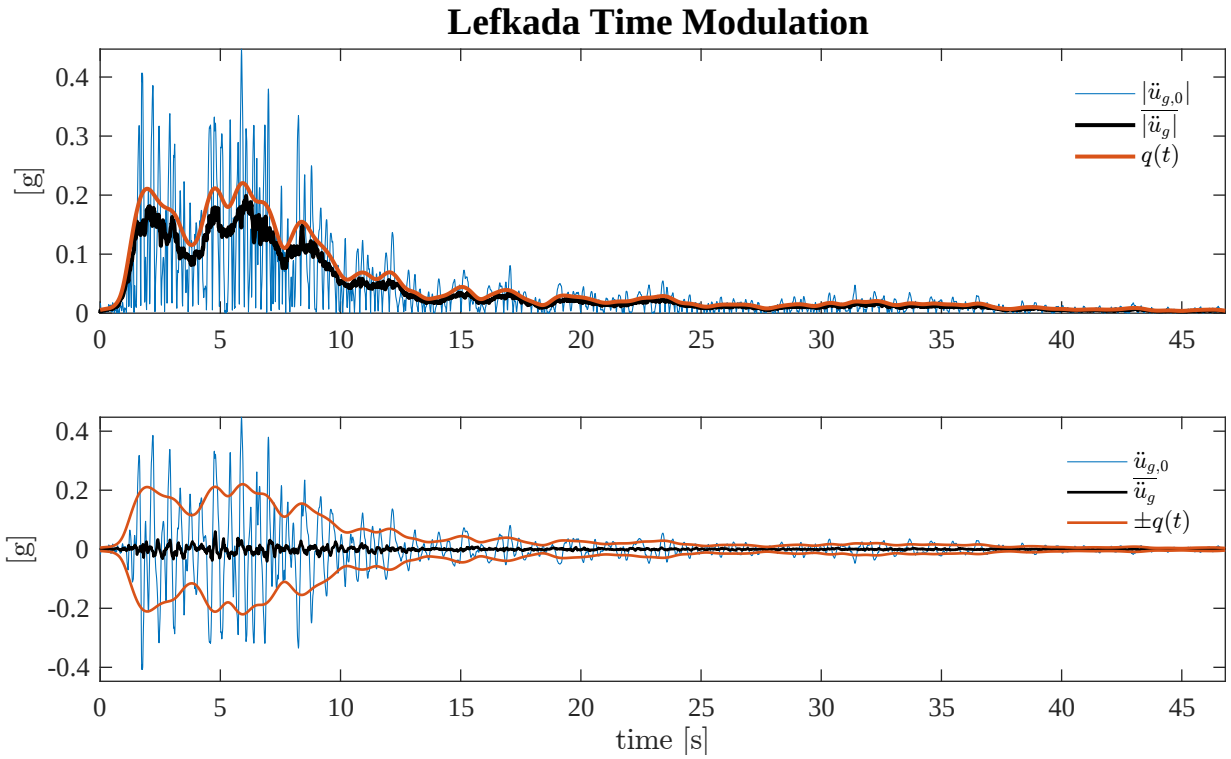

Figure 3.8: The original accelerations $\ddot{u}_{g,0}$ and mean value of simulated $\overline{\ddot{u}}_g$ accelerations compared to time modulation function $q(t)$. Upper figure show absolute values, lower figure actual values. The absolute mean values of the simulations fit well to the time modulation function $q(t)$.

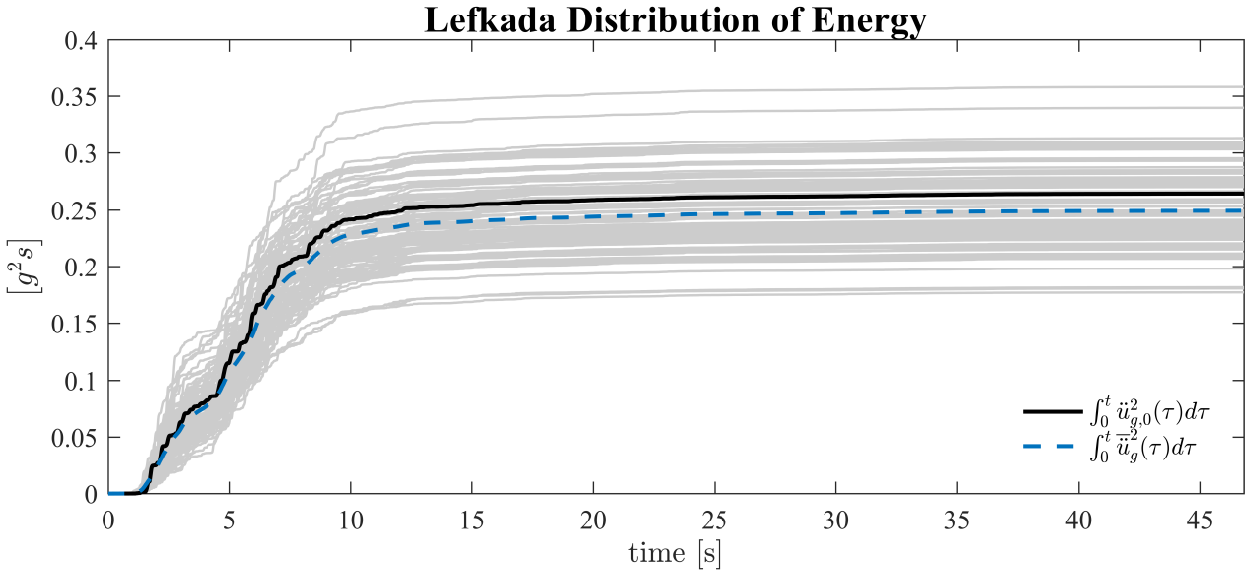

Figure 3.9: Cumulative distribution of energy of 100 simulations compared with original acceleration $\ddot{u}_{g,0}$ and mean of simulations $\overline{\ddot{u}_g}$. The mean of the simulations is well fitted to the original ground motion.

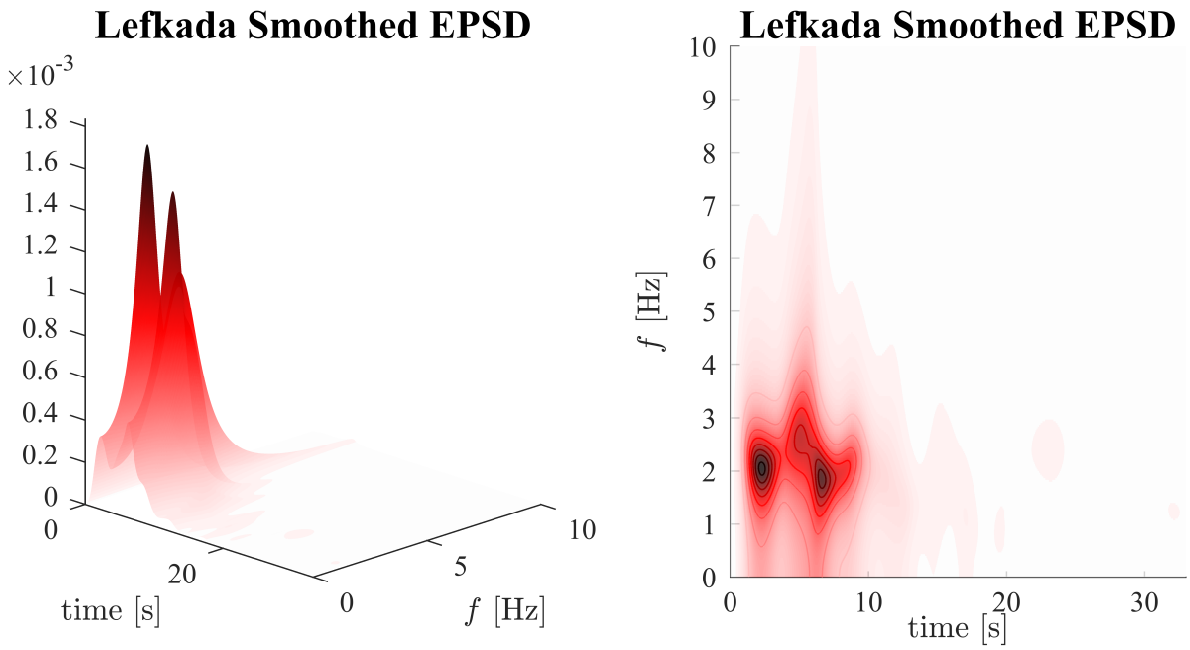

Figure 3.10: Smoothed and time modulated evolutionary power spectral density for original Lefkada ground motion. Highest value of EPSD for $t = 2.29$ s and $f = 2.0333$ Hz. The EPSD shows the variation of the stochastic model in time and frequency domain.

3.2 Choice of Prototype Scales

If the test specimen with height $H_0 = 0.5$ m were exposed to the 100 ground motion simulations of El Centro and Lefkada with original time steps, we expect the specimen to overturn for all 100 of the tests, as shown in table 3.5. In order to observe sustained rocking, the time steps are decreased according to equation 2.21. By scaling the time steps by a factor $\sqrt{\frac{R_{\text{experimental}}}{R_{\text{prototype}}}} = \sqrt{\frac{H_{\text{experimental}}}{H_{\text{prototype}}}} = \sqrt{\frac{H_0}{H}}$ we are able to represent the rocking response of a block with height H.

Shaking Table Limits The shaking table has displacement limit $u_{g,\text{lim}} = 250$ mm and velocity limit $\dot{u}_{g,\text{lim}} = 220$ mm/s. If the ground motions have displacements higher than the limit, the shaking table will experience a sudden stop. On the other hand if the velocities are slightly higher than the limit, the shaking table will still try to represent the ground motions, but by reduced accuracy compared to the *input* signal. Since the *measured* accelerations are used as input for the numerical comparison, the velocity limit is not an absolute limit. When time signals are squeezed, the maximum velocity $\dot{u}_{g,\text{max}}$ and the displacement $u_{g,\text{max}}$ decrease by factors $\sqrt{H_0/H}$ and $\sqrt{H_0/H}^2$ respectively.

Choice of Heights When the heights of the prototype models were chosen, the following criteria were stressed: The scaled simulations

1. should represent three different scales and thus three different values of the frequency parameter p.
2. should be able to produce a considerable amount of rocking motions without overturning.
3. must have $u_{g,\text{end}} \leq u_{g,\text{lim}}$ for all tests.
4. should have $\dot{u}_{g,\text{max}} \leq \dot{u}_{g,\text{lim}}$ for a low amount of the tests.

As seen in table 3.5, criterion 3 excludes heights lower than 3 m. To obtain a small number of overturns and a small number of velocities over the limit, height 5 m was chosen as the smallest specimen. For higher specimens criteria 2-4 are met, and heights 10 m and 20 m were chosen to represent three different prototype models.

3.3 Generation of Displacement Files

The shaking table is able to represent a ground motion with a given displacement time history as input. The CSV-inputfile (Comma Separated Values) consists of one column with time values in seconds and six equal columns with displacement values in millimeter. The values in all seven columns are written to the CSV-file with precision 6, i.e. 6 significant digits.

The generated ground motions tend to have small, finite end displacements $u_{g,\text{end}}$. In order to place the shaking table in its zero-position after each test, a zero-correction displacement was appended to each file as shown in figure 3.11. Firstly three seconds of a constant displacement equal to $u_{g,\text{end}}$ was added. In this way there is a clear distinction between the varying original displacement time history and the constant added values. Thereafter a cosine term equal to $0.5u_{g,\text{end}}(1+cos(\pi x))$, which attains values from $u_{g,\text{end}}$ to 0, is added. x is a vector with values from 0 to 1, discretized such that the mean velocity of the motion is 5 mm/s.

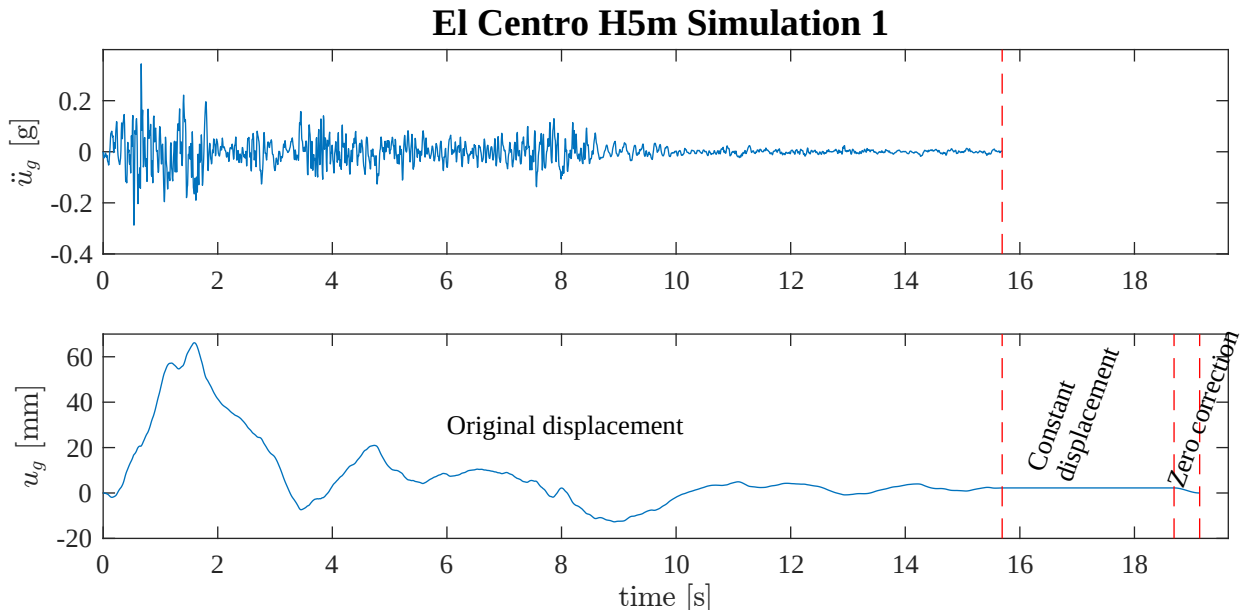

Figure 3.11: Generation of displacement u_g to input file from simulated acceleration $\ddot{u}_g$ and appending constant displacement $u_{g,\text{end}}$ and zero correction.

Table 3.5: Number of simulations that attain values above the velocity limit $\dot{u}_{g,\text{lim}}$ and displacement limit $u_{g,\text{lim}}$ of the shaking table and expected number of overturns. The values are calculated for 100 simulations with various time scaling based on the heights for both ground motions. The height of the test specimen is 0.5 m and has thus scaling 1. Number of overturns are calculated for slenderness $b/h = 0.15$, $\lambda = 0.6235$ and Housner coefficient of restitution. Prototype heights marked in grey are chosen. See appendix B for CDF plots of the numerical results of the chosen heights.
Means and medians are calculated based on those tests that did not overturn. The mean values are in general higher than the median values.

		Number of			Mean	Median
Ground motion	Height [m]	$\dot{u}_{g,\max} \geq \dot{u}_{g,\text{lim}}$	$u_{g,\max} \geq u_{g,\text{lim}}$	Overturns	$\theta_{\max}/\alpha$	$\theta_{\max}/\alpha$
El Centro	0.5	100	99	100	-	-
El Centro	1	98	72	96	0.82	0.89
El Centro	2	64	4	77	0.65	0.64
El Centro	3	34	0	64	0.53	0.48
El Centro	4	18	0	43	0.50	0.48
El Centro	5	7	0	32	0.42	0.40
El Centro	6	4	0	21	0.42	0.37
El Centro	7	2	0	12	0.37	0.32
El Centro	8	1	0	9	0.31	0.27
El Centro	9	0	0	3	0.29	0.24
El Centro	10	0	0	1	0.25	0.21
El Centro	15	0	0	0	0.16	0.15
El Centro	20	0	0	0	0.12	0.10
Lefkada	0.5	100	95	100	-	-
Lefkada	1	99	18	99	0.80	0.80
Lefkada	2	76	0	88	0.71	0.71
Lefkada	3	37	0	61	0.69	0.70
Lefkada	4	11	0	47	0.52	0.49
Lefkada	5	4	0	30	0.51	0.45
Lefkada	6	1	0	24	0.44	0.38
Lefkada	7	0	0	10	0.44	0.38
Lefkada	8	0	0	8	0.39	0.37
Lefkada	9	0	0	5	0.36	0.34
Lefkada	10	0	0	3	0.32	0.29
Lefkada	15	0	0	0	0.20	0.17
Lefkada	20	0	0	0	0.15	0.13

Chapter 4

Laboratory Work

The main goal of the laboratory work was to obtain experimental values for the rocking angle time history and the associated measured acceleration time history. The measured accelerations were used as input for numerical calculation of rocking response such that this response could be compared to the experimental one.

The rocking block was exposed to two different ground motions of 100 simulations each that were time scaled according to three different prototype heights, i.e. six test setups of 100 simulations. In this chapter the laboratory equipment and procedures are described, and figures 4.1 and 4.2 give a schematic overview of the laboratory. Figures 4.6 to 4.9 in the end of the chapter show complimentary pictures of the laboratory set up.

4.1 Shaking Table

The servohydraulic shaking table is built in 1997 and is able to represent shaking motion in one direction. As shown in figure 4.1 the shaking table is moved by the cylinder which is controlled by the controller. From the controller PC the shaking table could be governed manually or by input files with displacement or force time history. The servohydraulic cylinder that moves the table, has a maximal range of ±125 mm and ±100 kN and maximal velocity of ±220 mm/s.

The shaking table controller could be tuned in such a way that the shaking table is able to reproduce the motions in an appropriate manner. We are able to choose parameter values for stiffness K_p, inertia K_i and damping K_c. The values are chosen by trial and error with a special focus on the represented acceleration values. High stiffness K_p leads to a close match

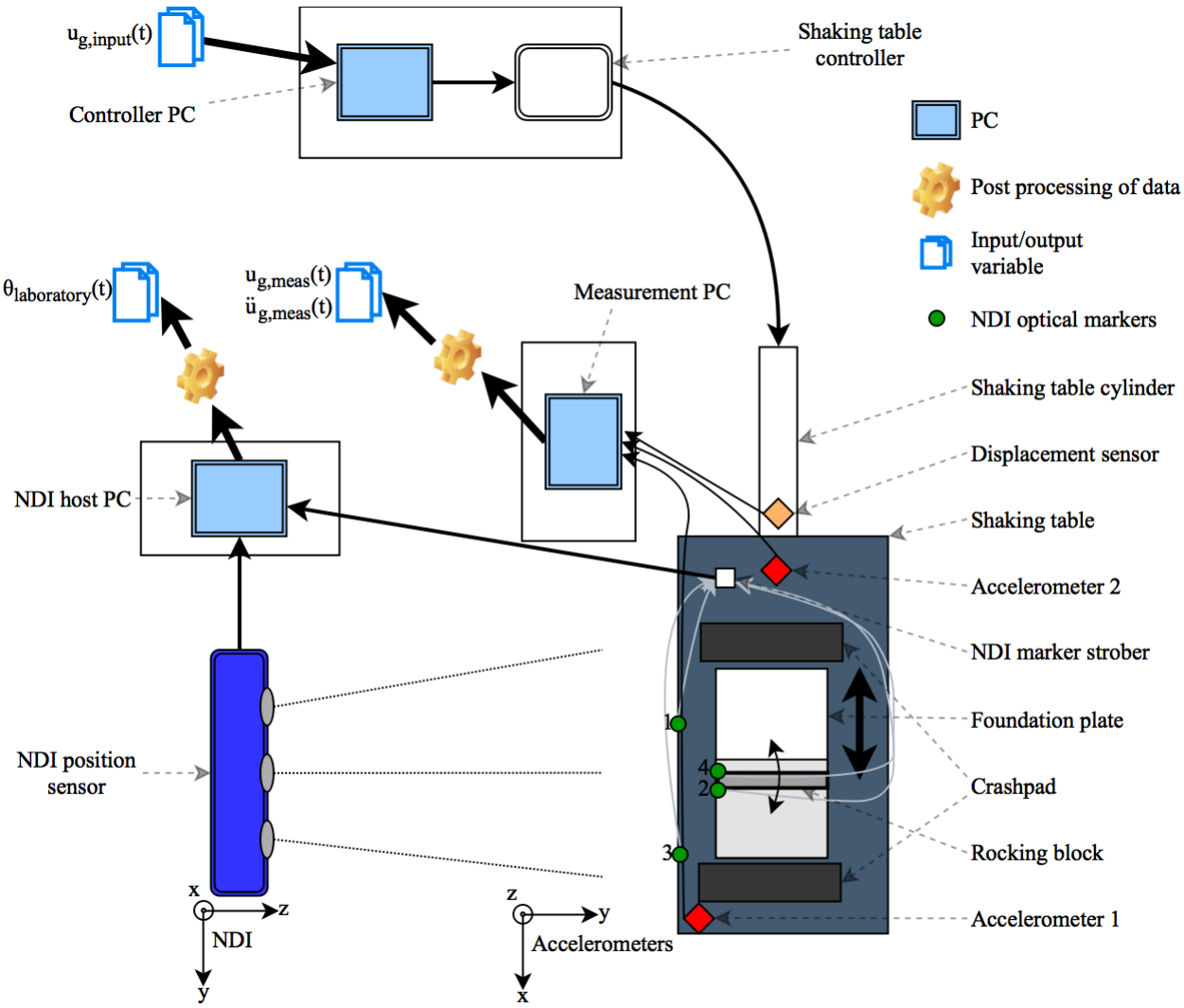

Figure 4.1: Schematic overview of laboratory setup.

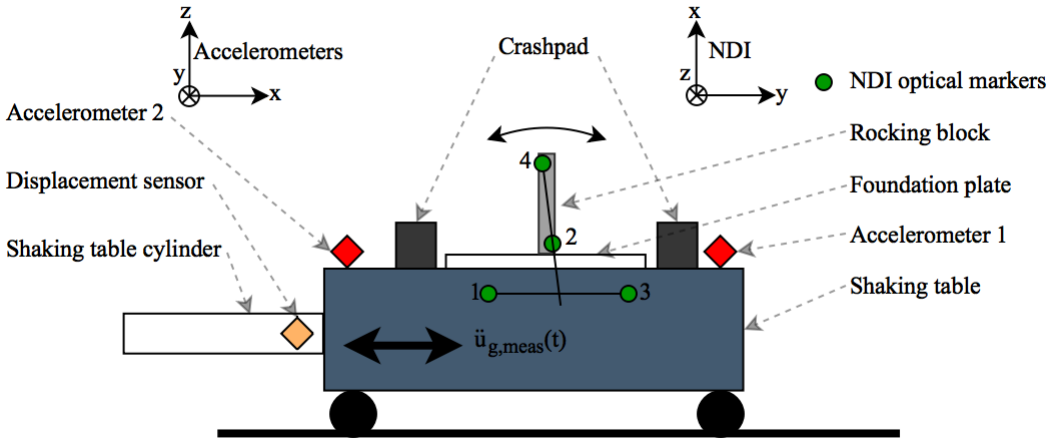

Figure 4.2: Setup of shaking table from the side.

between the prescribed and the actual displacement time history, but on the other hand will too high stiffness values imply that accelerations may be higher than realistic. For some high values of K_p, the cylinder reached the force limit and accelerations in the magnitude of 1.5 g was measured, which is clearly unrealistic for the simulated ground motions. Since the measured acceleration time history forms the basis for the numerical rocking response, the shaking table was tuned to reproduce realistic accelerations at the expense of exactness of represented displacement.

Table 4.1: Tuning values for the shaking table controller. The values for K_p and K_i for Tuning 1 were not noted explicitly, but were higher than the values for Tuning 2.

Tuning	K_p	K_i	K_c
1	>3.2	>0.04	0.03
2	3.2	0.04	0.03

When the system is under hydraulic pressure and the target displacement value is constant, the cylinder position is oscillating around the target displacement. Based on measured displacement files we see that the motion has an amplitude of about 0.05-0.15 mm and main frequency of about 1.5-2.0 Hz. An example from one test is shown in figure 4.3. This motion might be present also when the shaking table is moving and might influence the measurements.

As long as the shaking table is connected to the cylinder, it will move, and according to the time instant the prescribed displacement is started, the initial conditions will vary. The rocking response is sensitive to initial conditions, and consequently it is not expected that the rocking response of the block to one simulation is exactly repeatable. The same observation is also reported by Aslam et al. [1].

4.2 Shaking Table Measurements

As seen in figure 4.1 the measurement PC is connected to two accelerometers on the shaking table and a displacement sensor on the cylinder. Two accelerometers are chosen to have redundancy in case of failure in measurements, which was the case for some of the 700 tests. Measurements are recorded at sampling rate F_s = 500 Hz, displayed on the PC screen and finally saved to a CSV-file when the recording is stopped. The recording must be started and stopped manually, thus the duration of the records are longer than the duration of the respective ground motion simulation.

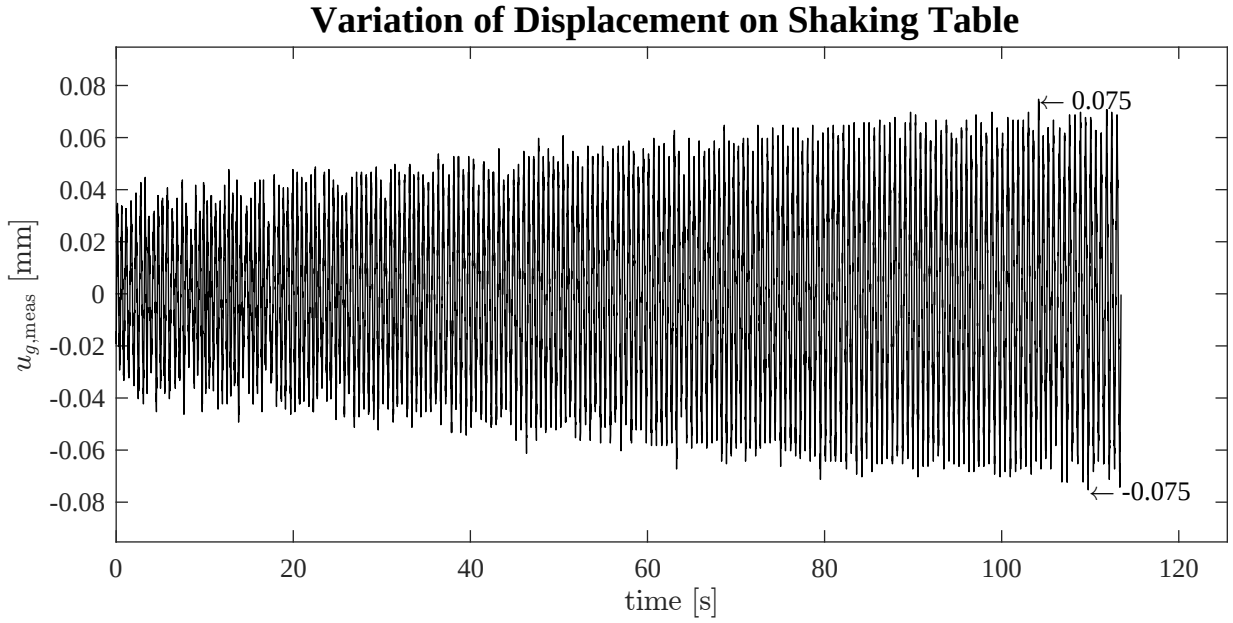

Figure 4.3: Actual variation of displacement of the shaking table for constant target displacement based on result from the 114 last seconds of test 2016_11_01_135701_018. Maximum amplitude 0.075 mm and main frequency 1.727 Hz. This motion might influence the measurements.

4.3 NDI Optical Measurements

To measure the rocking response of the rocking block, the optical measure system Optotrac Certus from the company Northern Digital Inc (NDI) is used. Hereafter this system will be referenced by the abbreviation NDI.

As seen on figure 4.1 the NDI system consists of a position sensor that tracks the positions and motions of infrared light emitting diodes (optical markers) within a specific area. The markers are connected to the host PC through cables and the marker strober, and motions are recorded with a sampling rate $F_s = 500$ Hz.

Calculation of Rocking Angle Marker 1 and 3 are attached to the shaking table and marker 2 and 4 are attached to the rocking block as shown in figure 4.2. The NDI software is able to calculate the acute angle $\theta_{\text{init}}(t) = \angle(l_{1,2}(t), l_{2,4}(t)$ between the lines $l_{1,2}(t)$ and $l_{2,4}(t)$ directly. We are interested in the rocking angle of the test specimen relative to the equilibrium state, in other words the change of the angle relative to the angle at rest. For a specimen that is at rest, the rocking angle is zero. Consequently we need to subtract the offset of about 87° to obtain the rocking angle.

$$\theta_{\text{laboratory}}(t) = \theta_{\text{init}}(t) - \theta_{\text{offset}} \tag{4.1}$$

The orientation of the position sensor was calibrated such that the y-axis of the position sensor coincides with the direction of motion of the shaking table. This calibration was performed by setting the shaking table to move back and forth and checking that z-positions of marker 1 and 3 did not change.

4.4 Test Specimen

The test specimens used in the experimental tests consist of a triple symmetric assembly of two hollow columns, two linking plates and four wedges as shown in figure 4.4. The wedges pictured in 4.4(a) are replaced by the wedges in 4.4(b). All parts are made of aluminum and connected by aluminum bolts, and the specimen is assumed to be rigid.

Specimen Parameters The total height of the specimen $H = 2h = 500$ mm is measured from the lowest part of the bottom wedge to the highest part of the top wedge. When the specimen is uplifting, it is tilting about the lower, outer corners of the wedge, a distance $B = 2b = (2+71+2)$ mm $= 75$ mm apart from each other. According to section 2.1 the slenderness b/h is

$$\frac{b}{h} = \frac{B}{H} = \frac{75}{500} = 0.15 \tag{4.2}$$

the slenderness angle α is

$$\alpha = \tan^{-1}\left(\frac{b}{h}\right) = \tan^{-1}(0.15) = 0.148889... \text{ rad} \approx 0.15 \text{ rad} \tag{4.3}$$

and the semidiagonal R is

$$R = \sqrt{b^2 + h^2} = \frac{1}{2}\sqrt{B^2 + H^2} = \frac{1}{2}\sqrt{75^2 + 500^2} \text{ mm} \approx 252.80 \text{ mm} \tag{4.4}$$

Double Column Design The initial design consisted of only one column and a wedge on top and bottom, however this assembly turned out to rotate about its longitudinal axis when exposed to shaking table motions. In order to avoid rotation and to model the targeted one degree of freedom system better, the design consisting of two columns was chosen as shown in figure 4.4.

The chosen design exhibits a main drawback: The foundation of the rocking specimen consists of two wedges and a linking plate instead of one piece. These three parts need to

be connected and tightened by uttermost precision to avoid twisting and to obtain a parallel rocking edge. If not, the specimen will rest on three of four edges and exhibit a wobbling motion instead of a clean rocking motion with one simultaneous impact on each side.

Consequently the rocking block was assembled on a flat steel table and tightened until the bottom surface was precisely in plane. Whether the surface is in plane or not, is easily observed by gently pushing and pulling the top of the specimen from side to side and feel for instabilities and wobbling motion. A perfect specimen should exhibit no tilting for a gentle push below the uplift criterion, and a simultaneous tilt about the entire bottom edge for a push over the uplift criterion.

Instabilities from Overturn Impacts As seen on figure 4.2 a crash pad, consisting of a wooden specimen and a rubber mat on top, was put on each side of the foundation plate to avoid damages of cables, bolts etc. and to limit impacts on the specimen when overturning. Nevertheless, during the test it was observed that especially the bolts on the top of the rocking block became looser after several impacts from overturns, which in turn lead to twisting of the block. Consequently the stability of the rocking block should be checked after each overturn, and if need be, the bolts should be re-tightened. For some of the tests this was not performed and the effect thereof is observed as discussed later. The test specimen used for the two first test groups is called Model 1, the second, equal test specimen used for the following five test groups is called Model 2.

4.5 Free Vibration Test

Since the test specimen is not a perfect rectangular cylinder with evenly distributed mass, the inertia must be experimentally determined. The inertia factor λ affects the frequency parameter p and thus the period of the rocking motion. Also the coefficient of restitution c could be experimentally determined. The coefficient of restitution affects the loss of energy and thus the decrease of rocking amplitude.

Free vibration tests are performed, and values for λ and c are tested to obtain a numerical rocking response which fits the laboratory response in a good manner. The obtained values are shown in table 4.2 and the corresponding numeric and laboratory response are shown in figure 4.5.

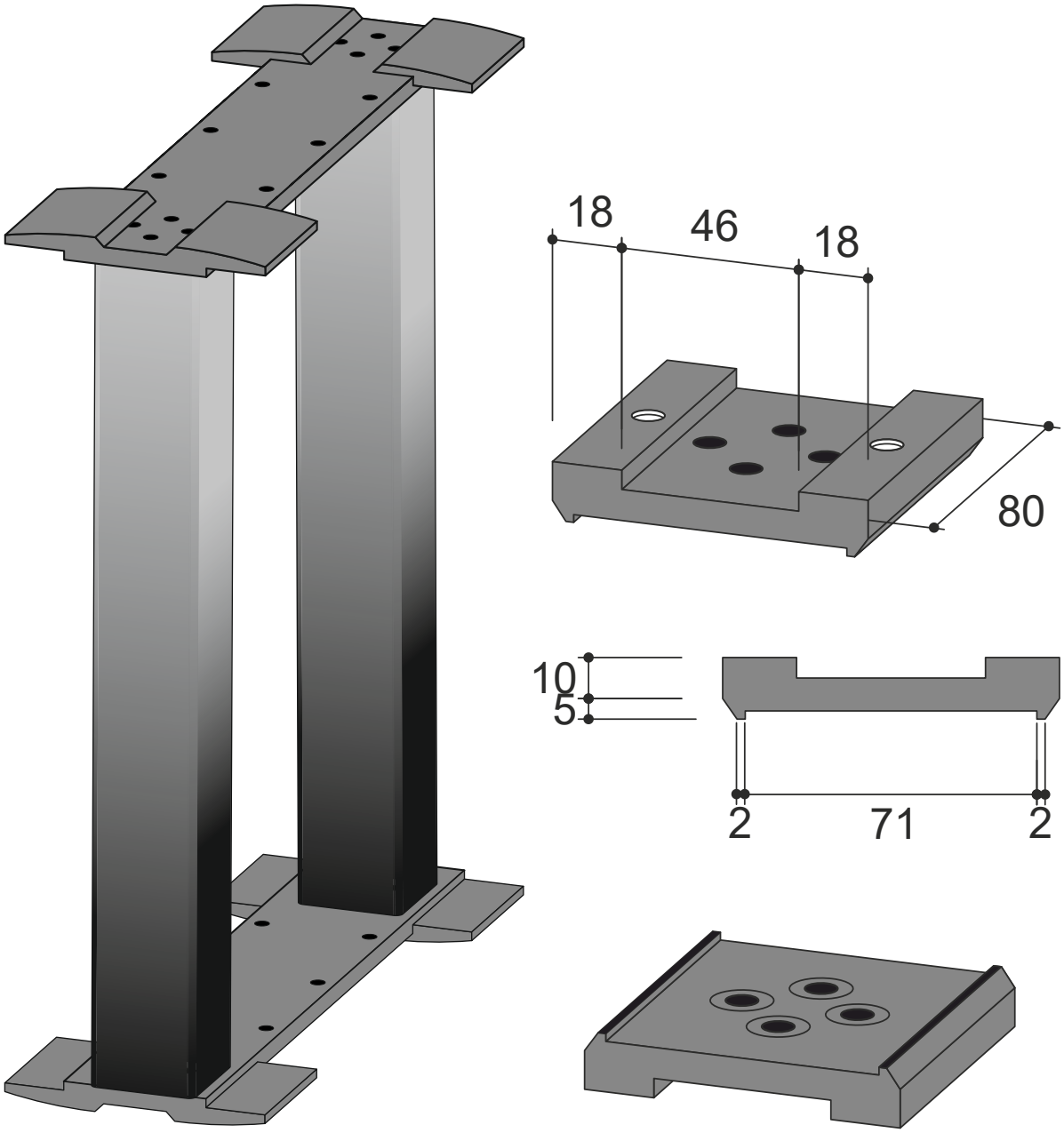

(a) Assembled rocking block consisting of two columns, two linking plates and four wedges. Total height H=500 mm.

(b) Correct wedges used in experiments with measurements in mm. Total width of bottom B=75 mm.

Figure 4.4: Test column with wedges as pictured in (b). *Figures from Jonas Bachmann.*

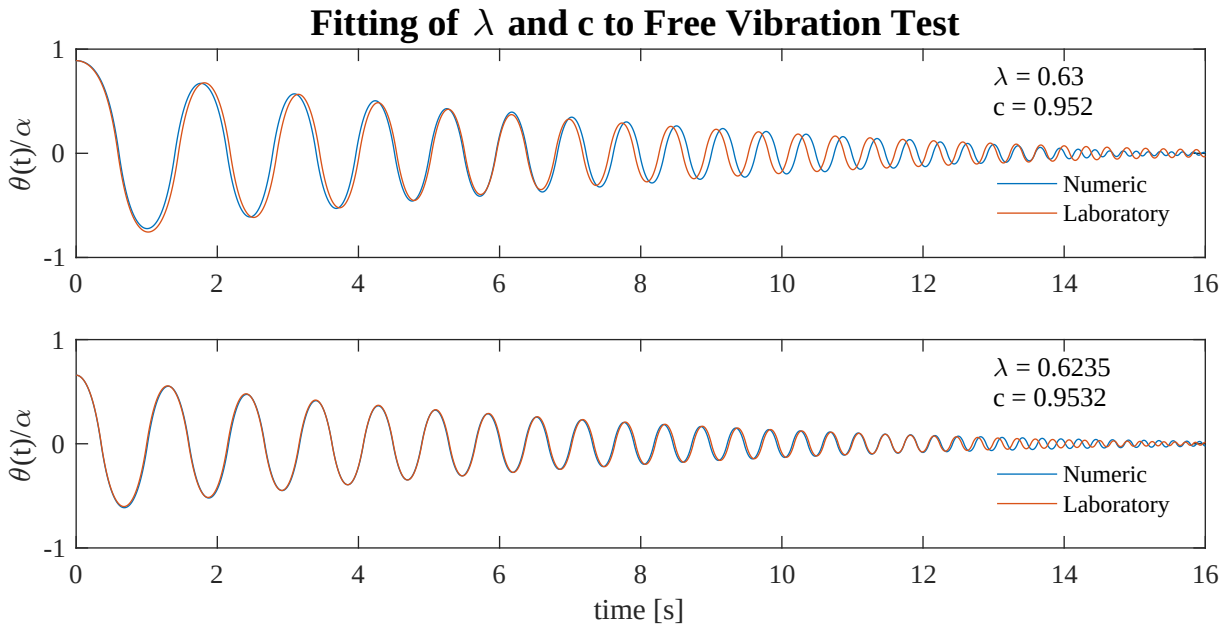

Figure 4.5: Free vibration response and fitting of values for λ and c. The upper graph corresponds to model 1, the lower to model 2.

Table 4.2: Experimental and analytical Housner values for coefficient of restitution c and experimental inertia factor λ for the two different models used. The Housner values are lower than the experimental, thus more energy is lost on each impact for $c_{Housner}(\lambda)$.

Model	λ	c_{Exp}	$c_{\text{Housner}}(\lambda)$	$c_{\text{Exp}} - c_{\text{Housner}}(\lambda)$	$\frac{c_{\text{Exp}} - c_{\text{Housner}}(\lambda)}{c_{\text{Exp}}}$
1	0.63	$0.9520 \approx 0.9757^2$	$0.9467 \approx 0.9730^2$	$5.3 \cdot 10^{-3}$	0.56 %
2	0.6235	$0.9532 \approx 0.9763^2$	$0.9465 \approx 0.9729^2$	$6.7 \cdot 10^{-3}$	0.70 %

4.6 Test Procedures

When the tests were performed, the following procedures were pursued for each test.

1. Check stability of column, and if needed, tighten the bolts until the bottom surface is in plane.
2. Check the position of the column. The initial position was measured to be perpendicular to the shaking table and then marked with pen on the table.
3. Choose and load displacement file into controller PC.
4. Start recording of NDI on host PC. The measurement stops automatically after a specified amount of time.
5. Start recording of shaking table on measurement PC.
6. Start shaking table movement from controller PC.

7. Observe movement of the rocking block.
8. End recording of shaking table after the shaking table has stopped, and save the file manually. Even if the block overturns in the beginning, the measured accelerations must be recorded until the shaking table has stopped its movement.
9. Note any comments or observations in log. Qualitative observations about each rocking motion were noted to have a possibility to verify the correspondence of a test and its measured rocking response, if need be.

Observation of Errors In total over 700 laboratory tests were performed, and the risk of human errors or unwanted events is imminent. Following test procedures, noting of observations and regularly controlling the output results, were found useful as means of avoiding and observing errors and mistakes. In addition to following the test procedures, the preliminary results were regularly checked, compared and validated on the computer. According to observations in the laboratory and on the computer, the test procedures were iteratively improved. Observations during the laboratory period lead to that some of the simulations needed to be retested. Other observed challenges could be dealt with by post-processing of measured data on the computer.

Name of Files A consistent naming procedure of the test results was crucial to be able to post-process the signals by loop-iterations in a computer script. Moreover a log was filled out during the lab period to connect each test result with the corresponding input displacement file that was tested. Any notes important for the post-processing were also noted in the log.

Output Result Files The NDI software automatically saves the calculated angle recordings as a CSV-file in the manner

`Artificial_Ground_Motions_Rocking_YYYY_MM_DD_HHMMSS_NNN_cal.csv`

where the timestamp `YYYY_MM_DD_HHMMSS` denotes the time when the new project was initiated and `NNN` is a counter from 001 to 999 indicating the test number. An example is given as

`Artificial_Ground_Motions_Rocking_2016_11_01_135701_001_cal.csv`

The corresponding recording of acceleration and displacement of the shaking table is saved manually as

`Artificial_Ground_Motions_Rocking_2016_11_01_135701_001_acc.csv`

where the suffix `acc` is the only difference.

Input Displacement Files The generated input displacement files were saved as a CSV-file in the following manner

`Artificial_Ground_Motions_Input_GM SCALE_N.csv`

where `GM` is the name of the ground motion, `SCALE` is the applied scaling and `N` is the simulation number. An example is given as

`Artificial_Ground_Motions_Input_Lefkada H5m_1.csv`

4.7 Description of Laboratory Tests

Preparations Model 1, Tuning 1 The laboratory equipment was set up October 25, 2016. Thereafter time was spent on getting used to the software, the equipment and the test procedures. The input and output files were tested, and MATLAB scripts were improved iteratively to be able to analyze and validate the results during the test period. The shaking table controller was tuned to represent the accelerations of El Centro H10m in an appropriate manner: Tuning 1 according to table 4.1. Free vibration tests were performed on Model 1 to obtain the values for c and λ as given in table 4.2.

The groups of ground motions that were tested, are described chronologically in the following as showed in table 4.3. The number of model and tuning coincides for all seven test groups.

El Centro H10m The first tests were performed November 1, 2016. Out of 100 tests only 8 overturned, leading to impacts that might loosen bolts. The bolts were not tightened, but nevertheless the column foundation remained stable throughout all tests, and the results are assumed to be sufficient for comparison with numerical response.

El Centro H5m, Model 1, Tuning 1 Out of 100 tests 50 overturned. After the fourth overturn, an instable foundation was observed, nevertheless the tests were continued without tightening of the bolts. Due to the following 46 overturn impacts, the degree of twisting of the foundation was varying throughout the tests.

Table 4.3: Overview of tests. Some of the testruns for El Centro H5m Model 1 (marked in grey) were performed with wobbling column foundation. All 100 tests for El Centro H5m were therefore retested with model 2.

Ground motion	Model	Tuning	Test project	Test number
El Centro H10m	1	1	2016_11_01_135701	001-040
			2016_11_02_125617	001-060
El Centro H5m	1	1	2016_11_08_134036	001-052
			2016_11_09_134129	001-048
Lefkada H5m	2	2	2016_11_11_093855	001-007
			2016_11_11_132038	001-047
			2016_11_14_104011	001-045
			2016_11_17_172214	001
Lefkada H10m	2	2	2016_11_14_125700	001-100
Lefkada H20m	2	2	2016_11_17_104502	001-100
El Centro H20m	2	2	2016_11_17_131517	001-100
El Centro H5m	2	2	2016_11_17_151155	001-100

The unstable foundation was resting on three of four edges: two edges on the right side and only one edge on the left side, directions as in figure 4.2 and 4.4. When the column was gently pushed to the right side, thus pivoting about the right parallel edge, the column tilted without wobbling or twisting. On the other hand, when the column was pushed to the left side, thus pivoting about the nonparallel, left edge, the column exhibited a small wobbling motion for even a gentle push.

It is reasonable to assume that the coefficient of restitution has changed, at least on the left, unstable edge, due to the changed impact mechanism. When the column foundation rested on three edges, it could be tilted a small angle from one side to the other without uplifting. Consequently this small, spurious rocking angle will influence the angle measured by the NDI, leading to higher angle values compared to what is expected from a perfectly plane foundation. Due to these imperfect initial conditions, there are many sources of errors in the results and many discrepancies compared to the analytical model applied in numerical response. The experimental rocking response to El Centro H5m was therefore rerun at a later time.

Preparations Model 2, Tuning 2 Due to the unstable column used in the previous test, a new, equal column, Model 2, was assembled and tightened until the bottom surface of the foundation was in plane. Free vibration tests were performed on Model 2 to obtain the values for c and λ as given in table 4.2. From now on the test procedure "Check stability of column, and if needed, tighten the bolts until the bottom surface is in plane." was followed. As seen

by comparing figures 3.2 and 3.4 with 3.7 and 3.9, the Lefkada simulations have higher peak accelerations and cumulative energy than the El Centro simulations. When the first Lefkada simulation was tested on the shaking table with the previous controller Tuning 1, the shaking table stopped due to exceeded force limit. The shaking table was retuned according to the values in table 4.1, and Tuning 2 was used for all the following test groups. Thus the number of model and tuning coincides for all seven test groups.

Lefkada H5m The measured acceleration signal from test `2016_11_14_104011_005` shows a spurious spike of 1.15 g in the period after the shaking table had stopped. The spike originates from an accidental impact on the accelerometer. This spike must be excluded before numerical response is calculated based on the measured acceleration signal.

The test of simulation number 100 had to be retested some days later because the NDI-recording was missing.

Lefkada H10m No remarkable events.

Lefkada H20m For tests `2016_11_17_104502_052-100` the cable connecting accelerometer 1 to the measurement PC was not properly connected, thus only recordings from accelerometer 2 are available.

El Centro H20m For tests `2016_11_17_131517_001-007` the cable connecting accelerometer 1 to the measurement PC was was not properly connected, thus only recordings from accelerometer 2 are available.

El Centro H5m, Model 2, Tuning 2 The displacement input-files used for these tests are the same as used for El Centro H5m, Model 1, Tuning 1. Due to the rationale mentioned in the end of section 4.1, and due to the fact that the tuning of the shaking table is different, the measured accelerations are not expected to be equal to the respective measurements from the previous tests.

If the numeric response of El Centro H5m is calculated based on input accelerations, instead of measured accelerations, the response would not be equal for Model 1 and 2 because the respective c- and λ-values given in table 4.2 are used. See figures in appendix B.

The last laboratory test was performed November 17, 2016.

Figure 4.6: Picture of shaking table and test specimen. Notice the two pairs of optical markers on the side of the shaking table and on the test specimen. See figures 4.1 and 4.2 for further descriptions.

Figure 4.7: Overview picture of laboratory set up. The NDI optical sensor is seen to the left, the shaking table and the test specimen to the right. The three PCs are seen in the background. See figures 4.1 and 4.2 for further descriptions.

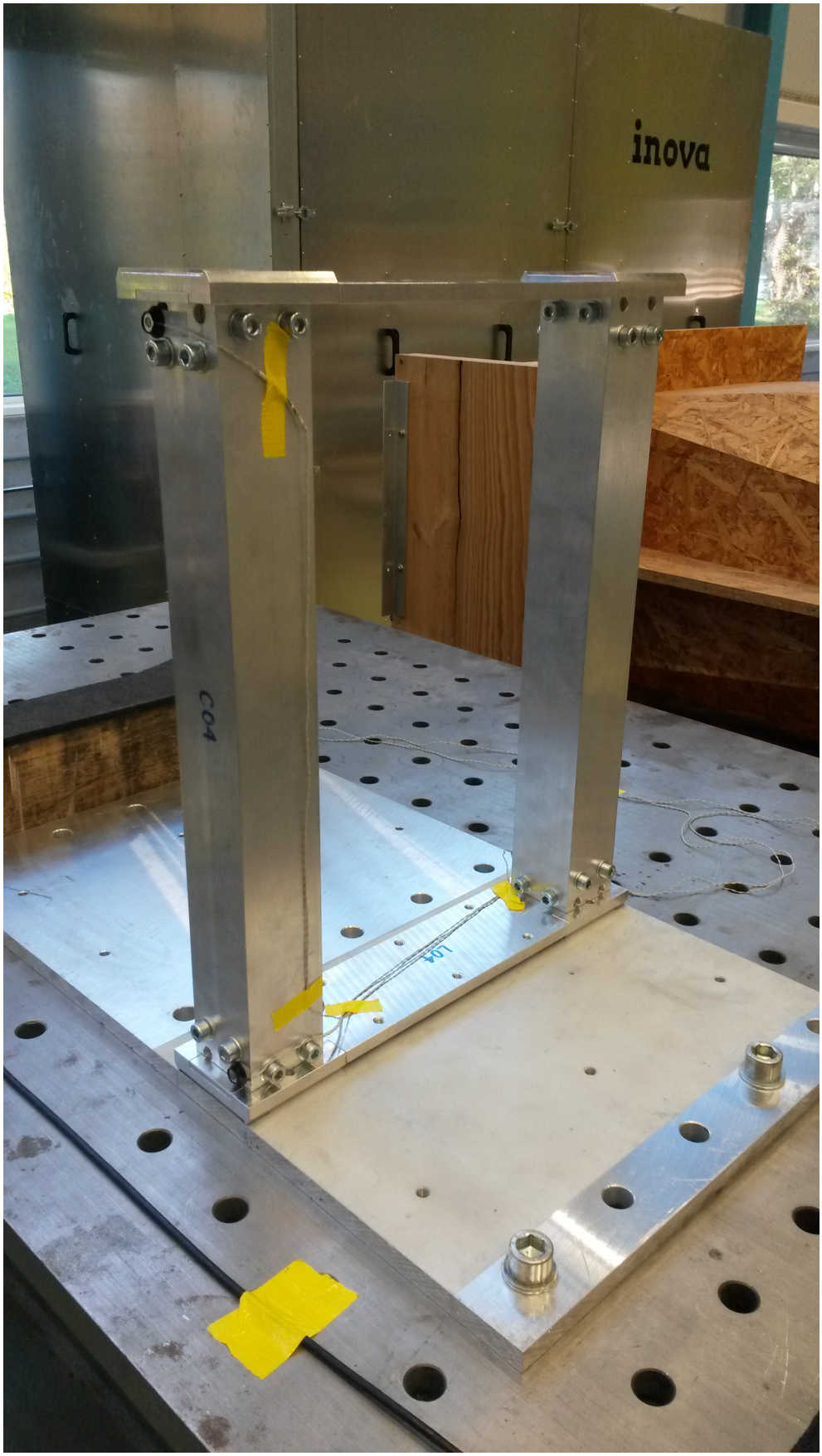

Figure 4.8: Close picture of test specimen. The grey cables are connecting the optical markers with the NDI host PC. See figures 4.1 and 4.2 for further descriptions.

Figure 4.9: Rocking test specimen before overturning. Overturning lead to impacts that slightly influences the measured accelerations. The impacts lead additionally to that the bolts connecting the wedges and the columns become looser and must be re-tightened. See figures 4.1 and 4.2 for further descriptions.

Chapter 5

Post Processing of Laboratory Results

The measured test results need to be post-processed in order to obtain the maximum rocking angle and compare the results of laboratory response with that of numerical response. The certain steps performed to obtain these values, are described in this chapter.

All test results are named according to the rules described in section 4.6 and saved in folders according to their test project. A MATLAB script iterates through the logfile with records for each test, imports the associated output files and links the meta-information about the associated, scaled ground motions that are tested.

5.1 Adjusting Offsets of Measured Variables

All the variables that are measured in the laboratory, show near-constant non-zero values when we expect zero-values, e.g. when there is no movement of the shaking table. Moreover if we consider the initially measured variable $X_{\text{init}}(t)$, the expected value $E[X_{\text{init}}(t)] = X_{\text{offset}} \neq 0$. To obtain physically realistic results with a zero mean for the variables, we subtract the mean of the first M recorded points

$$X_{\text{offset}} = \frac{1}{M} \sum_{i=1}^{M} X_{\text{init},i} \tag{5.1}$$

from the initially measured value at every point i

$$X_{\text{meas},i} = X_{\text{init},i} - X_{\text{offset}} \tag{5.2}$$

The measurement records are started before the shaking table movement is initiated, thus the mean of the first M points is assumed to represent the offset of the measure device. For the acceleration and theta values $M = 100$ is chosen. For a sampling rate $F_s = 500$ Hz that implies that the mean is calculated based on the values of the first 0.2 seconds.

Accuracy of Method The accuracy of this method of offset correction is not determined explicitly, but the offset correction is also performed with the built-in MATLAB function `detrend` for comparison. The `detrend` function calculates and subtracts the least square fit of a linear trend of the input signal. See discussion in section 8.10 for details.

5.2 Measured Rocking Angle

As explained in section 4.3 the measured rocking angle $\theta_{\text{laboratory}}(t)$ is calculated by equation 4.1 by subtracting the offset such that the angle is zero at rest. The offset $\theta_{\text{init}}(t)$ has a value of about $87° \approx 1.52$ rad due to the placement of the NDI optical markers on the rocking block, se figure 4.2.

$$\theta_{\text{laboratory}}(t) = \theta_{\text{init}}(t) - \theta_{\text{offset}} \qquad \text{(4.1 revisited)}$$

Maximum, Absolute Value The value of interest for further comparisons is θ_{max}, the maximum, absolute value of the rocking angle. The value is normalized by the critical slenderness angle α.

$$\theta_{\text{max}} = \max(\text{abs}(\theta_{\text{laboratory}}(t))), \qquad \text{[rad]} \tag{5.3}$$

Since we might observe $\theta_{\text{max}} \geq 1.0\alpha$ without overturning, $\theta_{\text{max}} \geq 1.5\alpha$ is set as the discretized definition of overturning. All values higher than 1.5α are set to 1.5α. The maximum value below 1.5α that was observed, was 1.030α. The domain of θ_{max} is consequently given as

$$\theta_{\text{max}} \in [0, 1.5]\,\alpha \tag{5.4}$$

Examples of initial measured signal $\theta_{\text{init}}(t)$ and normalized, corrected rocking angle $\theta_{\text{laboratory}}(t)/\alpha$ are shown in figure 5.1.

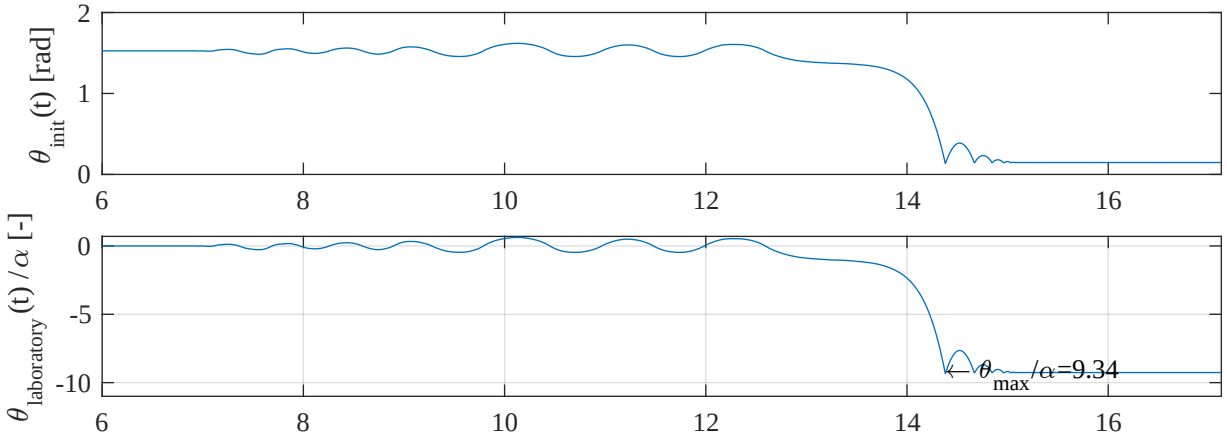

(a) Overturn. $\theta_{\max}$ is set to 1.5α.

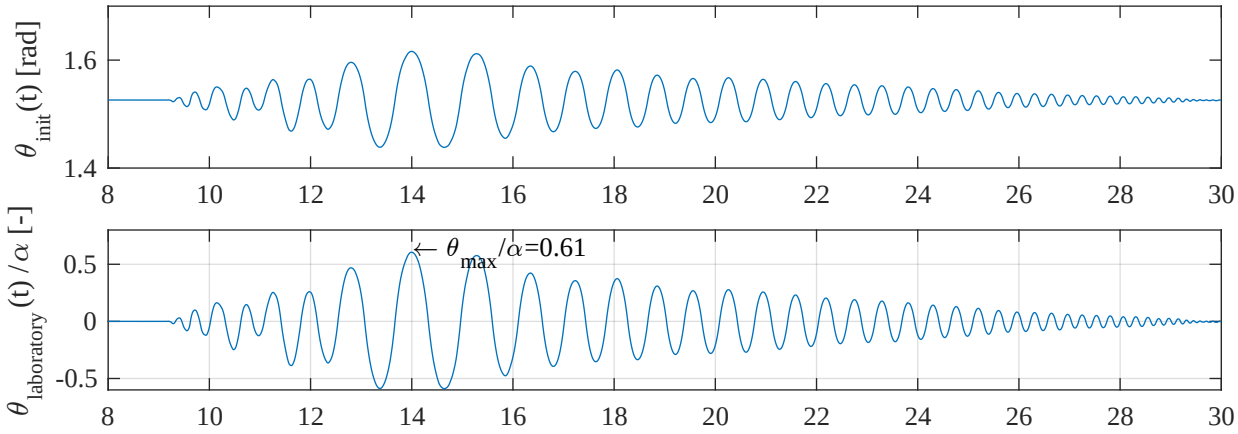

(b) Sustained, long rocking.

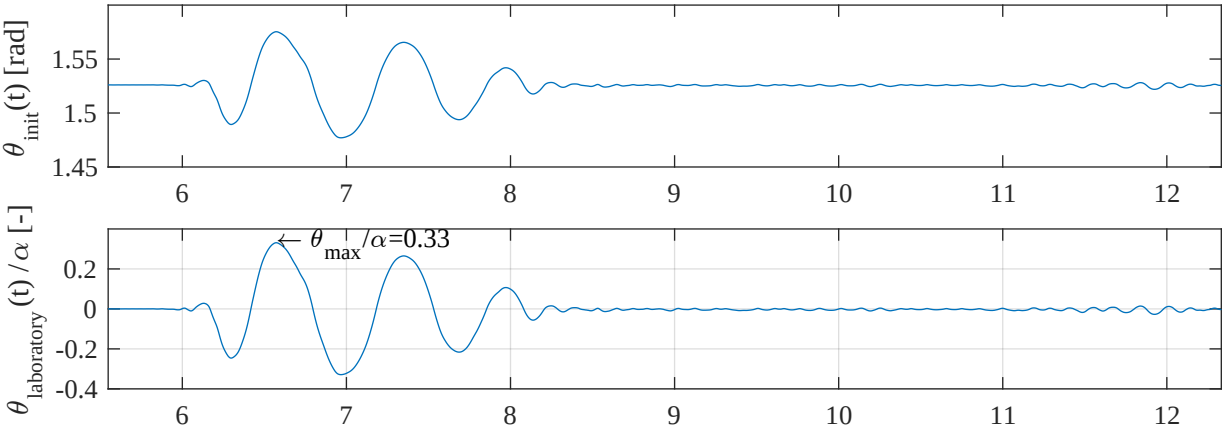

(c) Sustained, short rocking.

Figure 5.1: Initial measured signal $\theta_{\text{init}}(t)$ and normalized, corrected rocking angle $\theta_{\text{laboratory}}(t)/\alpha$. Plots (a), (b) and (c) show measured response to El Centro H10m simulations 6, 14 and 21 respectively. Time axis given in seconds.

5.3 Measured Accelerations

The measured accelerations need to be imported and post-processed to serve as input for numerical response calculations. The offset must be subtracted, the main component of the acceleration must be calculated and the accelerations with highest peak values from either accelerometer 1 or 2 is chosen as input. See figure 5.3 for an overview.

Main Component The accelerometers record accelerations in three directions and are attached to the shaking table surface with tape as shown in figure 5.2. Consider an initial acceleration record $\ddot{u}_{g,\text{init},i,j}$ in direction $j = x, y, z$ for time t_i where $i = 1, .., N$ for N record points. The recorded acceleration values $\ddot{u}_{g,\text{init},i,j}$ have an offset $\ddot{u}_{g,\text{offset},j}$ in each direction. To obtain physically realistic results $\ddot{u}_{g,\text{meas},i,j}$, the offset corrections are calculated by equations 5.1 and 5.2.

The accelerometers are aligned such that the x-axis coincides with the direction of movement of the shaking table. Since the accelerometers hardly could be aligned in an exact manner, the main component of the acceleration for all the N recording points is calculated in the x-y-plane as

$$\ddot{u}_{g,\text{meas},i} = \text{sgn}(\ddot{u}^*_{g,\text{meas},i})\sqrt{\ddot{u}^2_{g,\text{meas},x,i} + \ddot{u}^2_{g,\text{meas},y,i}}, \qquad i = 1, ..., N \tag{5.5}$$

where $\ddot{u}^*_{g,\text{meas},i}$ is the acceleration component $\ddot{u}_{g,\text{meas},x,i}$ or $\ddot{u}_{g,\text{meas},y,i}$ that has the largest absolute value. The accelerations in z-axis are not taken into account.

Figure 5.2: Accelerometer 1 attached to the shaking table.

The acceleration signal are cut such that eventual spurious spikes from the period before or after the shaking table started to move, are avoided. The time instants t_0, for the first

acceleration value to be included, is determined by the first acceleration value to fulfill 80 % of the uplift criterion

$$\ddot{u}_{g,\text{meas}}(t_0) \geq 0.8g\tan(\alpha) \tag{5.6}$$

The numerical rocking response script takes only acceleration values greater than the uplift criterion into account, as described in section 5.4. The last time instant, t_{end}, is determined by

$$t_{\text{end}} = t_0 + T + t_{\text{added}}/2 \tag{5.7}$$

where T is the duration of the input displacement signal and $t_{\text{added}} = 3$ s is the duration of added constant displacement as shown in figure 3.11.

The accelerations are measured by two accelerometers. Due to the fact that some of the measurements for accelerometer 1 are lacking, see section 4.7, the two signals must be compared for each test result. The offset-corrected and time-cut acceleration signal with the highest absolute value, is chosen as input signal for further numerical response calculations.

As seen on figure 5.3, measured accelerations from responses where the block overturned, has a spike from the overturning impact. Such spikes are not observed for the y-signals for those responses without overturning. These spikes introduce additional inaccuracy of the acceleration signals.

Displacement Records Displacement time history is recorded at the shaking table cylinder in one direction. To obtain physically realistic results, the offset must be calculated by equations 5.1 and 5.2.

5.4 Calculation of Numerical Results for Rocking Angle

The numerical rocking response is calculated by a MATLAB script written by advisor Jonas Bachmann. The script F could be explained by the simplified equation

$$\theta(t) = F[\ddot{u}_g(t), R, \alpha, \lambda, c] \tag{5.8}$$

where $\ddot{u}_g(t)$ is the acceleration time history, R is the semidiagonal of the prototype, α is the slenderness angle, λ is the inertia factor and c is the coefficient of restitution. The script gives

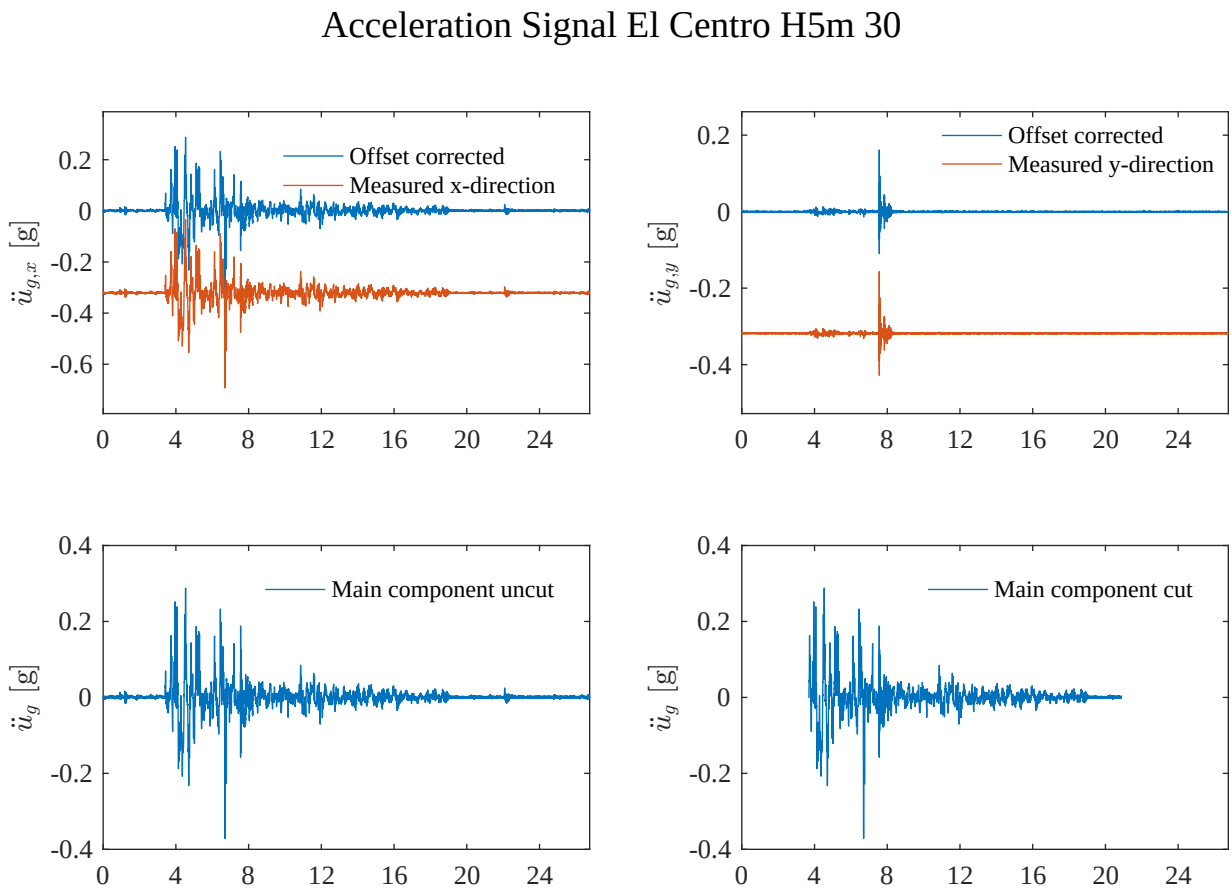

Figure 5.3: The offset corrected x- and y-components of the measured acceleration signal are used to calculate the main component of the accelerations. The main component signal is then cut to avoid disturbance and to facilitate post-processing. The spike of the y-signal after 8 seconds coincides with the time of overturning impact. This spike is not seen on y-signals from measurements where the block did not overturn.

the numerical solution to the nonlinear state space equations

$$\{y(t)\} = \begin{Bmatrix} \theta(t) \\ \dot{\theta}(t) \end{Bmatrix} \tag{5.9}$$

and

$$\boldsymbol{f}(t) = \{\dot{y}(t)\} = \begin{Bmatrix} \dot{\theta}(t) \\ -p^2 \left[\sin\left[\alpha \operatorname{sgn}\left[\theta(t)\right] - \theta(t)\right] + \frac{\ddot{u}_g(t)}{g} \cos\left[\alpha \operatorname{sgn}\left[\theta(t)\right] - \theta(t)\right] \right] \end{Bmatrix} \tag{5.10}$$

based on equation 2.6 where the frequency parameter $p = p(\lambda)$ is calculated by equation 2.9. t is the time vector discretized with time instants t_i.

Time Instant of Uplift The response calculation is started at the first time instant t_i where the uplift condition is met, i.e. $|\ddot{u}_g(t_i)| \geq g\tan(\alpha)$. Thereafter the time history response is calculated by a loop for every time instant $t_j > t_i$:

Loop Calculations and Checks

- Solve equations 5.9 and 5.10 according to the chosen tolerance limits.
- If overturn: $|\theta(t_j)| \geq 1.5\alpha \implies$ Calculation is stopped.
- If impact, decrease the angular velocity: $\theta(t_j) = 0 \implies \dot{\theta}(t_j) = \sqrt{c}\dot{\theta}(t_{j-1})$, where c is the coefficient of restitution given by either equation 2.12, $c = c_{\text{Housner}}(\lambda)$, or by experimental tests, $c = c_{\text{Exp}}$.
  - If $\dot{\theta}(t_j) \leq 0.0005$ rad/s $\implies$ The calculation is provisionally stopped for very small angular velocities, but it must be checked whether there exist later accelerations that fulfill the uplift criterion.
    - If $|\ddot{u}_g(t_k)| \geq g\tan(\alpha)$ for $k > j \implies$ Start new calculation from t_k.
- End loop and return $\theta(t)$.

Response to Different Accelerations and Coefficients of Restitution For each test result the rocking response is calculated with four different combinations of accelerations and coefficients of restitution:

- Measured accelerations, $\ddot{u}_{g,\text{meas}}$
  - Housner coefficient of restitution, c_{Housner}
  - Experimental coefficient of restitution, c_{Exp}

- Simulated accelerations, $\ddot{u}_{g,\text{sim}}$
  - Housner coefficient of restitution, c_{Housner}
  - Experimental coefficient of restitution, c_{Exp}

The goal of this project is to verify the response calculated with measured accelerations against the measured rocking response. The calculations based on simulated accelerations are included for comparison, see appendix B for figures.

Chapter 6

Statistical Analysis

6.1 Definitions

We define the statistical variable $\theta_{\max}$ as the maximum absolute rocking angle, where the values for overturning are set to 1.5α. The state of overturning is a discrete variable with only two outcomes: either the column overturns or it remains stable. The maximum absolute rocking angle, where there is no overturn, is a continuous variable that can attain all values in the interval $[0, 1.5\alpha)$. To analyze the continuous variable separately, we rather define the statistical variable

$$\beta_{\max} = \theta_{\max}, \quad \text{where} \quad \theta_{\max} < 1.5\alpha \tag{6.1}$$

which describes the maximum rocking angle for those tests that did not overturn.

Definitions The statistical measures that are applied in this project are defined as:

P(OT) Probability of overturning, $P(\theta_{\max} \geq 1.5\alpha)$. Percentage of the values that equals 1.5α.

n Number of $\beta_{\max}$-values, which the following statistical measures are based on. P(OT) = $1 - \frac{n}{N}$ when there are N $\theta_{\max}$-values.

Mean Mean μ of the $\beta_{\max}$-values. The mean is affected by extreme values of the sample.

Min The minimum value of $\beta_{\max}$, which equals the miniumum of $\theta_{\max}$.

Q(p) The p-percentile value of the $\beta_{\max}$-values.

Q25 The 25-percentile (or first quartile) value of the $\beta_{\max}$-values. 25 % of the values in the sample are equal to or lower than Q25.

Q50 The median, 50-percentile (or second quartile) value of the $\beta_{\max}$-values. 50 % of the values in the sample are equal to or lower than Q50. The median is not affected by

extreme values in the sample.

Q75 The 75-percentile (or third quartile) value of the $\beta_{\max}$-values. 75 % of the values in the sample are equal to or lower than Q75.

Max The maximum value of the $\beta_{\max}$-values.

IQR IQR = Q75-Q25. The interquartile range of the $\beta_{\max}$-values, which is a measure of statistical dispersion that is not affected by extreme values in the sample.

Conservative Prediction The numeric model is considered to produce conservative predictions

- where the predicted probability of overturning is *larger* than that of the laboratory results.
- where the predicted minimum, quartile, mean or maximum values are *larger* than those of the laboratory results.
- where the predicted CDF-graph of $\beta_{\max}/\alpha$ exists lower than or left of the CDF-graph of the laboratory results.

Where the opposite is true, we have non-conservative predictions. In table 8.1, 8.2 and 8.3 conservative nominal errors are positive and non-conservative values are negative.

6.2 Box Plots

A sample of values could conveniently be visualized by box-and-whisker-plots, henceforth called box plots. The boundaries of the plot is determined by quartile values as defined above, and the spacing between the boundaries indicates the degree of dispersion and skewness of data. An explanatory diagram of a box plot is shown in figure 6.1.

The limits for the upper w_u and lower whisker w_l are defined as

$$w_u = Q75 + 1.5(Q75 - Q25) = Q75 + 1.5IQR$$
$$w_l = Q25 - 1.5(Q75 - Q25) = Q25 - 1.5IQR$$

and outliers are points that have values outside the whisker limits. The whiskers are plotted at the lower and the higher value within the limits for the lower and upper whisker respectively. If and only if the the tested sample follow a normal distribution, it is expected that about 0.7 % of the values are outliers. Many outliers in a sample might be a sign of measure-

ment errors, systematic failures or that the theoretical model is not valid in this area. Outliers might also be a sign of values from another population or of an unsymmetrical distribution.

The box height indicates the size of the interquartile range (IQR), which includes the mid-50-percentage of the values. The mean is sensitive to outliers, whereas the median, Q50, denotes the middle value of the sorted values. Thus the median is a more robust estimator of the central tendency of the sample in question.

6.3 Cumulative Distribution Function Plots

A cumulative distribution function (CDF) $F_X(x)$ determines the probability that the underlying random variable X attains values lower than or equal to x:

$$F_X(x) = P(X \leq x) \tag{6.2}$$

The CDF attains probability values between 0 and 1 and is a continuous, non-decreasing function of x. The empirical CDF of the underlying random variable X could be calculated and plotted based on n measurements. The empirical function is a non-decreasing step function that increases with $1/n$ for each of the ordered values, and converges to the underlying CDF by increased number of measurements n if the samples represent the same distribution as X.

Different Interpretation of $\beta_{\max}/\alpha$ and $\theta_{\max}/\alpha$ The empirical CDF of $\beta_{\max}/\alpha$ and $\theta_{\max}/\alpha$ must be interpreted differently. They are equal only if $n = N$, i.e. if there are no overturns in the sample. The empirical CDFs of $\beta_{\max}/\alpha$ are related to the minimum, maximum and quartile values as defined above and based on the number of measurements given by n. Probability values related to this CDF are calculated on the subset $\beta_{\max}/\alpha$. The higher the n, the finer is the graph. The graph reaches a probability of 1 for the largest value of $\beta_{\max}/\alpha$. The percentile values Q(p) are related to the CDF as

$$F_X\big(Q(p)\big) = P\big(X \leq Q(p)\big) = p\,\% \tag{6.3}$$

To obtain real probability values for the whole sample, the percentage must be scaled. For a set of totally N $\theta_{\max}/\alpha$-values, and a subset of n $\beta_{\max}/\alpha$-values, we have the following

relations

$$\begin{aligned} P(\beta_{\max}/\alpha \leq Q(p)) &= p\,\% \\ P(\theta_{\max}/\alpha \leq Q(p)) &= p \cdot \frac{n}{N}\,\% \end{aligned} \tag{6.4}$$

The percentile values for the whole set consisting of N values, can not be calculated implicitly by the percentile values of the subset. They must be calculated on the whole set including overturn values.

The empirical CDFs of $\theta_{\max}/\alpha$ are calculated based on all $N = 100$ maximum values. Nevertheless, the values associated with overturning are all set to the same value, 1.5α, so the the step-line is as coarse as that of $\beta_{\max}/\alpha$. The probability value of the horizontal line between $\theta_{\max}/\alpha \approx 1$ and $\theta_{\max}/\alpha < 1.5$ equals the probability of *not* overturning, $\mathrm{P}(\overline{\mathrm{OT}})$, i.e. probability of sustained rocking. The value for probability of overturning presented in table 8.2, is given as $\mathrm{P(OT)} = 1 - \mathrm{P}(\overline{\mathrm{OT}})$. The graph reaches a probability of 1 for $\theta_{\max}/\alpha = 1.5$ if there are overturn in the sample. The derivative of the CDF is the probability density function. Thus the slope is a measure of probability density. A gentle slope means low density, while a steep slope means high density.

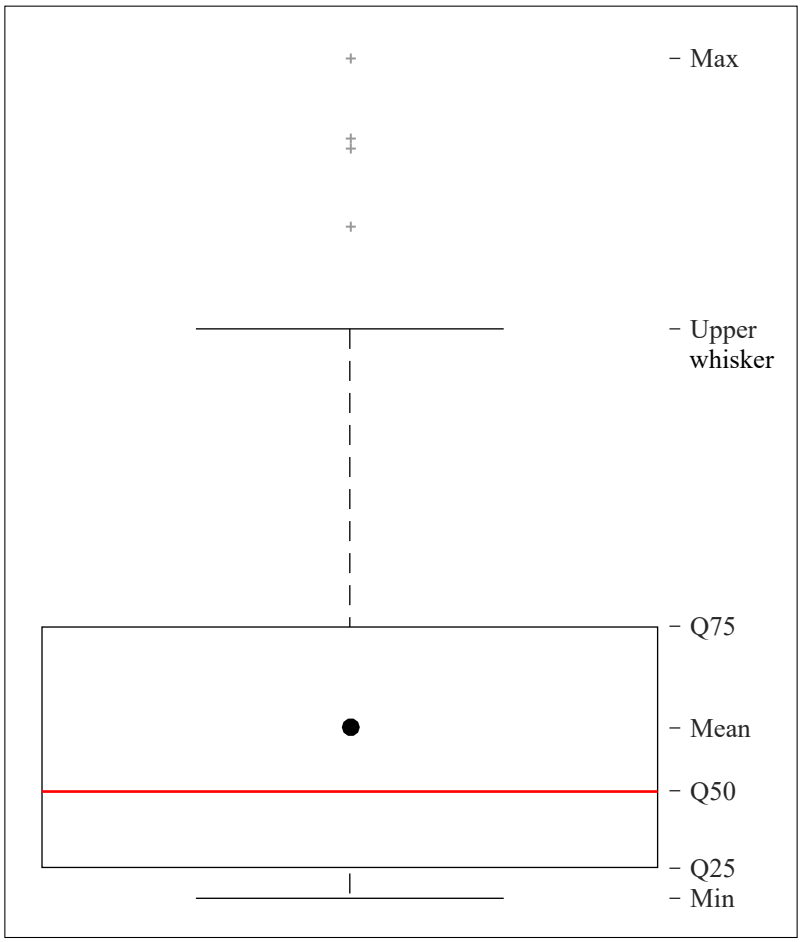

Figure 6.1: Box plot of $\beta_{\max}/\alpha$ with explanations. Grey +-signs are outliers. The underlying values are equal for figure 6.2.

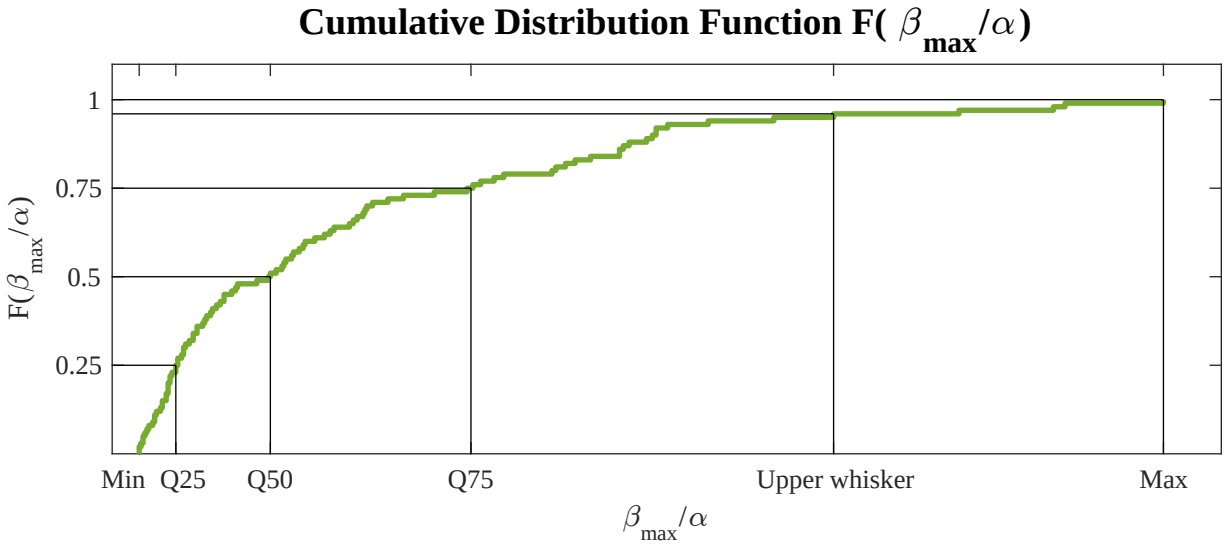

Figure 6.2: CDF plot with explanations. Example for Q75: there is a probability of 75 % that the values in the sample are lower than Q75. Min and lower whisker are here the same value. The interquartile range is IQR = Q75-Q25. The underlying values are equal for figure 6.1. The steep slope for the values below Q50 means that there is a high density of values in this interval. The gentle slope for values larger than Q75 means that there is a low density of values in this interval.

Part III

Results

Chapter 7

Similar Statistical Properties of Measured Ground Motions

A main assumption of this project is that the rigid rocking oscillator is subjected to an ensemble of ground motion accelerations that share similar statistical properties. By generation of the artificial ground motions, as described in section 3.1, the ensemble has same properties in time and frequency domain. The shaking table is not able to reproduce the ground motions perfectly. To verify that also the measured accelerations has similar statistical properties, we study the energy distribution and the elastic response spectra of accelerations.

7.1 Measured Accelerations and Energy Distribution

The measured accelerations that are used as input for the numerical rocking response model, is in general not expected to be the same as those used as input for the shaking table. The shaking table behaves like an unknown transfer function that takes integrated displacement signals as input and produces a transformed output ground motion. This continuous ground motion of the shaking table is measured by accelerometers and discretized with a given sampling rate. Then the accelerations are post processed as described in section 5.3. The goal in this project is to explore the response of a rocking oscillator to an ensemble of ground motions with same statistical properties. To substantiate this in time domain, we compare the energy distribution of the post processed measured accelerations.

As seen in figure 7.1 to 7.7 the 100 measured accelerations in each ensemble are plotted together with the cumulative distribution of energy calculated as in equation 3.1. The time

measures for reaching a certain percentage of the cumulative energy (or Arias intensity) are calculated based on the mean of all energy distributions within the ensemble and showed in the energy distribution plots and in table 7.1. The time measures are calculated on the prototype scaled and cut accelerations. For comparison in the table, the time measure is upscaled to the original, unscaled length and an offset is added such that the t_5-values are equal to the mean of simulations value.

From table 7.1 it is observed that there is a clear correlation between the time measures of the measured accelerations and the simulated accelerations. The largest difference is observed on the t_{95}-values, and El Centro have in general more similar values than Lefkada.

From figures 7.1 to 7.7 it is seen that there is a clear correlation between shapes of the energy distribution curves within each ensemble. For six of the ensembles there are one or two obvious outliers with higher values on the y-axis, but nevertheless the shape of these curves are similar to the other curves. Such outlier curves are also observed for the original simulations as seen in figure 3.4 and 3.9.

Conclusion There is an apparent correlation between the distribution of energy in time domain within each ensemble of measured accelerations. These distributions are comparable to the distributions of the simulations that were used as input for the shaking table. We conclude that the measured accelerations within each ensemble have similar statistical properties in time domain.

Table 7.1: The time t_n for reaching n % of the Arias intensity is calculated for the mean of each ensemble. Each time measure is upscaled to original length by $\sqrt{\frac{H_{\text{prototype}}}{H_{\text{experimental}}}}$ for comparison with the measures for the mean of the simulations and the original targeted signal. Due to that the measured accelerations are cut, an offset is added such that the t_5-values are equal. The total duration of the original signals are 50 s for El Centro and 47 s for Lefkada. The time measures are well fitted.

		Offset [s]	t_5 [s]	t_{45} [s]	t_{75} [s]	t_{95} [s]	t_{5-95} [s]
El Centro	Original	-	1.5	4.4	11.7	25.6	24.1
	Simulations	-	1.2	4.4	12.0	25.7	24.5
	H5m M1 measured	0.59	1.2	4.0	10.9	25.7	24.5
	H5m M2 measured	0.75	1.2	4.2	11.0	26.1	24.9
	H10m measured	0.70	1.2	3.9	10.0	25.4	24.2
	H20 measured	1.00	1.2	3.7	10.0	26.0	24.8

Lefkada	Original	-	1.7	5.2	7.2	12.3	10.6
	Simulations	-	1.7	5.1	7.0	12.2	10.5
	H5m measured	1.15	1.7	5.4	7.8	13.5	11.8
	H10m measured	1.22	1.7	5.3	7.1	12.1	10.4
	H20m measured	1.30	1.7	5.2	6.9	10.8	9.1

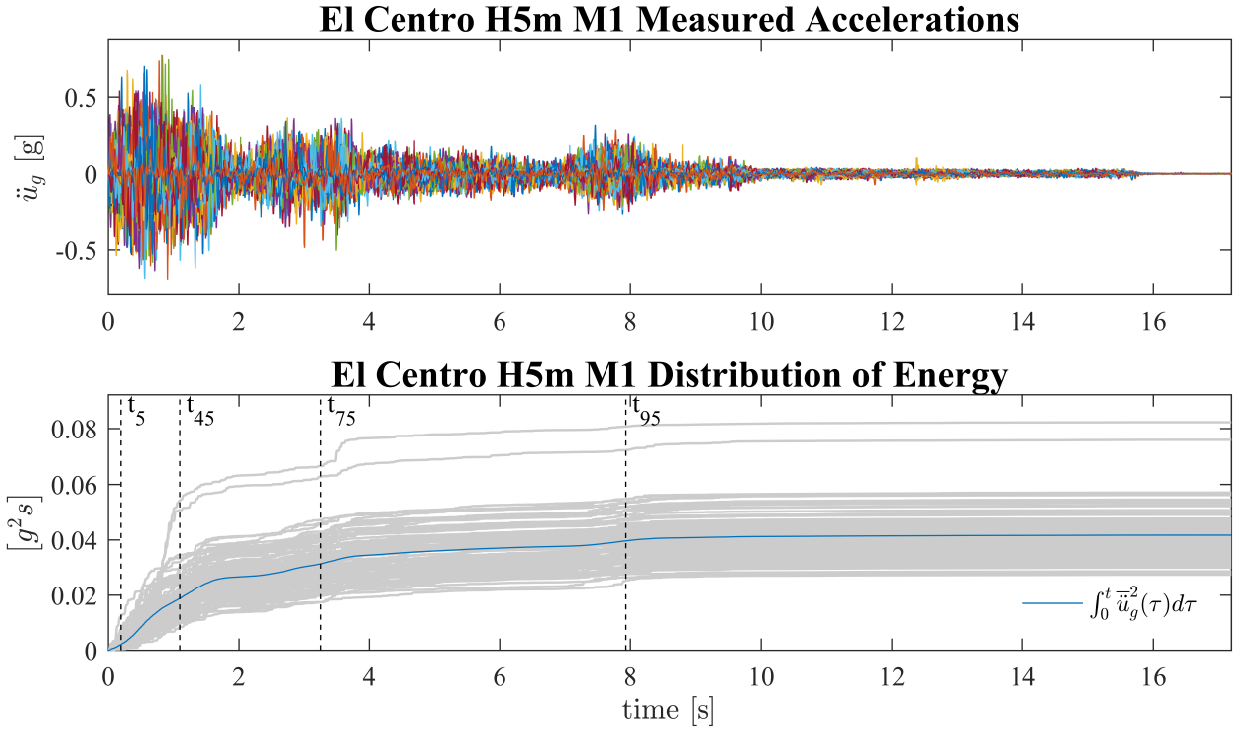

Figure 7.1: Accelerations and distribution of energy for El Centro H5m M1.

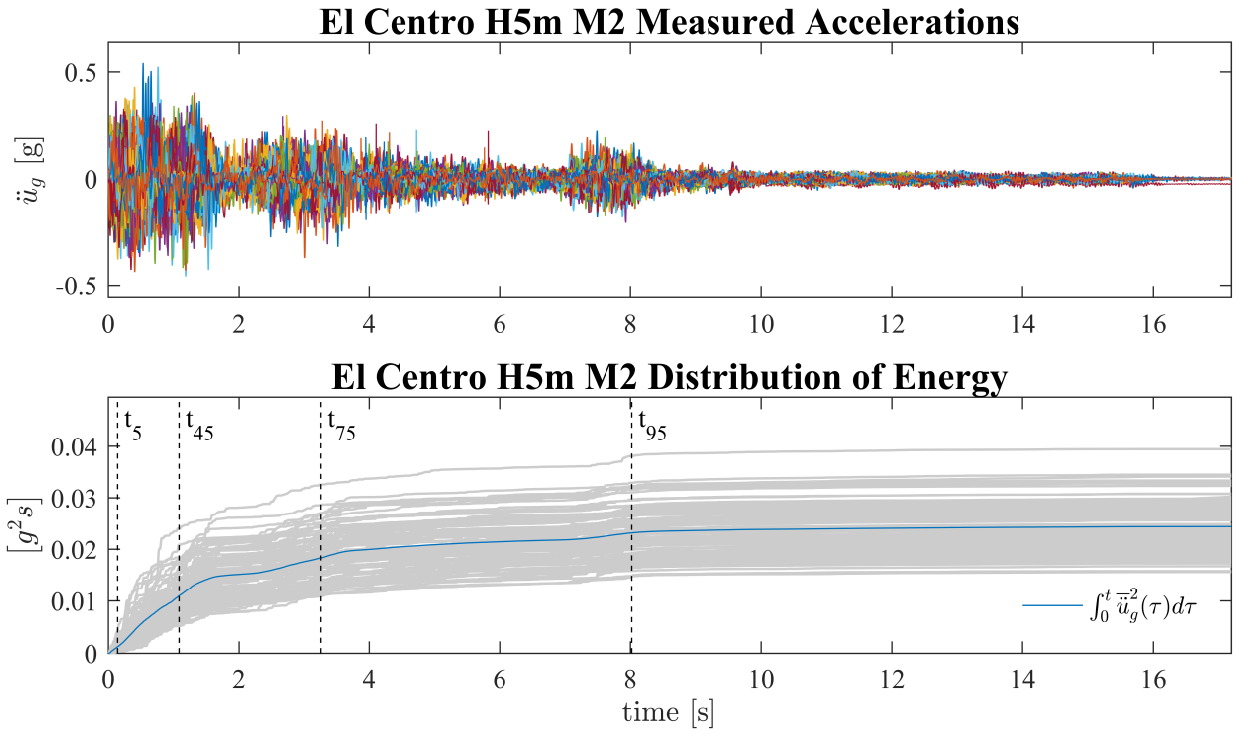

Figure 7.2: Accelerations and distribution of energy for El Centro H5m M2.

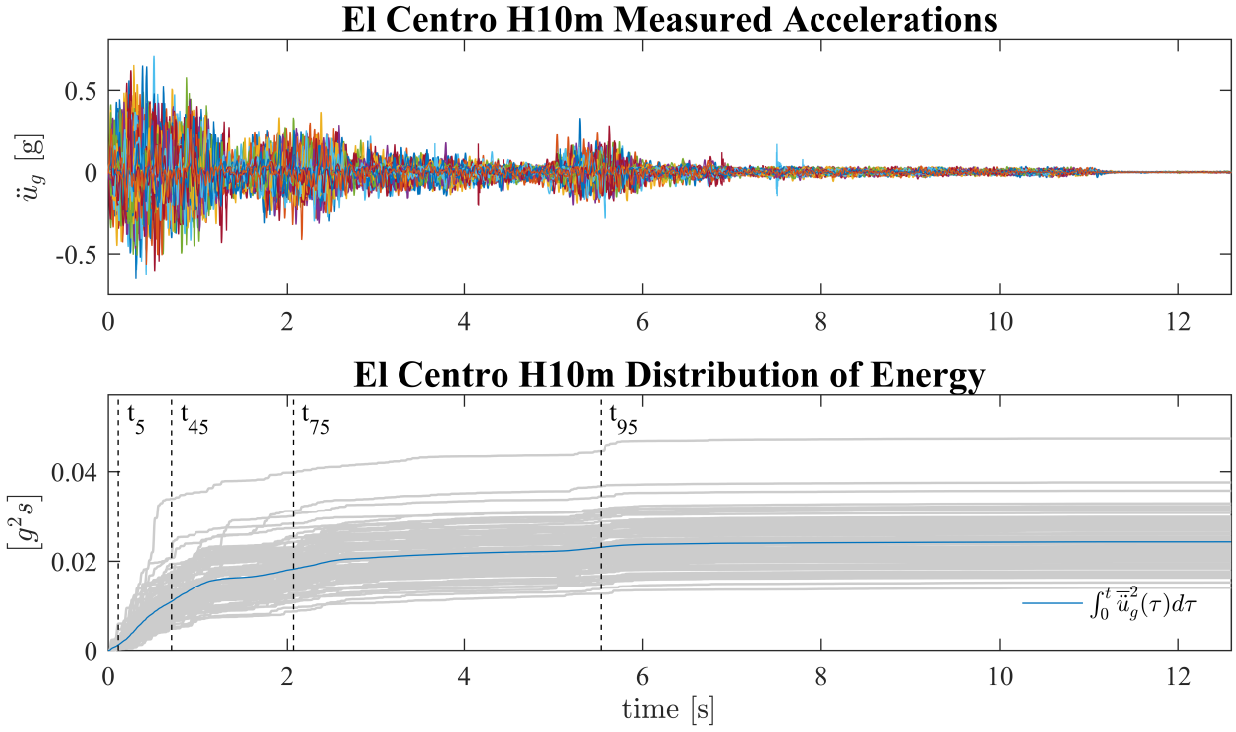

Figure 7.3: Accelerations and distribution of energy for El Centro H10m.

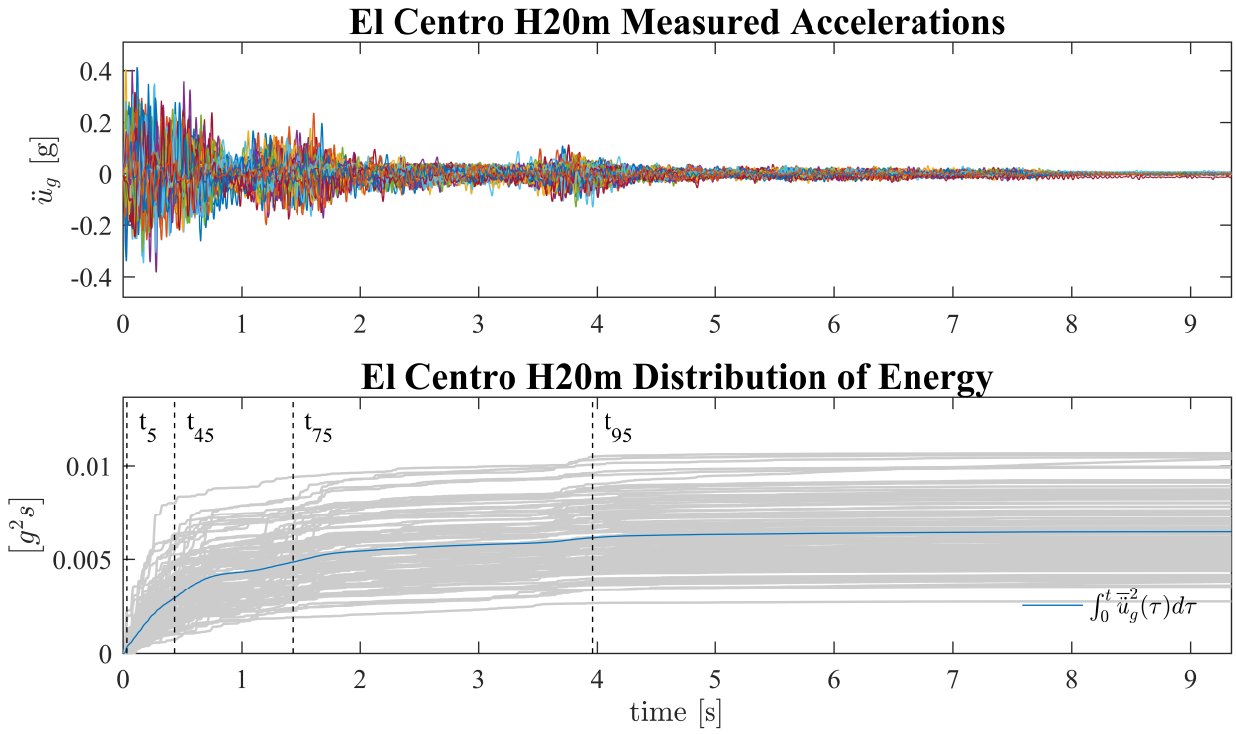

Figure 7.4: Accelerations and distribution of energy for El Centro H20m.

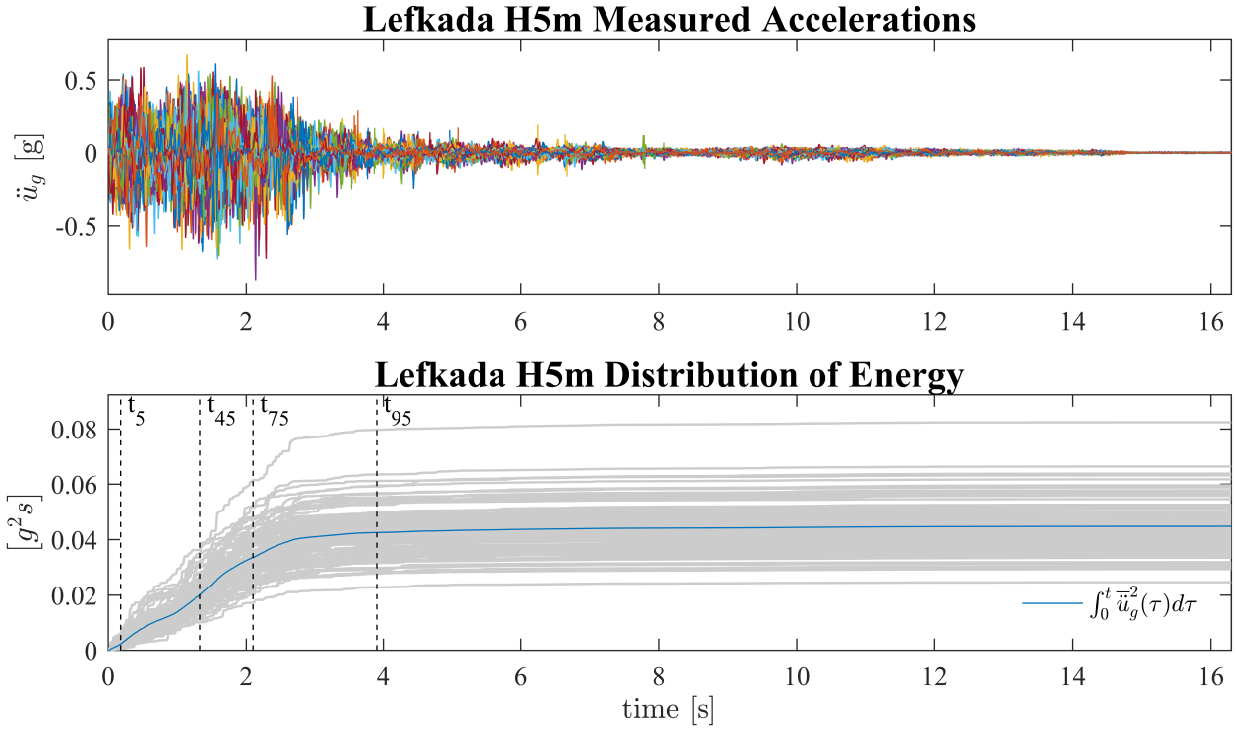

Figure 7.5: Accelerations and distribution of energy for Lefkada H5m.

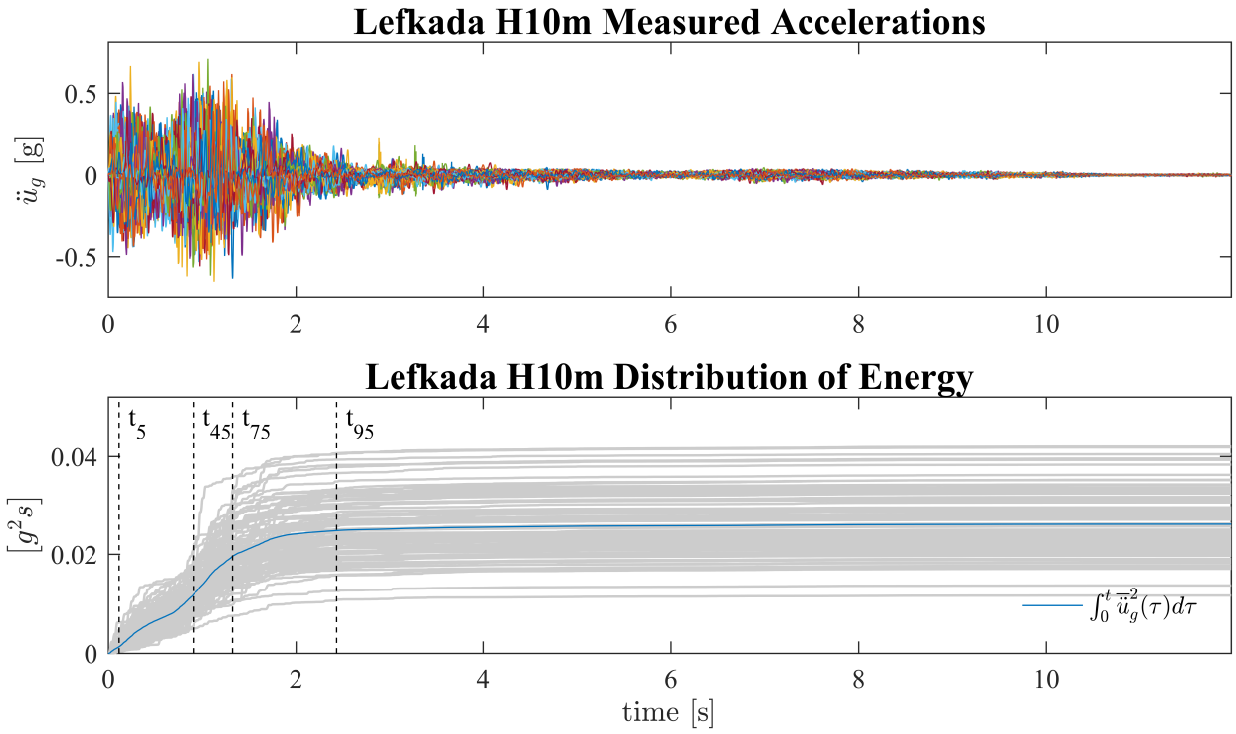

Figure 7.6: Accelerations and distribution of energy for Lefkada H10m.

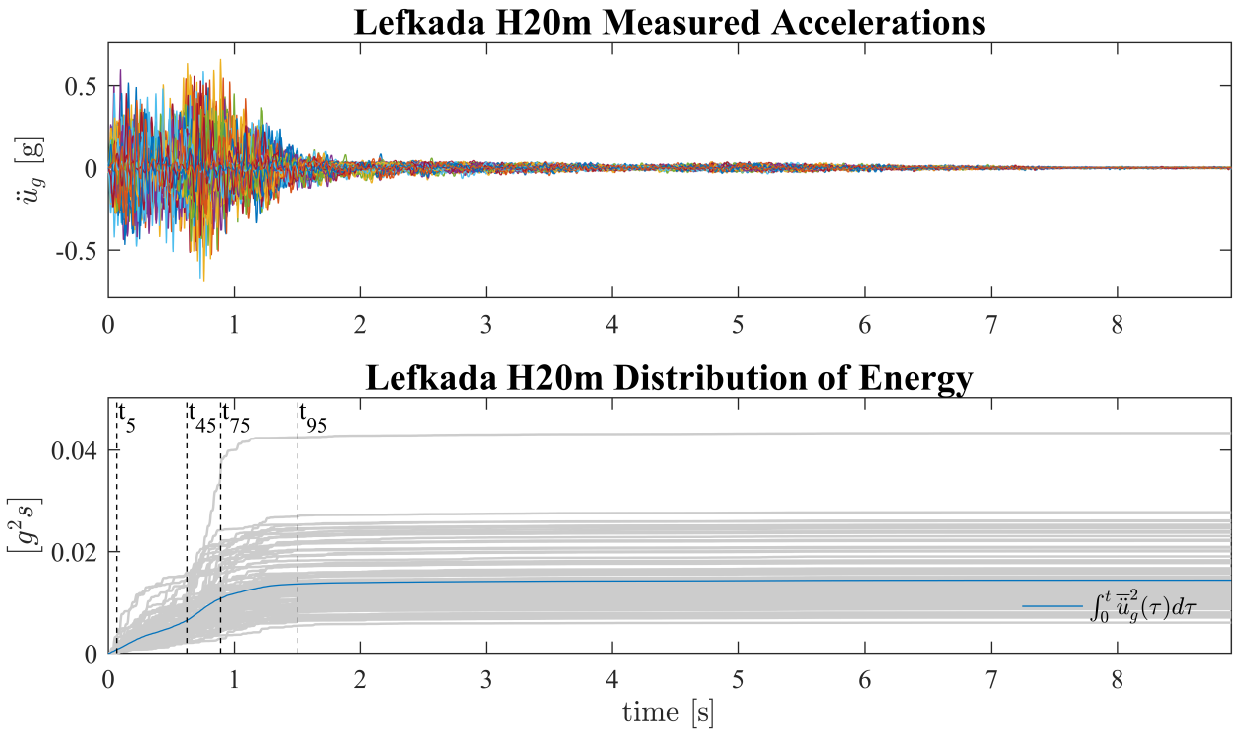

Figure 7.7: Accelerations and distribution of energy for Lefkada H20m.

7.2 Elastic Response Spectra of Accelerations

The elastic response spectra are calculated based on measured $\ddot{u}_{g,\text{meas}}$ and simulated accelerations $\ddot{u}_{g,\text{sim}}$. The spectra describes how the maximum amplification of a single degree of freedom system responds to different natural periods. A response specter is a means to compare the frequency content of the ensemble of accelerations to each other.

The natural vibration period T_s of the single degree of freedom system that is chosen, varies from $T_{s,0} = 0.01$ s to $T_{s,max} = 3.0$ s with a period time step $dTs = 0.01$ s. The damping coefficient is chosen as $\zeta = 0.02$. The time history response $\ddot{u}(t, T_s, \zeta)$ of the system to the ground motion acceleration $\ddot{u}_g(t)$ is calculated by Newmark's noniterative formulation as described in Chopra [4] section 5.4.3. The following plots show the maximum absolute value $\ddot{u}_{t,\max}(T_s, \zeta)$ of the total acceleration response $\ddot{u}_t(t, T_s, \zeta)$ for each natural vibration period T_s.

$$\begin{aligned} \ddot{u}_t(t, T_s, \zeta) &= \ddot{u}(t, T_s, \zeta) + \ddot{u}_g(t) \\ \ddot{u}_{t,\max}(T_s, \zeta) &= \max|\ddot{u}_t(t, T_s, \zeta)| \end{aligned} \tag{7.1}$$

Description of Plots In the following seven figures the elastic response spectra are shown to logarithmic scale. In the lower left corner the black spectra are based on 100 simulated accelerations. In the right corner the black spectra are based on measured accelerations. The original specter denotes the response specter of the target ground motion that the simulations are generated from. This blue line is equal in all three subplots in each figure. The mean of the 100 spectra is shown as an orange line for both simulated and measured accelerations. These means are compared with the original specter in the top subplot. All accelerations are to the same time scale for each figure. For El Centro and Lefkada H10m, figure 7.10 and 7.13, the spectra of those measured accelerations that led to overturning in the laboratory, are colored yellow. There is no apparent difference between the spectra of those who led to overturning and those who did not.

Different Tuning of Shaking Table In figure 7.8 and 7.9 the response spectra of El Centro H5m M1 and M2 are shown. The spectra of the simulated accelerations are equal in both figures, but the measured accelerations are different due to different tunings of the shaking table. Thus the spectra of the measured accelerations are different for M1 and M2 as well. For M1 the peak of the measured is considerably larger than the peak of the simulated. For M2 there is no significant difference in peak value. Moreover, when we consider all seven

elastic spectra, we observe that El Centro H5m M1 and El Centro H10m are the only spectra where there is a significant difference in peak heights. For the other five spectra based on accelerations with tuning and model 2, the peak heights of simulated and measured are quite equal.

Difference of Spectra based on Simulated and Measured Accelerations Consider the simulated acceleration spectra of El Centro H5m M1 in figure 7.8. The 100 simulated spectra envelopes the original specter for 0.01 s $< T_s <$ 0.40 s and show a low, broad peak of 1.071g for 0.12 s $< T_s <$ 0.15 s . The mean resembles a smoothed version of the original specter. For $T_s <$ 1.0 s the original specter has values lower than most of the simulations, meaning that the simulations overestimates the response for this interval of natural periods.

Consider now the measured acceleration spectra. The mean of the 100 measured spectra show a distinct, narrow peak of 1.7g for $T_s = 0.05$ s. For $T_s > 0.6$ s the mean of the simulated and measured spectra are almost equal. Also the measured specter of M2 in figure 7.9 shows a peak for the mean $T_s = 0.05$ s, but the peak value is reduced to 1.007g. All the seven spectra based on measured accelerations show a distinct peak for $T_s = 0.05$ s or $T_s = 0.06$ s. Consequently the accelerations that the shaking table generates based on the simulated accelerations, have a significant frequency content in this region of natural periods.

The spectra of the other ground motions are shown in figure 7.10 to 7.14, and they show similar properties as for El Centro H5m. The time scales are different, thus the peak period of the simulated and original spectra are shifted, but the peak period for the measured spectra remain constant. The spectra of the 100 measured accelerations do not necessarily envelope the original specter, as most of the simulation spectra do.

Similarities Between Spectra Within Ensemble Based on the seven figures of elastic spectra it is evident that the shaking table is not able to reproduce the exact same accelerations that are used as input. Moreover the frequency content has a more narrow peak, and the peak natural period is between 0.05 s and 0.06 s for all prototype scales. Nevertheless, there is an apparent correlation between the 100 spectra within each ensemble of accelerations. In fact the measured spectra have in most cases a smaller dispersion than the simulated spectra. It is also observed that the accelerations that lead to overturning, do not have significantly different response spectra. In general it seems that the elastic response spectra within each ensemble of measured accelerations has similar properties, and thus that each

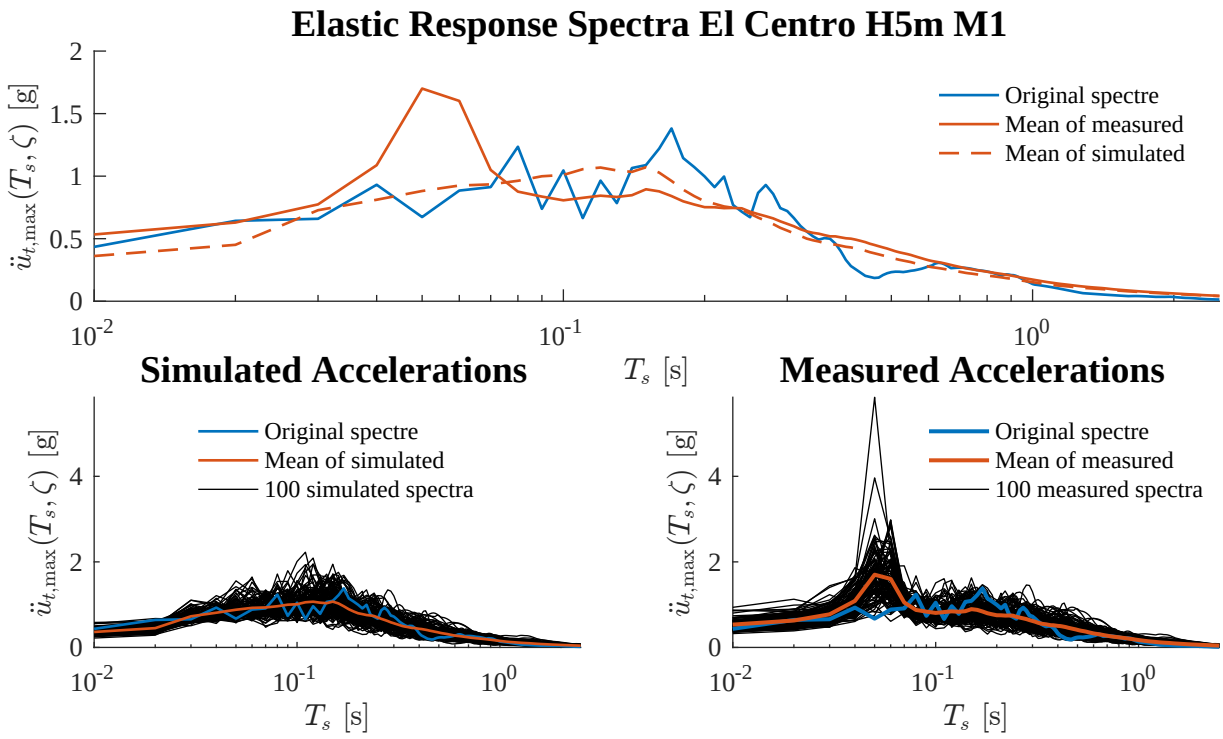

Figure 7.8: Elastic spectra El Centro H5m M1. Mean of measured: peak of 1.7g for $T_s = 0.05$ s. Mean of simulated: peak of 1.071g for $T_s = 0.15$ s. Notice the difference in peak height for the spectra based in simulated and measured accelerations, this difference is caused by Tuning 1.

ensemble has similar statistical properties in frequency domain.

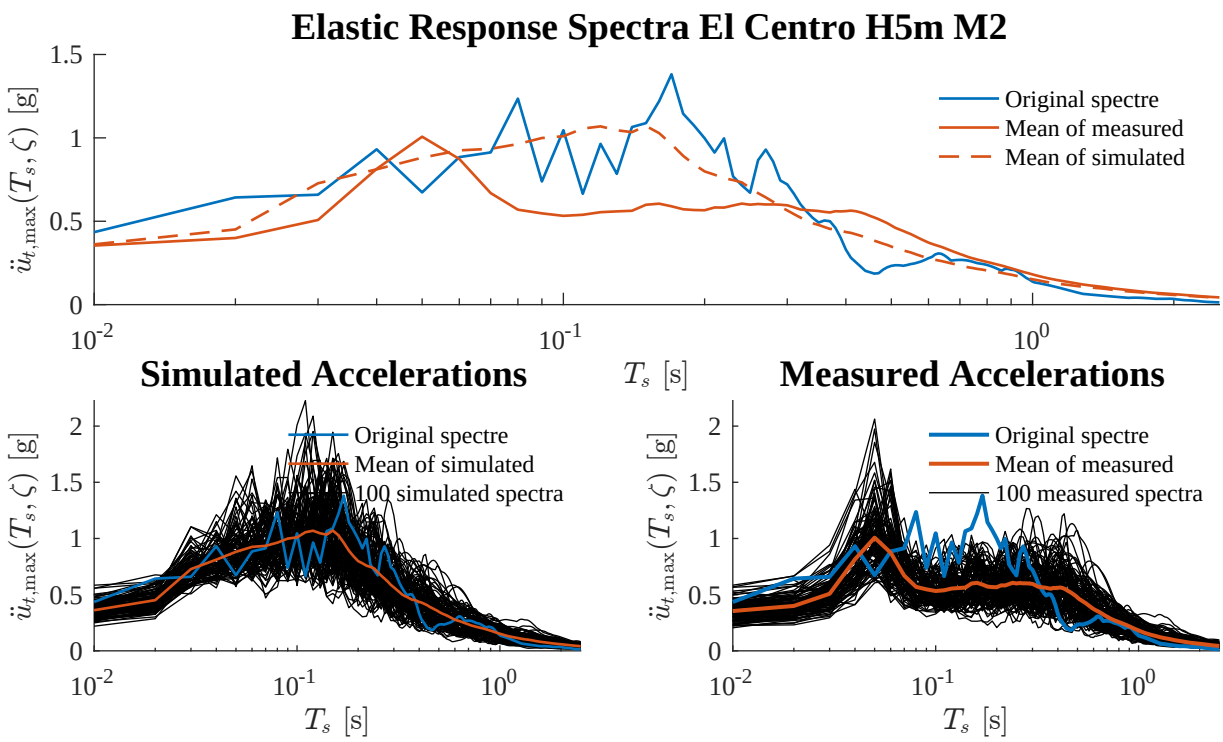

Figure 7.9: Elastic spectra El Centro H5m M2. Mean of measured: peak of 1.007g for T_s = 0.05 s. Mean of simulated: peak of 1.071g for T_s = 0.15 s.

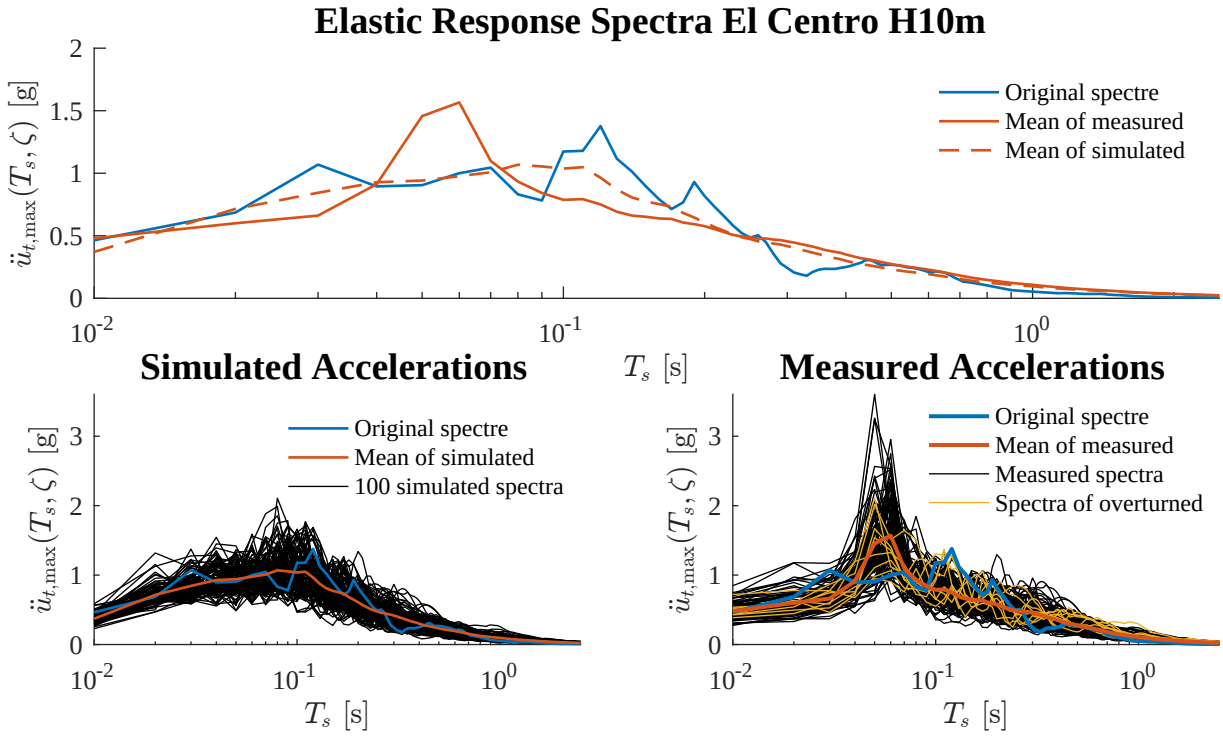

Figure 7.10: Elastic spectra El Centro H10m. Mean of measured: peak of 1.566g for T_s = 0.06 s. Mean of simulated: peak of 1.068g for T_s = 0.08 s. Notice the difference in peak height for the spectra based in simulated and measured accelerations, this difference is caused by Tuning 1.

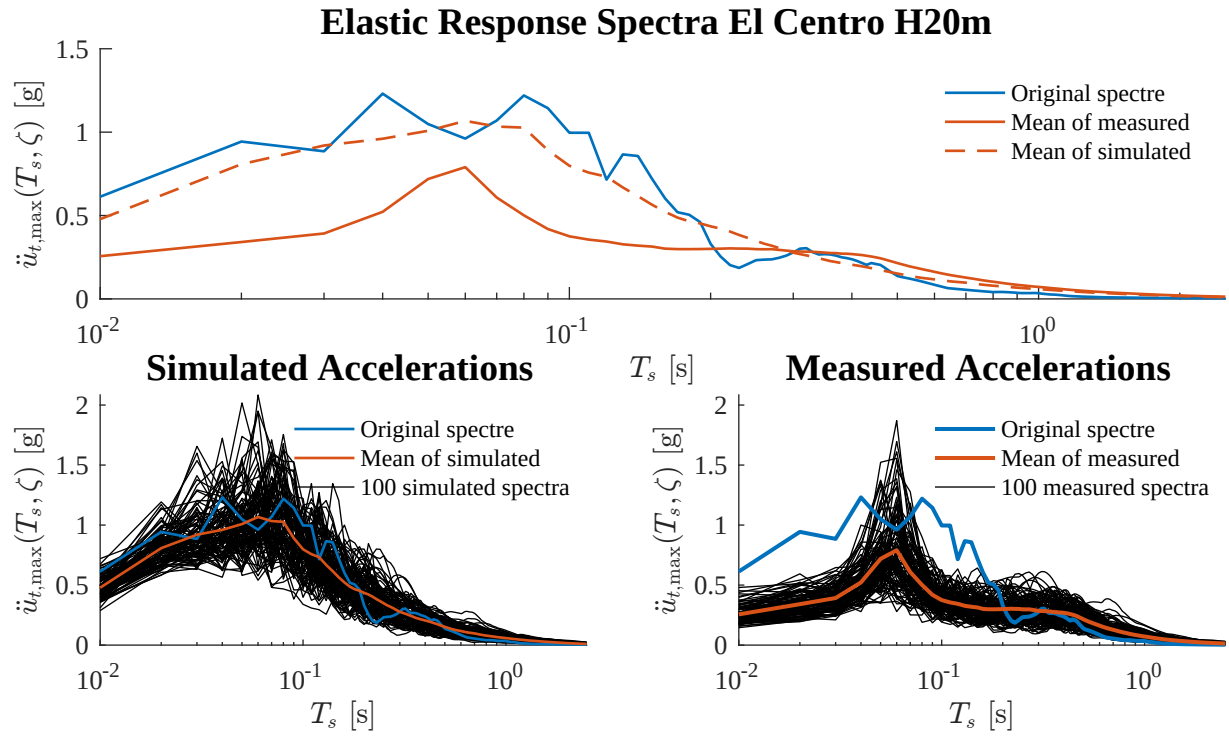

Figure 7.11: Elastic spectra El Centro H20m. Mean of measured: peak of 0.79g for $T_s = 0.06$ s. Mean of simulated: peak of 1.068g for $T_s = 0.06$ s.

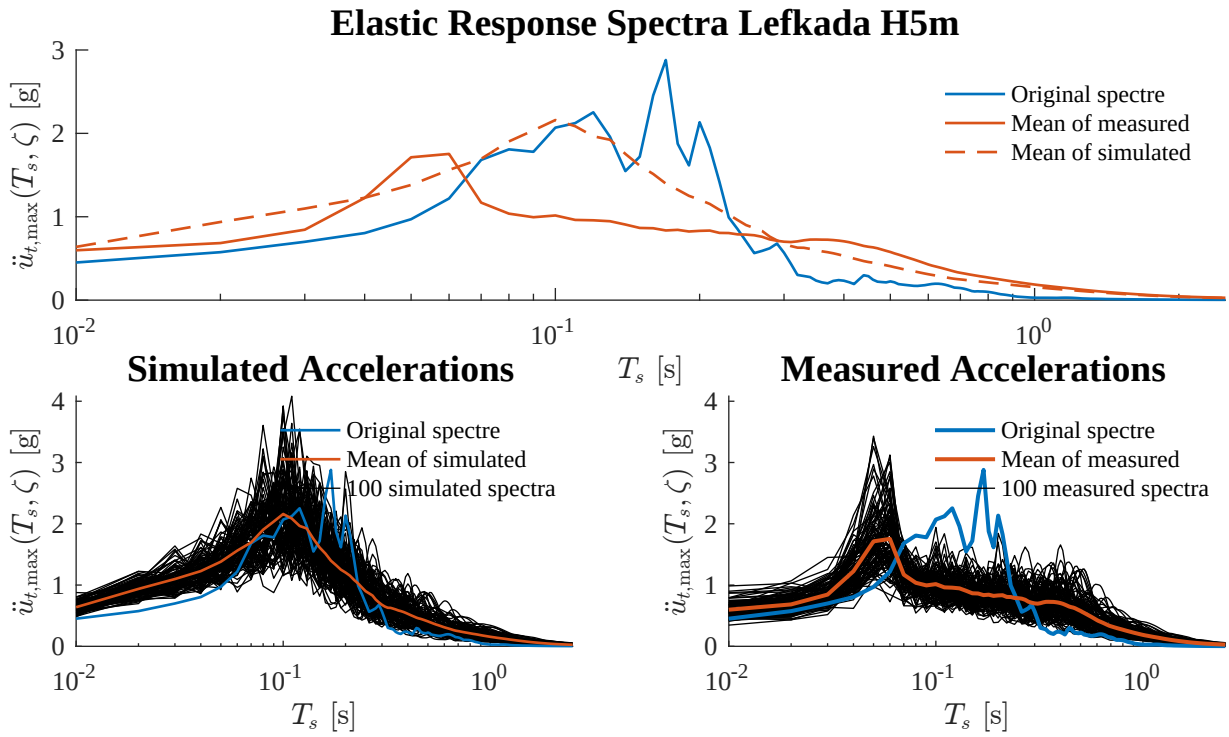

Figure 7.12: Elastic spectra Lefkada H5m. Mean of measured: peak of 1.754g for $T_s = 0.06$ s. Mean of simulated: peak of 2.16g for $T_s = 0.10$ s.

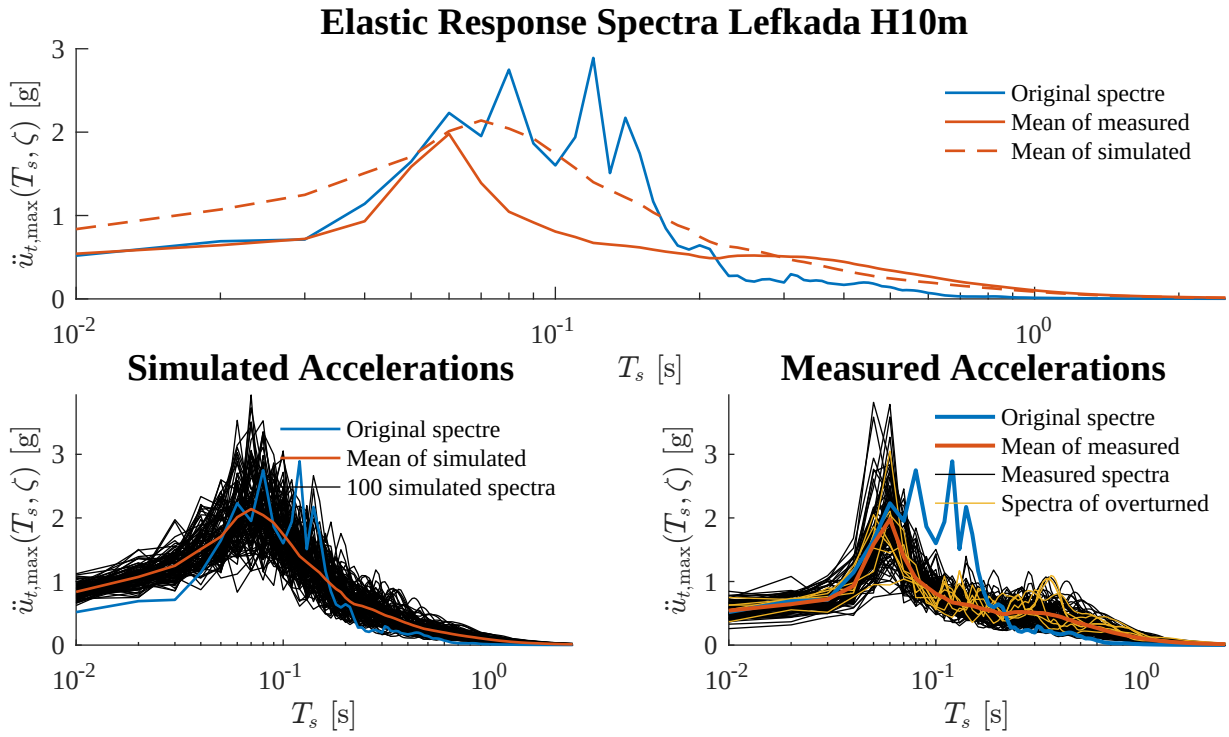

Figure 7.13: Elastic spectra Lefkada H10m. Mean of measured: peak of 1.979g for $T_s = 0.06$ s. Mean of simulated: peak of 2.14g for $T_s = 0.07$ s.

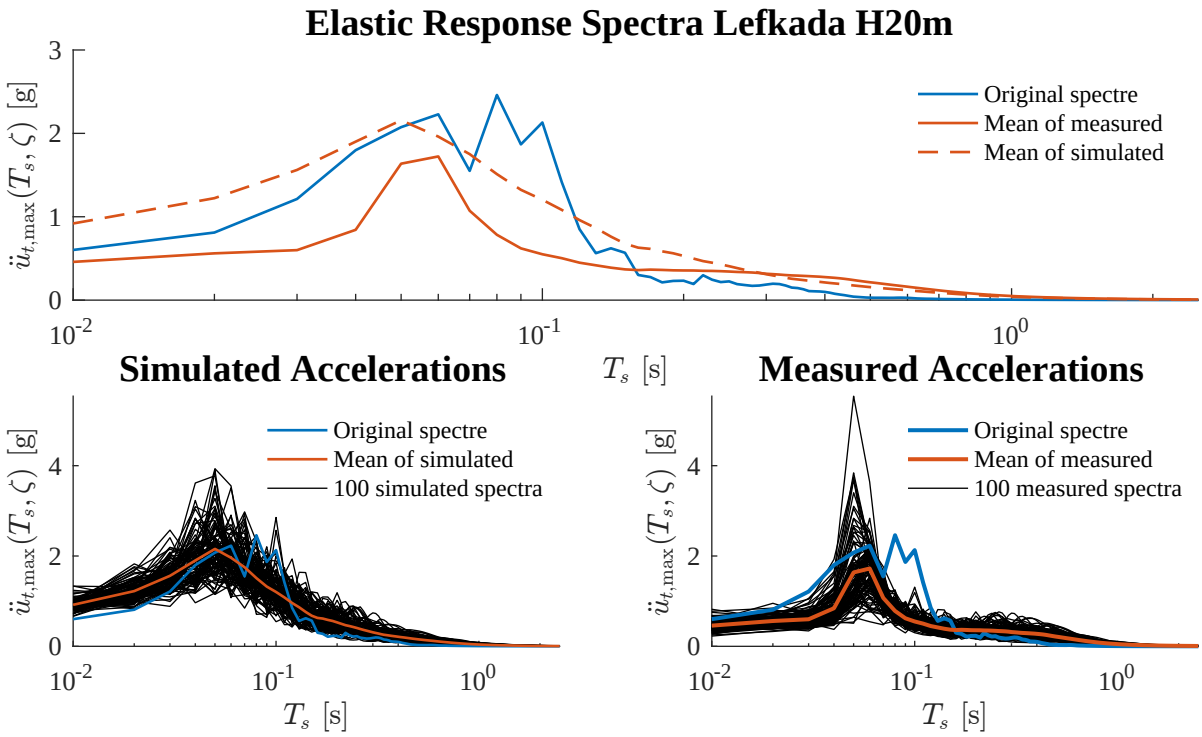

Figure 7.14: Elastic spectra Lefkada H20m. Mean of measured: peak of 1.723g for $T_s = 0.06$ s. Mean of simulated: peak of 2.157g for $T_s = 0.05$ s.

Chapter 8

Laboratory Response Compared to Numerical Response

The results are represented by the statistical measures explained in chapter 6. These values are best interpreted visually by box plots and CDF plots as described in section 6.2 and 6.3. All box plots are shown together in appendix A. The underlying numbers are presented in tables at the end of this chapter. Table 8.1 show the minimum, maximum and quartile values of the response that did not overturn. Also the nominal and relative error are calculated. Table 8.2 presents the probability of overturning and its errors based on different offset methods. Table 8.3 compare mean and median values and their errors based on different offset methods.

8.1 All Ensembles

The empirical CDF of $\beta_{\max}/\alpha$ and $\theta_{\max}/\alpha$ are plotted in figures 8.1 and 8.2 for El Centro and Lefkada respectively. Notice the different interpretation of these plots as explained in section 6.3.

There is a clear correlation between the distributions of the predicted results and the laboratory results. For all ensembles the slope of the curves change similarly for the green laboratory lines and for the red and blue predicted lines, based on c_{Housner} and c_{Exp} respectively. For most of the interval the curves lie close to each other, thus having close percentile values. On the CDF plots including overturn values for both El Centro and Lefkada, there are notable discrepancies on the overturning values for H5m. The red line of c_{Housner}, which are

calculated with most damping, i.e. lowest coefficient of restitution, are lower for El Centro and higher for Lefkada. The overturning lines for H10m are closer to each other, but here the opposite trend is seen on the red lines. It is higher for El Centro and lower for Lefkada.

Plots of $\theta_{\max}$ Compared To $\beta_{\max}$

For H5m for both ground motions between 34 % and 49 % of the tests overturn, so the graph of $\beta_{\max}$ is substantially shifted upwards compared to that of $\theta_{\max}$. For El Centro H5m M2 the response with c_{Housner} has P(OT) = 45.0 %. By comparing graph (a) and (b) of figure 8.1, the red line is shifted upwards in (a), the larger the $\beta_{\max}/\alpha$-value, the larger is the shift. The discrepancy between the three lines for $\theta_{\max} > 0.6\alpha$ in (b) is noticeably reduced in (a). Also for Lefkada H5m in figure 8.2 (a) and (b) similar observations can be made, and the discrepancy for $\theta_{\max} > 0.6\alpha$ is reduced here as well. The increasing discrepancy between the lines for the graphs in (b) comes as a result of the difference in probability of overturning for the three different lines.

For H20m for both ground motions there are no overturns, so $\beta_{\max} = \theta_{\max}$, and the graphs are equal. For H10m between 5 % and 9 % of the tests overturn, so the graph of $\beta_{\max}$ is slightly shifted upwards compared to that of $\theta_{\max}$. We can draw the same conclusions for H10m as for H5m regarding decreased discrepancy between the lines for high values.

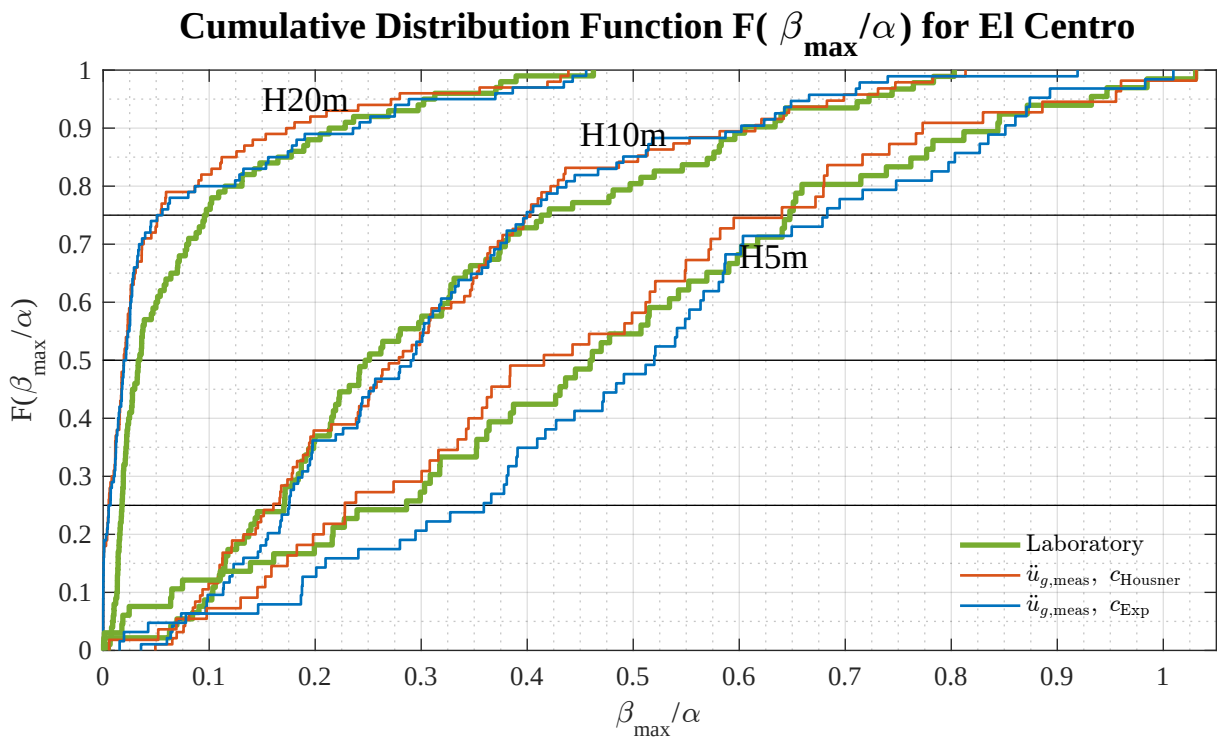

(a) Empirical CDF of maximum rocking angle β_{max}/α *excluding* the overturn values. The graph is comparable to statistical measures in table 8.1 and to the associated box plots in figure A.1.

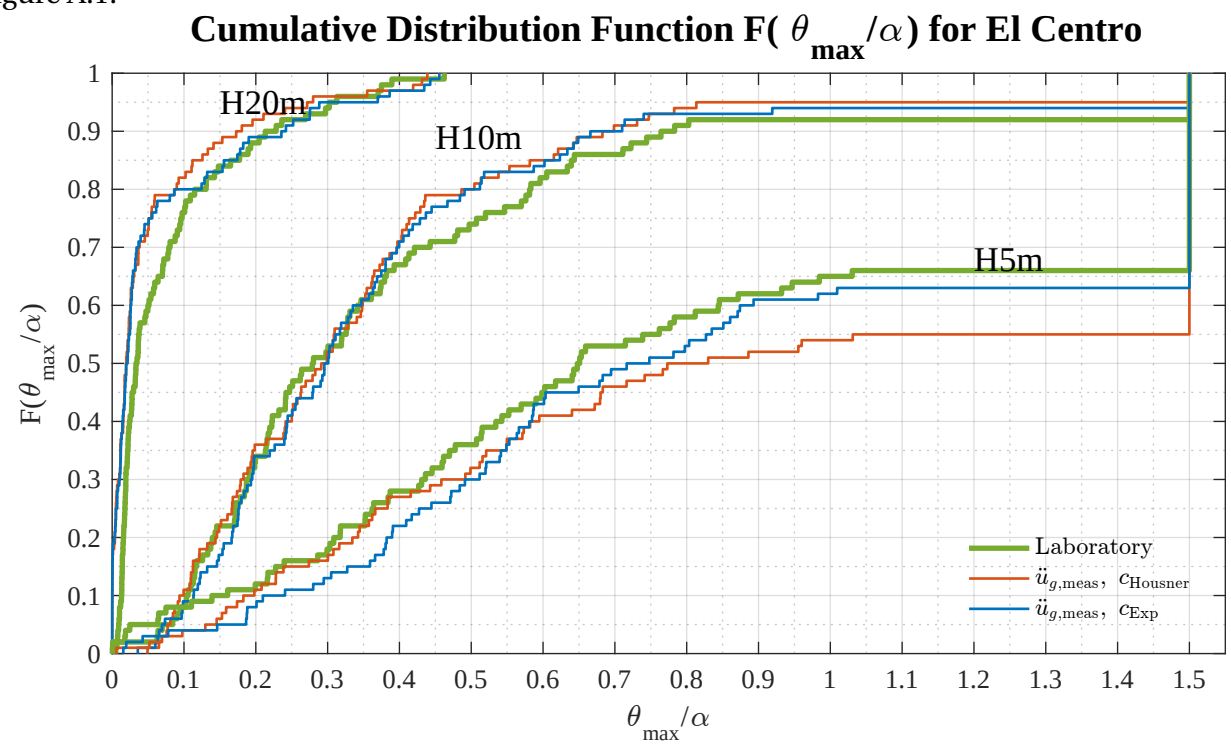

(b) Empirical CDF of maximum rocking angle θ_{max}/α, *including* the overturn values. The graph is only comparable to probability of overturning in table 8.1.

Figure 8.1: Empirical CDF for El Centro. (Values for H5m M2). There is an apparent correlation between the predicted and the laboratory graphs. H10m is best fitted. When considering relative errors are also the graphs of H5m good fitted. The H20m graphs show similar slopes, but are not well fitted when relative errors are considered. Notice that the red line for H5m predicts considerably *more* overturns than the green and and blue lines.

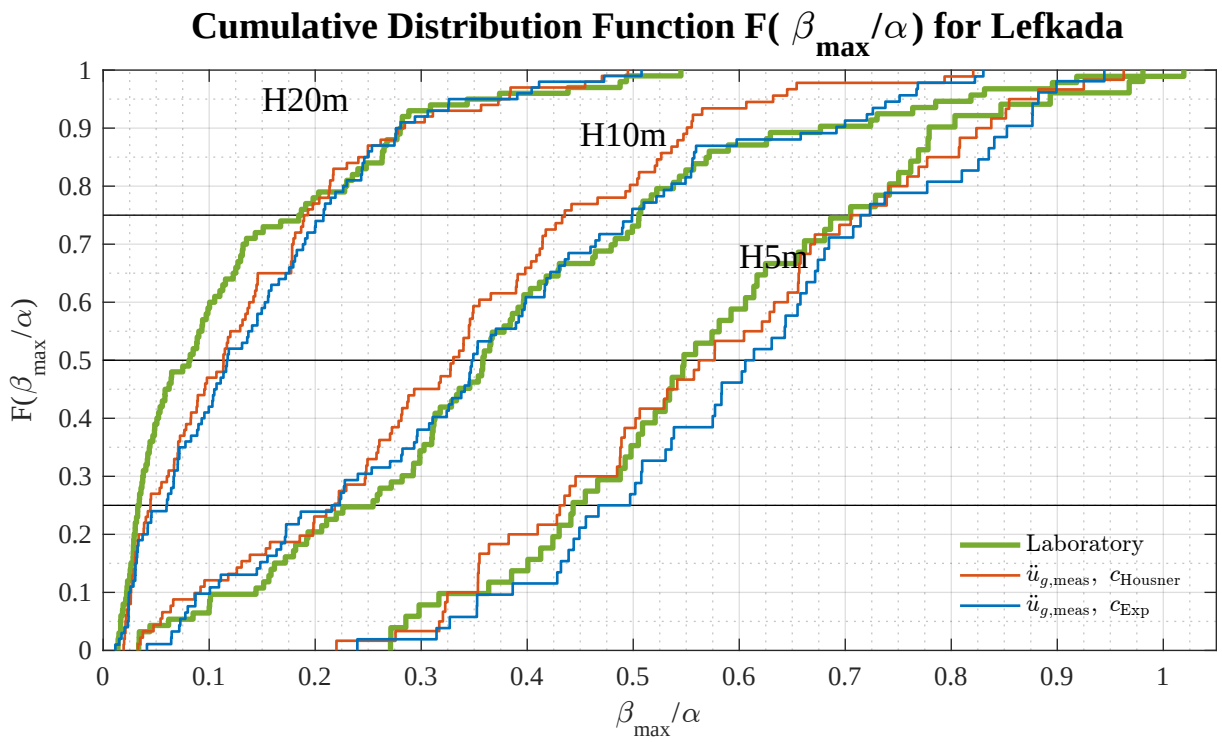

(a) Empirical CDF of maximum rocking angle β_{max}/α, *excluding* the overturn values. The graph is comparable to statistical measures in table in table 8.1 and to the associated box plots in figure A.2.

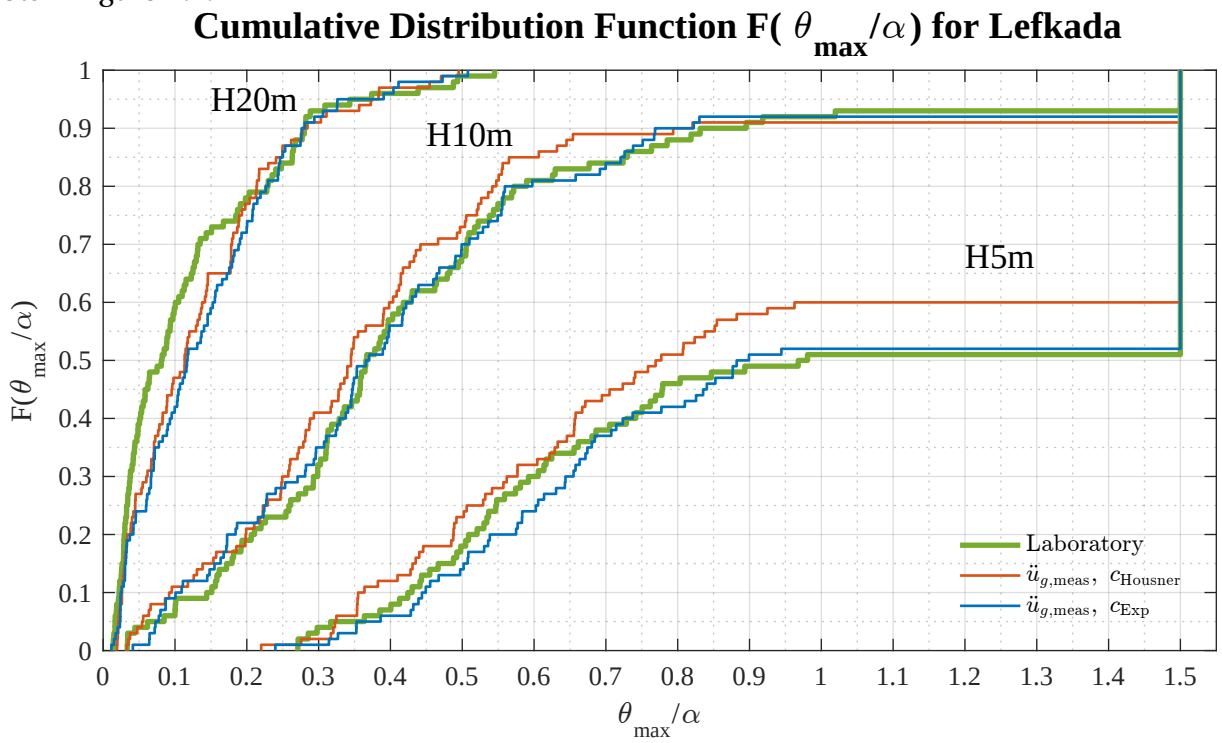

(b) Empirical CDF of maximum rocking angle θ_{max}/α, *including* the overturn values. The graph is only comparable to probability of overturning in table 8.1.

Figure 8.2: Empirical CDF for Lefkada.There is an apparent correlation between the predicted and the laboratory graphs. The lines of both H5m and H10m are good fitted. Notice that the red line for H5m predicts considerably *less* overturns than the green and and blue lines, compare with for El Centro. The lines of H20m are good fitted for low and high values, but not in the middle.

8.2 Observations on Coeffecient of Restitution

As seen in table 4.2 the Housner coefficient of restitution c_{Housner} is lower than the experimental c_{Exp} for both models. This means that rocking motion with c_{Housner} will lose around 0.7 % more energy per impact. One might expect that the numerical response with c_{Housner} will exhibit smaller values for the maximum rocking angle β_{max} than the response with c_{Exp}.

Effect on Maximum Angle As seen in table 8.1, the results with c_{Housner} show both higher and lower values than those of c_{Exp}. The general effect is better seen in the CDF plots in figure 8.1(a) and 8.2(a). The red c_{Housner} lines lie to the left of the blue lines c_{Exp} for most of the β_{max}-interval for all heights in both plots. The red lines lie to right of the blue lines only for small regions.

In general it seems that a smaller coefficient of restitution leads to smaller maximum rocking angles for the whole ensemble of ground motions when all other parameters are equal. In other words, more rapid energy loss leads to smaller maximum rocking angles in an average sense. When considering the relative error on the quartile values for all test groups there is no obvious trend regarding which coefficient of restitution that predicts the values with least error.

Effect on Overturning Consider the CDF plots including overturn values. The blue lines of c_{Exp} are close to the green lines of the laboratory tests for both ground motions and for H5m and H10m. The nominal error of the predictions relative to the laboratory values are ± 3 out of 100 tests for both prototypes. While for the red lines c_{Housner} the nominal error is 11 and -9 for H5m and -3 and 2 for H10m. Thus the greatest difference is seen for predictions on both H5m tests. Since the difference values are both positive and negative, the predictions are both conservative and non-conservative. As seen in in table 8.2, a slight change of the accelerations reverses the observations on which coefficient of restitution that leads to smallest error, as discussed in section 8.10. In general the overturning values are not well predicted when relative errors are considered. The c_{Housner}-value implies larger damping than with c_{Exp}, but there is no clear trend that implies that larger damping lead to fewer overturns.

8.3 El Centro H5m M2

The distributions for El Centro M2 fit well to each other. The prediction lines in the CDF plot in figure 8.4 show relative errors between -19 % and 26 % on Q25, between -10 % and 13 % on Q50 and between -2.9 % and 5.3 % on Q75. The red line of c_{Housner} is in general best fitted to the green laboratory line, which is also observed by the box plots in figure 8.3. The red line is non-conservative and the blue line of c_{Exp} is conservative for most of the domain, which follows the general trend observed in subsection 8.2. The slopes of the curves vary similarly, and there is an apparent correlation between the predicted and laboratory distributions.

The probability of overturning equal to 34 % is not good estimated. The predictions are between 37 % c_{Exp} and 45 % for c_{Housner}, which equals a relative error up to 32 %. Even though predictions with c_{Housner} implies more energy loss per impact, there is observed significantly more overturns. This effect is albeit not predictable, as seen by comparing the results with different offset correction in table 8.2.

For comparison of the the results with the flawed test of El Centro H5m M2, see section 8.9.

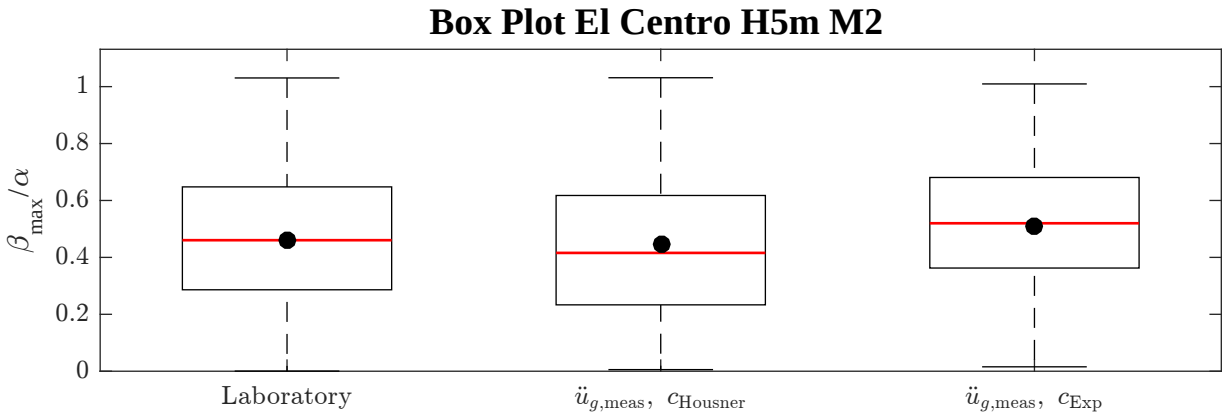

Figure 8.3: Box plots of the maximum rocking angle β_{max}/α for El Centro H5m. Notice the difference in height of the box for laboratory results. The median values differ with -10 % and 13 %, but the mean is better fitted for $c_{Housner}$ with error of only 3 %

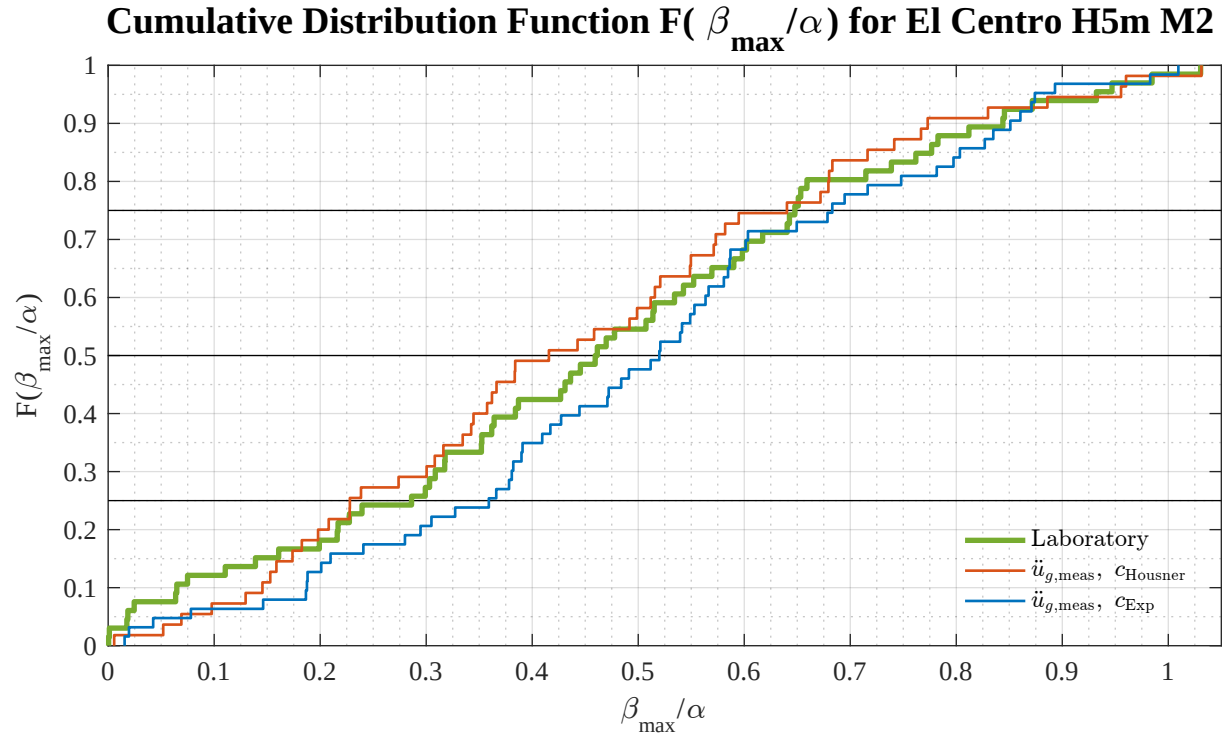

Figure 8.4: Empirical CDF for El Centro H5m M2. The red line is in general higher than the green laboratory line, but the Q25 and Q75 values are similar, as seen on the box plot. The blue line has significantly larger value for Q25.

8.4 El Centro H10m

The CDF graphs for El Centro H10m in figure 8.6 fit in general well. In the interval $0.06 < \beta_{max}/\alpha < 0.4$ the fit of both predictions is close. The relative error at Q25 is between 2.8 % and -5.1 %, while the values at Q50 are increased to 17 % and 12 %. At Q75 the relative error is decreased to 5.3 % and -2.9 %. For the interval $0.4 < \beta_{max}/\alpha < 0.6$ both prediction lines lie to the left of the laboratory line, giving non-conservative predictions. For $\beta_{max}/\alpha > 0.6$ the fit is yet again close. For most of the β_{max}-values the prediction with $c_{Housner}$ fits the laboratory line better. The minimum and maximum values differ with up to 0.049 and 0.106 respectively, but these extreme values belongs to the tail of the distribution and are indeed not expected to be well predicted in a set of 100 values. The interquartile range is predicted with a relative error of -9.0 % and -2.8 %, thus the predictions give lower dispersion of the results than the laboratory results, which is non-conservative.

The predicted probabilities of overturning are 6 % and 5 % compared to 8 %, which leads to non-conservative relative error of -25 % and -38 %, as shown in table 8.2.

When considering the box plot in figure 8.5, the three boxes are similar. The predicted medians are similar, but higher than the laboratory median. The means are on the other hand well fitted an higher than the median values. In general there is a good fit of the predicted and laboratory distributions.

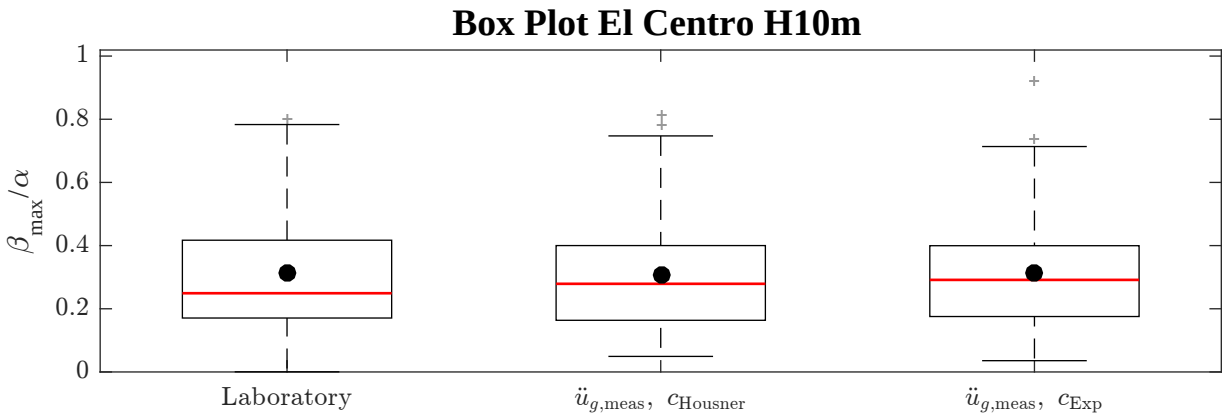

Figure 8.5: Box plots of the maximum rocking angle β_{max}/α for El Centro H10. There is a good fit of the distributions. The mean values are better fitted than the medians with less than 1 % error compared to less than 17 % error.

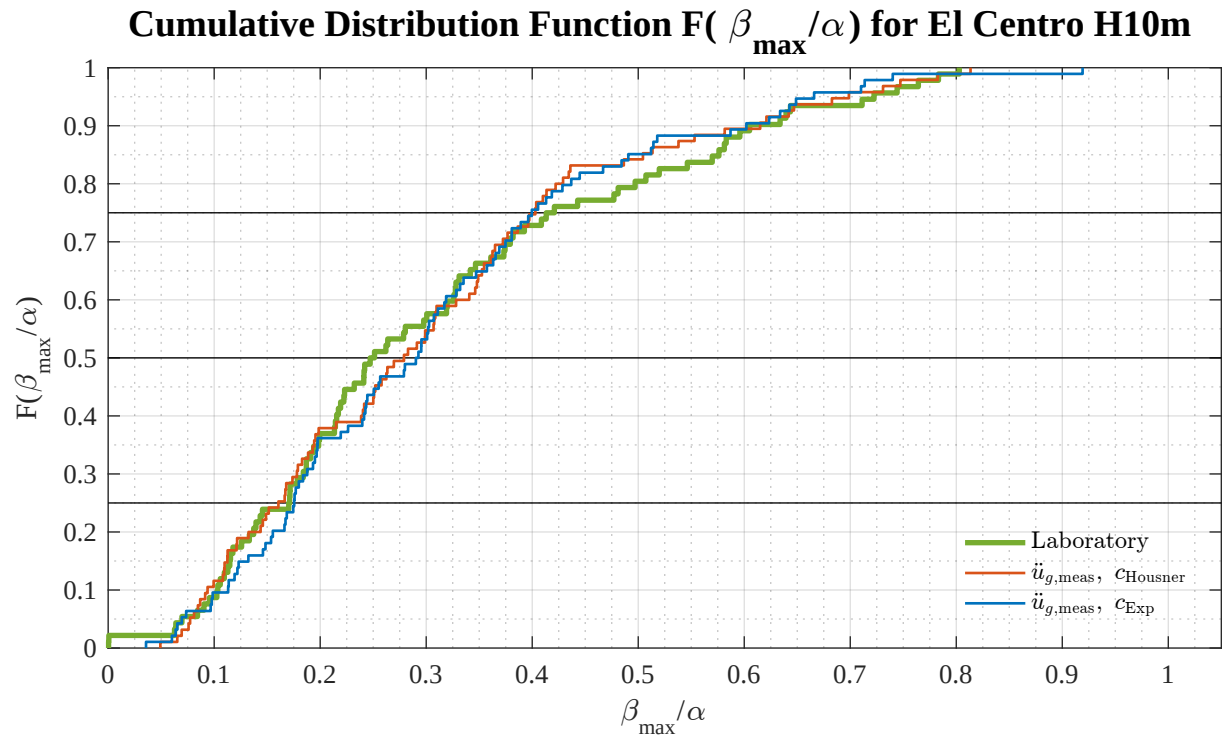

Figure 8.6: Empirical CDF for El Centro H10m of values excluding overturns. There is in general a good fit of the prediction lines to the laboratory line.

8.5 El Centro H20m

The CDF graphs for El Centro H20m in figure 8.8 *does not* fit as good as expected. For the three quartile values Q25, Q50 and Q75 there is a relative error in prediction between -39 % and -71 %. For $\beta_{max}/\alpha > 0.011$ the blue prediction line of c_{Exp} fits better to the green laboratory line, the red line of $c_{Housner}$ still shows errors to the same degree.

Both prediction lines have 23 values below $\beta_{max}/\alpha = 0.00495$ which is the minimum value of the measured laboratory results. This minimum value equals a rocking angle of 1.89°.

The values that represent the laboratory results are maximum values of the offset-corrected signal. This offset-correction introduces uncertainty in addition to the uncertainty of the measurements itself. What we interpret as measured maximum rocking angles in this low-value-region might be heavily influenced by inaccuracies in measurements, post-processing, numerical noise or motions that not represent rigid rocking.

Possible Error Causes One of the measured acceleration signals, simulation 92, has peak value $\ddot{u}_{g,p}$ = 0.141 g, which is below the theoretical uplift criterion. For the numerical predictions the values are 0, i.e. no rocking, but the laboratory value from this test is $0.00657\alpha = 0.056°$. According to the log note for this test, no rocking was observed by the naked eye. When examining the plot of the NDI records of rocking motion, there is a significantly increased amplitude of the motion for a duration of 4 seconds, which is about the duration for reaching 95 % of the Arias intensity, see figure 7.4. This increase in amplitude means that the angle between line 1-3 and line 2-4 of figure 4.2 is changed. This change is interpreted as rocking motion when we assume that the column is rigid. If the column is not totally rigid, this change in amplitude might also be interpreted as elastic vibrations of the column or the connection between the bottom wedge and the column. In the numerical model, the column is assumed perfectly rigid.

Uplift Criterion An other explanation might be that the theoretical criterion for uplift as given in equation 2.2, does not describe the uplift criterion of the test specimen precisely. Assume that the total height of the test specimen is given as H = 500 ± 2 mm and the total width is given as B = 75 ± 1 mm. Then the theoretical value for the uplift criterion attain

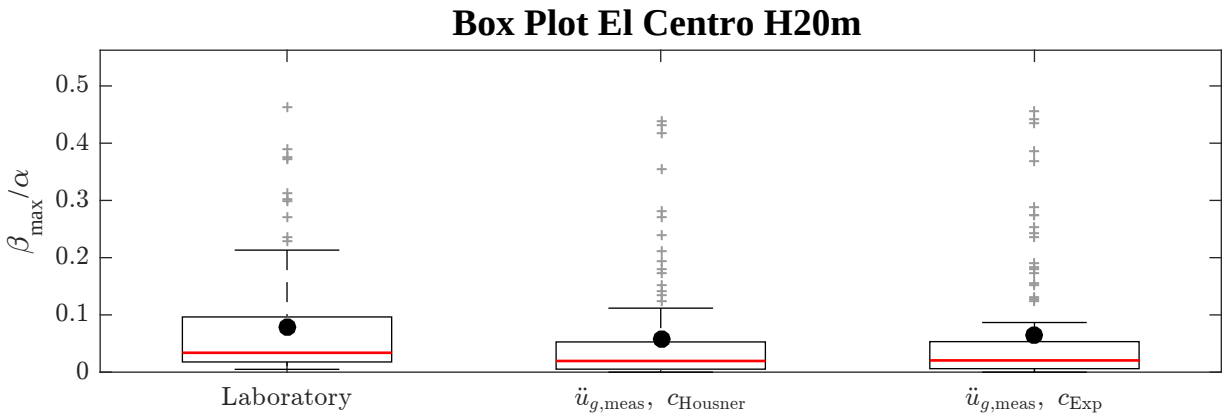

Figure 8.7: Box plots of the maximum rocking angle β_{max}/α for El Centro H20m including all values. Notice the high amount of outliers and the difference of height and location of the predicted boxes compared to the laboratory box. The 23 lowest predicted numerical values are so low that similar laboratory values hardly could be measured, thus there is a notable difference in the distributions.

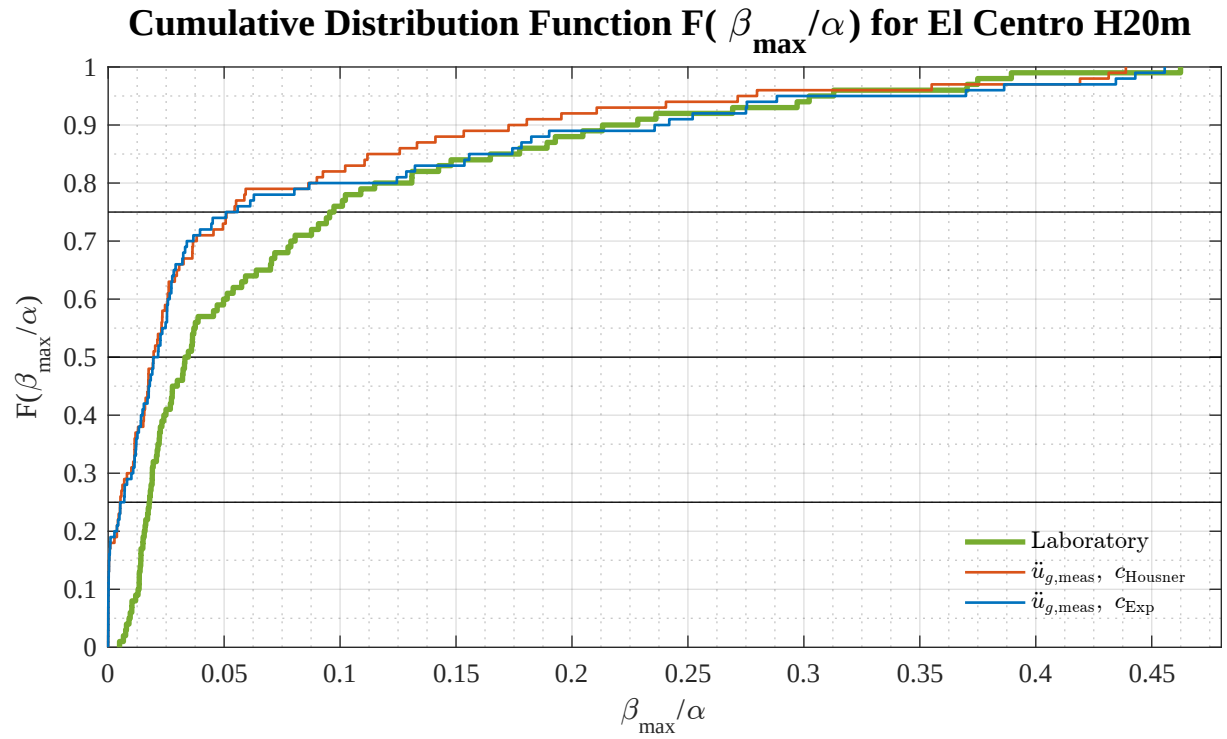

Figure 8.8: Empirical CDF for El Centro H20m of all values. The predictions have 23 values below 0.005α, which is the minimum measured laboratory value (for El Centro H20m), thus there is considerable discrepancy in the whole domain.

values between

$$\begin{aligned} \frac{75-1}{500+2}g \leq \ddot{u}_g \leq \frac{75+1}{500-2}g \\ 0.1474g \leq \ddot{u}_g \leq 0.1526g \end{aligned} \tag{8.1}$$

The uplift criterion is then given as $\ddot{u}_g = 0.15g \pm 0.0026g$ with these hypothetical uncertainty values, which is still higher than the lowest peak acceleration of 0.141 g. Nevertheless, the script is calculating the response for the deterministic value of 0.15g only. The actual limit of overturning for our specimen is not tested experimentally. The measured response for shaking table motions with peak acceleration below the uplift criterion is also not tested.

Lower Bound for Measurement The box plots of El Centro H20m in figure A.1 show a significant difference between the two predictions and the laboratory results. First of all there are many outliers: 19, 15 and 10 for c_{Exp}, c_{Housner} and laboratory results respectively. Outliers in the box plots could mean that the values might be influenced by errors or that the values represent different distributions. For the prediction values 19 and 18 values are below 10^{-3} for c_{Exp}, c_{Housner} respectively. The laboratory results are obtained by correcting the offset by an approximation of the mean and then returning the maximum absolute value of the entire signal. It is therefore likely that one of the 15 000 values measured in a 30 second-signal has one value greater than 10^{-3}. This value is then interpreted as the maximum rocking angle from the laboratory. From the box plot we can also observe that the mean values are considerably larger than the median values, and for the predictions the means are even larger than Q75. The means are heavily biased by the outliers with values up to 0.462, while all Q75 values are lower than 0.096. The predicted dispersion, given by IQR, is notably lower than for the laboratory results.

If we construct the CDF of the prediction lines only for $\beta_{\max} \geq 0.00495\alpha$, which is the lowest laboratory value, we get the plots in figure 8.10. These lines fit considerably better for the values where $\beta_{\max} \leq 0.04\alpha$. The red line of c_{Housner} fits good for almost the entire domain. When we compare the associated, reduced box plots in figure 8.9, the amount of outliers is considerably reduced and the IQRs are more equal. The predicted medians are still notably lower than for the laboratory values. Nevertheless, these distributions seem more equal, which might imply that we are not able to measure rocking angles somewhere below 0.00495α with sufficient accuracy. For all 700 tests there are four laboratory values that are

determined to be between 0.00039α and 0.00062α, which evidently are lower than 0.00495α, but nevertheless their accuracy remain unknown. These values are obtained for El Centro H5m M2 and El Centro H10m.

Also other methods of calculating the offset are tested. The built in MATLAB function `detrend` computes a least-square fit line which is subtracted from the original signal. Using this offset correction did neither reduce the error nor determine maximum values lower than 0.00495α for El Centro H20m. With this offset correction method the lowest laboratory value for all 700 tests was determined to 0.00038α. The effect of different offset correction methods is further discussed in section 8.10.

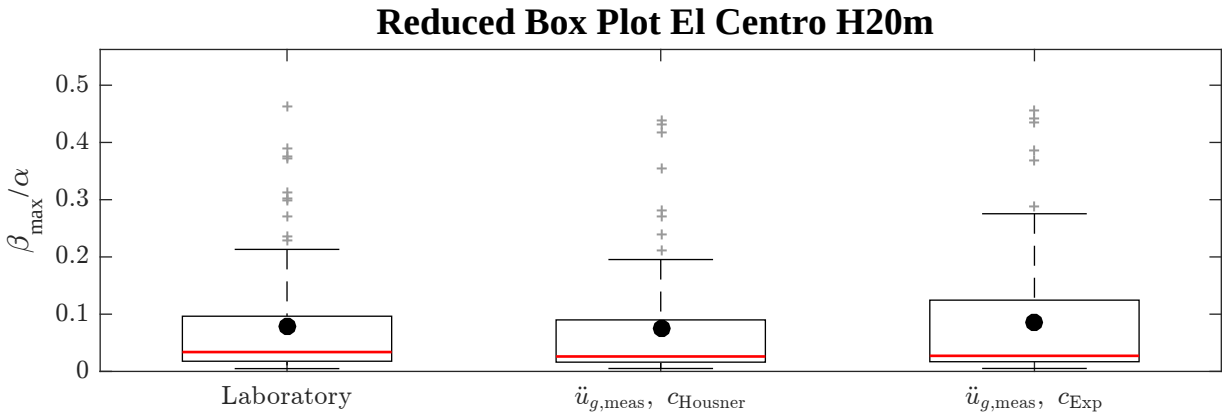

Figure 8.9: Box plots of the maximum rocking angle $\beta_{\max}/\alpha$ for El Centro H20m values excluding predicted values that are lower than the minimum measured value from the laboratory. The box plots are more similar when the low predicted values are excluded.

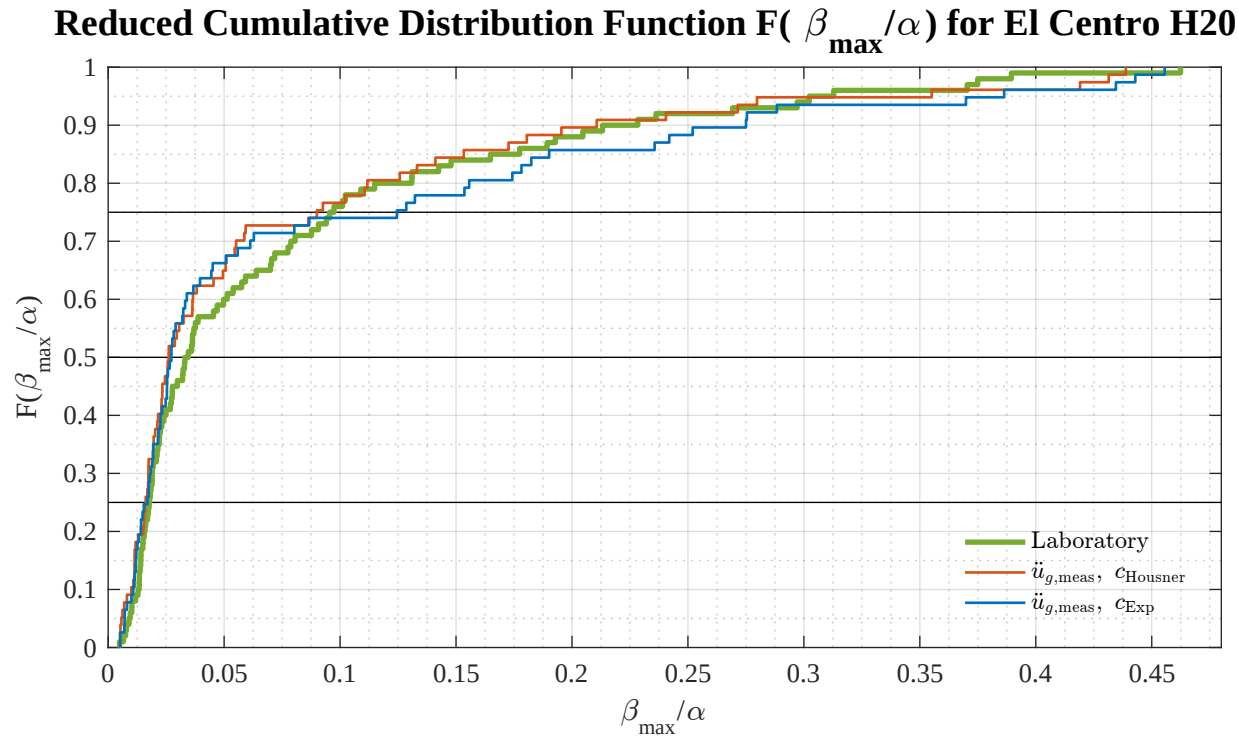

Figure 8.10: Empirical CDF for El Centro H20m of values excluding predicted values that are lower than the minimum measured value from the laboratory. The fit of the lines is notably better for the 40 % lowest values. The predicted lines are based on 77 values, while the laboratory line is based on 100 values, which influences how coarsely the lines are plotted.

8.6 Lefkada H5m

The prediction lines for Lefkada H5m fit well to the laboratory line in figure 8.12. The relative error at Q25 is between -3.0 % and 8.1 %, at Q50 between 3.9 % and 11.3 % and at Q75 between 2.0 % and 2.7 %. The red line based on c_{Housner} shows a better fit to the laboratory line than the blue prediction line with c_{Exp} for the entire domain. The blue line shows conservative predictions for most of the domain, while the red line has smaller errors and lies on both conservative and non-conservative side of the laboratory line. Also the interquartile region is relatively well fitted with relative error between -6.8 % and 11 %. Thus the dispersion of the values for all three responses are similar. In general for Lefkada H5m the predictions of β_{max} with c_{Housner} has smaller error values than the predictions with c_{Exp}.

The probability of overturning is predicted with relative error of -2 % for c_{Exp} and -18 % for c_{Housner}. $c_{\text{Housner}} < c_{\text{Exp}}$, so here an increased loss of kinetic energy, smaller c, lead to less overturns, which is the opposite effect than for El Centro H5m.

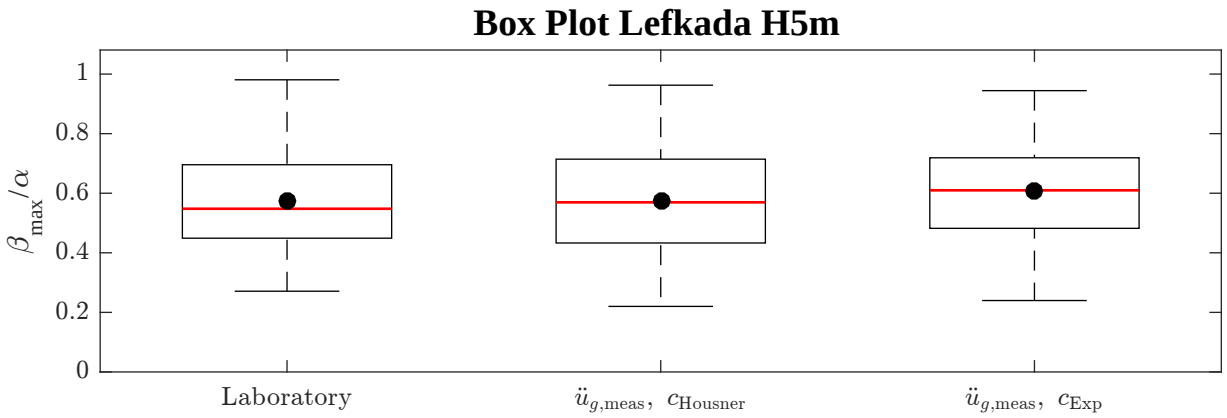

Figure 8.11: Box plots of the maximum rocking angle β_{max}/α for Lefkada H5m. The distributions are well fitted with errors on the mean less than 6 % and errors on the median less than 11 %.

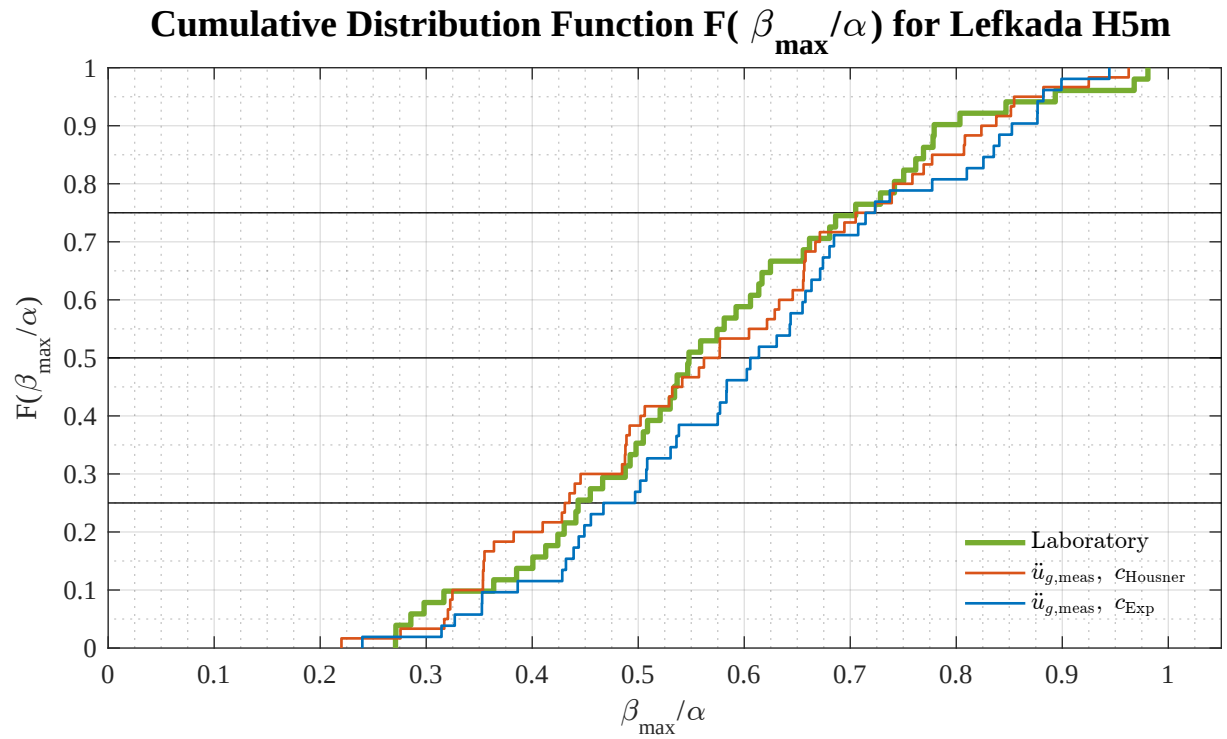

Figure 8.12: Empirical CDF for El Centro H5m. The predicted lines are well fitted to the laboratory lines. The largest errors on quartile values are observed for the blue line.

8.7 Lefkada H10m

For Lefkada H10m the two prediction lines are non-conservative in most of the domain as shown in figure 8.14. The blue line of c_{Exp} fits considerably better to the laboratory line than the red line of c_{Housner}. The relative error at Q25 is -11 % for both, at Q50 is between -2.7 % and -7.8 % and at Q75 is between -1.3 % and -14 %. As seen in the plot, the fit of the blue line for c_{Exp} is notably close for $0.35 < \beta_{\text{max}}/\alpha < 0.73$. The red line of c_{Housner} show larger, non-conservative errors for the entire domain.

The probability of overturning is fitted for c_{Exp} with a nominal error of 1%, which equals a relative error of 14 %. The prediction of probability with c_{Housner} has a relative error of 29 %.

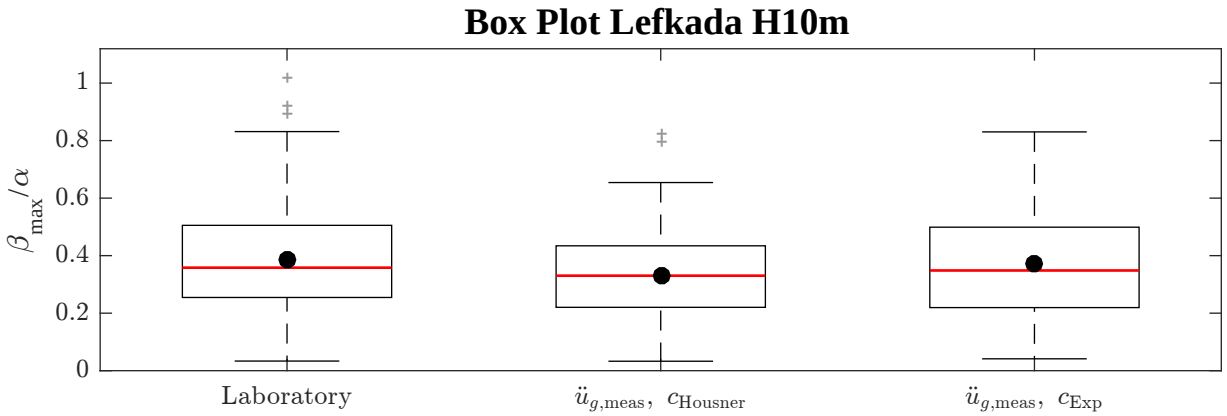

Figure 8.13: Box plots for Lefkada H10m. The box for predictions with c_{Housner} is smaller than the two others. c_{Housner} means more energy loss compared to c_{Exp}, and in this case the maximum response is reduced for the whole distribution.

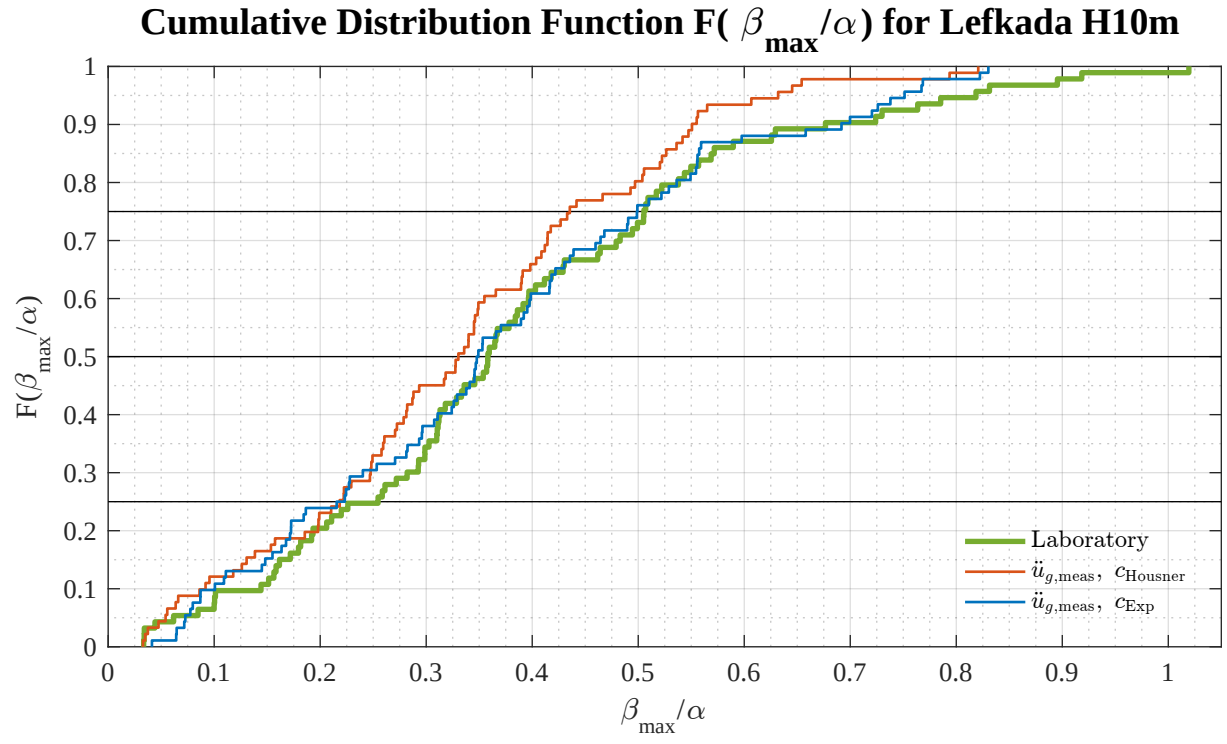

Figure 8.14: Empirical CDF for Lefkada H10m. The blue line is best fitted for all quartile values, especially the median and Q75 are predicted well. The red line predict smaller values for the entire distribution.

8.8 Lefkada H20m

For Lefkada H20m in figure 8.16 there is a considerable discrepancy for $0.03 < \beta_{\max} < 0.19$, which almost coincides with the interquartile range for all three lines. The minimum measured value is 0.033 which is almost seven times higher than the minimum measured value for El Centro H20m. The lines fit here well for the lowest 20 values, which was not the case for El Centro H20m in figure 8.8. In the box plot in figure 8.15 we observe that the interquartile region is well fitted although the relative errors on the quartile values attain values between 34 % and 80 % for Q25 and between 39 % and 44 % for Q50. The relative error on Q75 is notably smaller and between 3 % and 12 %. The blue line of c_{Exp} has almost constant nominal error between 0.022 and 0.036 on the three quartile values. The red line of c_{Housner} shows smaller errors, but the error on the median is considerable for both predictions.

From the box plot we observe that there is only a limited number of outliers, and the distributions seem relatively equal. There is thus not a notable sign of measurement errors or unexpected influences. The minimum measured peak acceleration is 0.218g, which is considerably higher than the theoretical uplift criterion. The uncertainty on the real limit for uplift will therefore mainly introduce errors if the angular velocity in the numerical predictions is lower than the cutoff-limit and there is later accelerations that fulfill the uplift criterion. Consequently uncertainty on the real limit for uplift is not expected to affect these results to a high degree.

8.9 El Centro H5m M1 and M2

The measured laboratory response for the two tests of El Centro H5m are compared in CDF plots in figure 8.17. CDF plots including the prediction lines for $\ddot{u}_{g,\text{meas}}$ are shown in figure 8.18. Since the number for model and tuning coincide, we refer to them together as M1 and M2

In figure 8.17 there is a significant difference in the graphs for $\theta_{\max} < 0.2\alpha$. The first tests performed with M2 has a minimum value of 0.128α while the second tests show 9 values below this. When comparing all 2×3 minimum values in table 8.1 and figure 8.18, we see that the numerical results based on measured accelerations fit quite well to those of the laboratory results for both M1 and M2. The measured accelerations are unequal for M1 and M2 due to the different tuning of the shaking table. The combination of an unstable foundation

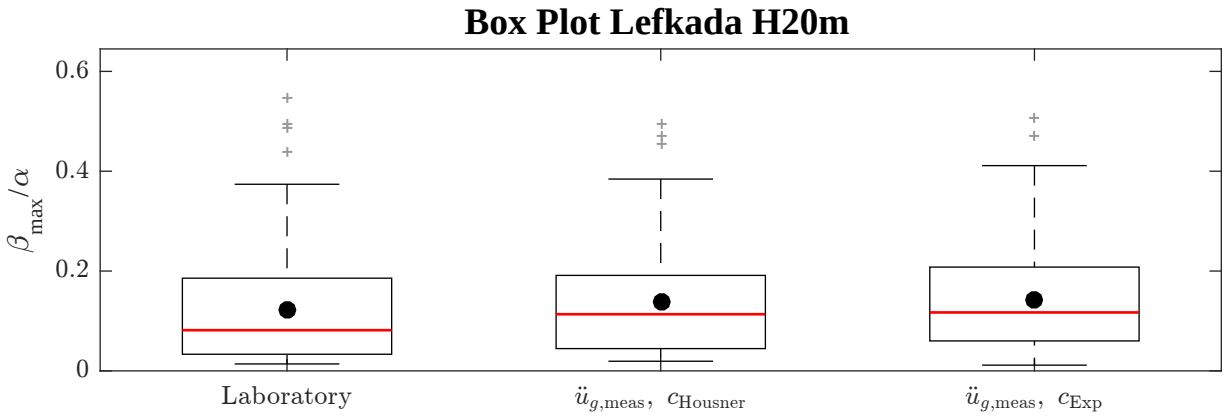

Figure 8.15: Box plots for Lefkada H20m. The two predicted boxes are more equal to each other than the laboratory box. The IQR of the predictions are given with an error of only 3 % and 4 %, even though the Q25 has an error up to 80 % and the median up to 44 %. The means are better estimated, but still have errors between 13 % and 18 %.

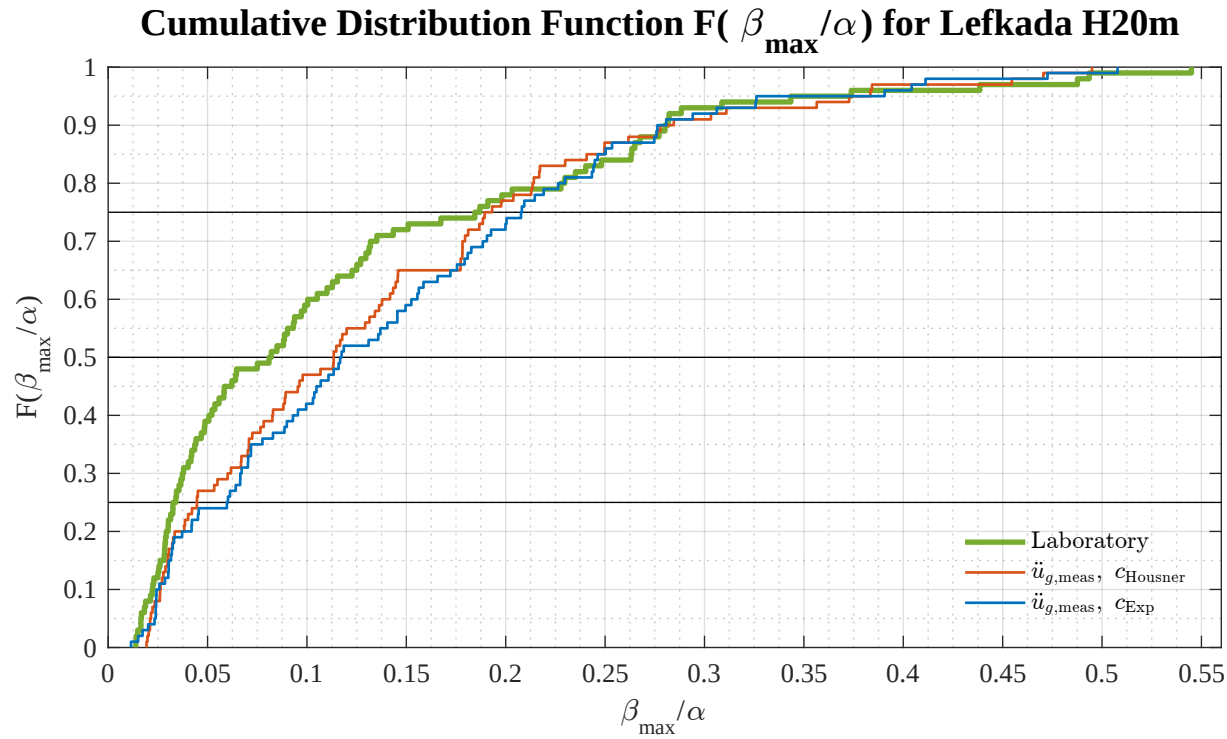

Figure 8.16: Empirical CDF for Lefkada H20m. Here the lowest values are significantly better predicted than for El Centro H20m. The two predicted lines are close to each other, and the red line, with more energy loss, predicts lower values than the blue for the entire distribution. From the Q25 to Q75 for the laboratory results there is a notable discrepancy between the laboratory and the predicted lines.

and applied accelerations that lead to higher minimum values also for the numeric results, might explain why the laboratory results for M2 start first at 0.128α.

When we compare the probability of overturning as shown in table 8.2 and figure 8.17(b), M1 has a measured probability of 50 % and M2 34 %. The laboratory probability for M1 is higher than that of the numerical probabilities - thus the numerical model underestimates the probability of overturning. For M2 we observe the opposite case - the numerical model overestimates the probability. For both M1 and M2 the maximum error in number of overturns is 11. The numeric results from simulated accelerations are shown in figure B.1 and B.2 in the appendix. Due to the slightly different values for c and λ as showed in table 4.2, the numerical graphs based on the same simulated accelerations are notably different.

When we compare the box plots of M1 and M2 in figure 8.19, we observe that the interquartile range of laboratory M1 is much higher than that of the predictions. This IQR is also higher than all IQRs for M2. This means that the dispersion of the laboratory results for M2 is significantly higher than what is expected by the numeric results, which is not seen for any of the other test groups. A larger IQR means in other words that the probability density in the mid region is lower than for the comparable distributions. Consequently the density in both ends become higher than for the comparable distributions, which is also observed by in the CDF plots by less steep curve in the middle. We observe more maximum rocking angles in both the low and high angle region than expected with a perfectly stable foundation. The twisting of the foundation for M1 was varying during the test, leading to non-constant initial conditions for the rocking motion. Varying initial conditions leads to the conclusion that the measured maximum rocking angles for M2 arises from not one single distribution, and that this combined distribution hardly could be predicted precisely by the applied stationary numeric model.

The relative errors of the quartile values for M1 are considerably larger than those of M2, as seen in table 8.1. The largest relative error for M1 is 72 % while it is 26 % for M2. The median of M1 c_{Exp} has an error of only 0.2 %, but as seen on the CDF graphs of figure 8.18 (a) this small error is purely coincidental.

Conclusions Overall the laboratory results from M1 *does not* fit well to the numerical results. This is mainly caused by the unstable foundation leading to non-constant initial conditions. Both the numerical and laboratory results for M1 does not compare well to those of M2. This difference is mainly caused by the unequal tuning of the shaking table and slightly

different values for c and λ.

Nevertheless, the results for M2 *does* fit well to each other, and these results are used for further validation of the numerical model. The prediction lines for M2 show relative errors between -19 % and 26 % on Q25, between -10 % and 13 % on Q50 and between -2.9 % and 5.3 % on Q75. In figure 8.18 (b) the red line of c_{Housner} fits the laboratory line better for most of the domain. The red line is non-conservative and the blue line is conservative for most of the domain, which follow the general trend observed in subsection 8.2.

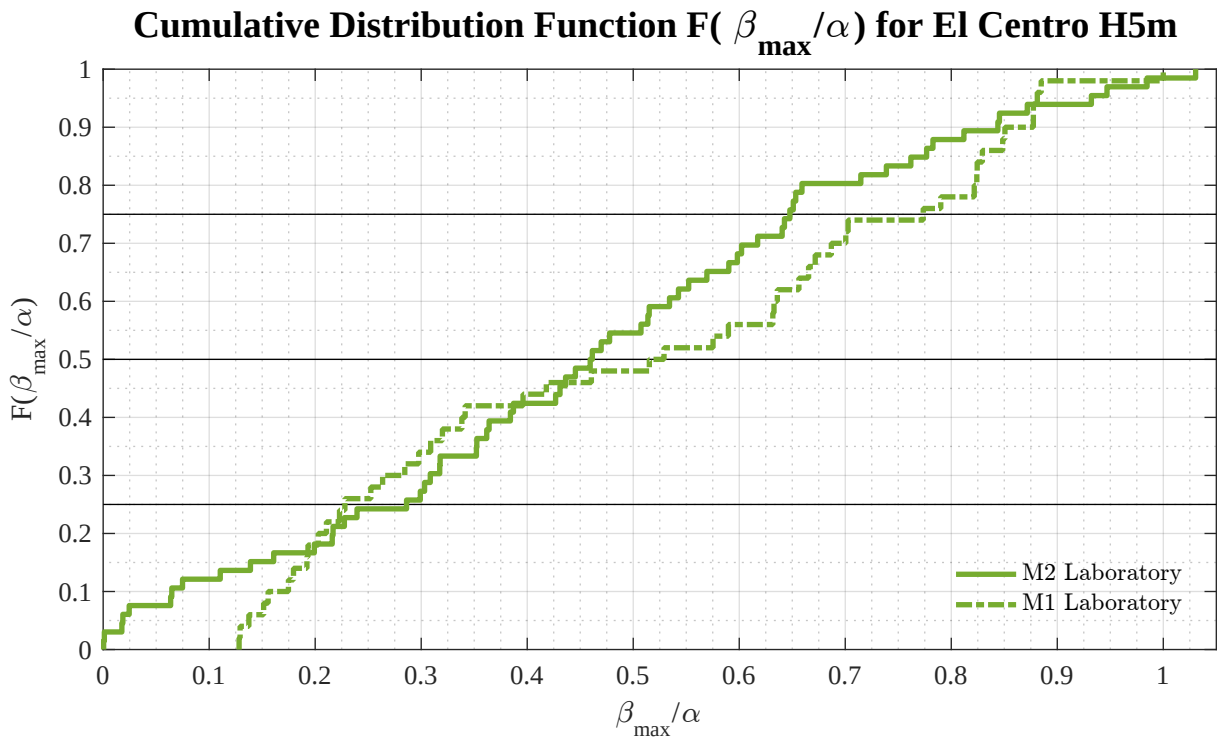

(a) Empirical CDF excluding overturn values. The graph of M1 is based on 50 values and shows a more distinct change of slope with higher density for low and high angles. The M2 graph is based on 66 values and shows a smoother line and more even density of angle values.

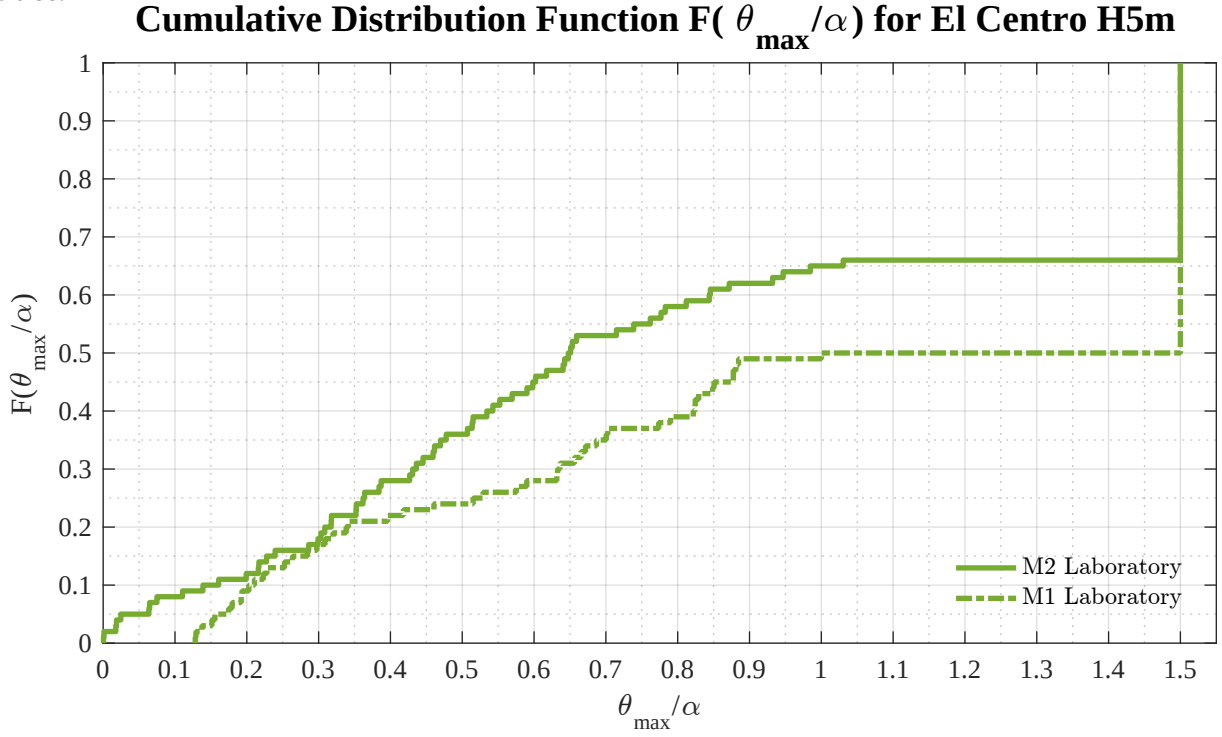

(b) Empirical CDF including overturn values. There is a difference of 16 overturns out of 100, where the unstable M1 shows most overturns.

Figure 8.17: Comparison of empirical CDF of El Centro H5m laboratory values for M1 and M2. The graph of M1 shows no values for $\beta_{max}/\alpha < 0.128$. The M1 and M2 curves are significantly different for the entire domain of rocking angles.

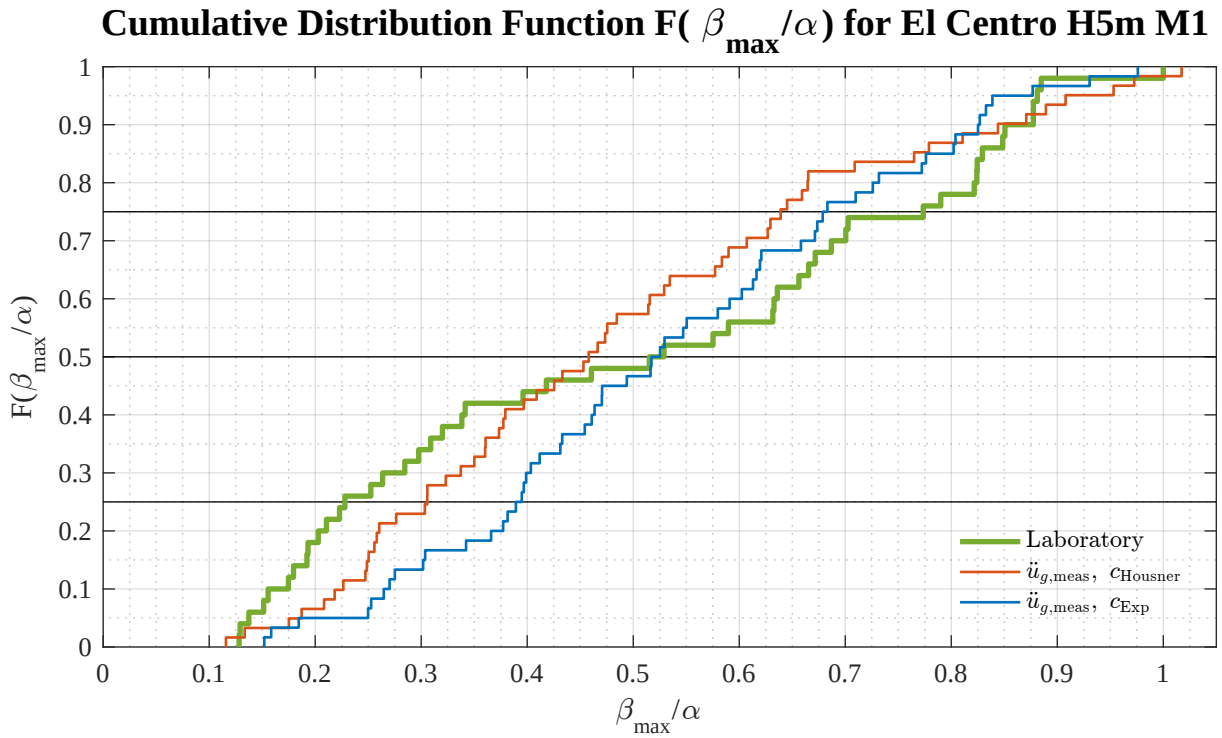

(a) For $0.40 < \beta_{max}/\alpha < 0.62$ the slope of the green line is significantly lower than for the prediction lines. This means that there are fewer laboratory results in this region compared to the predictions as seen in the box plot in figure 8.19 as well.

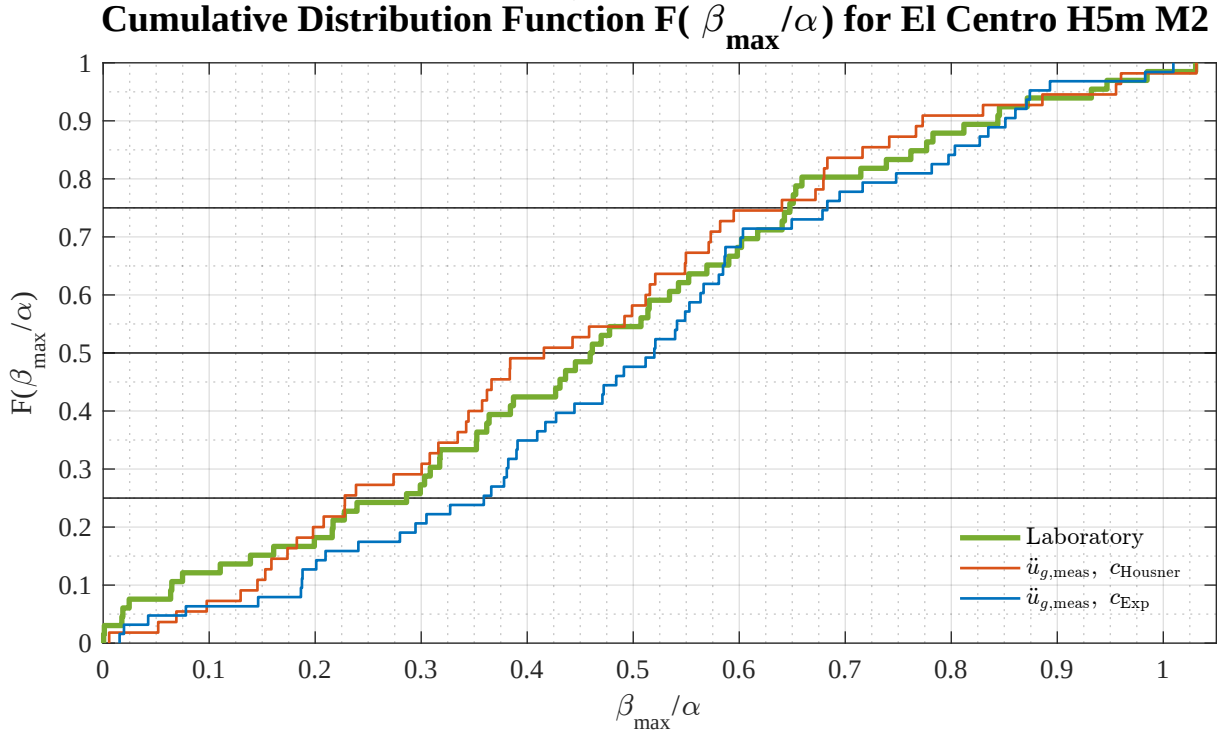

(b) The three graphs fit notably better for all β_{max}/α values compared to M1.

Figure 8.18: Comparison of empirical CDF for El Centro H5m M1 and M2. The curves have different minimum values for M1 and M2 because of different tunings of the shaking table. The M2 curves are significantly better fitted than the M1 curves.

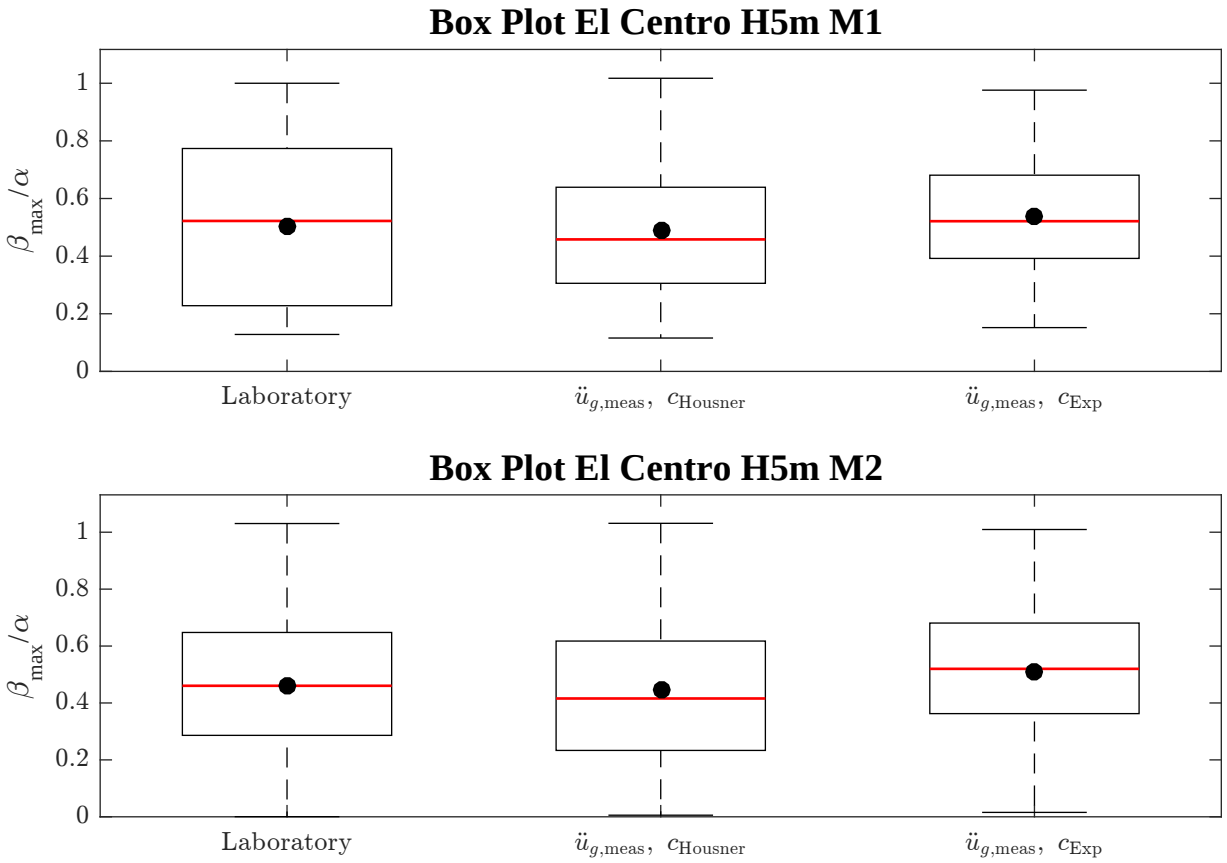

Figure 8.19: Box plots of the maximum rocking angle $\beta_{\max}/\alpha$ for El Centro H5m. Notice the difference in height of the box for laboratory results, which might be interpreted as a sign of two different distributions.

Table 8.1: Minimum, maximum and quartile values excluding overturns. Nominal, Δ, and relative, |Δ|/Q, errors of quartile values from table. The nominal error values show the discrepancy of the numerical predicted values to the laboratory values. Green values denote relative error less than 10 %, orange values between 10 % and 20 % and red values larger than 20 %. n is the number of samples that the statistical values are based on, which is 100 - number of overturns. Offset correction based on mean of the first 100 points. All values except for n are given as β_{max}/α [-]. The largest nominal error value Δ is $0.07\alpha \approx 0.6°$ and largest relative error value |Δ|/Q is 80 % (El Centro H5m M1). Lefkada shows in general smaller nominal errors than El Centro. The nominal errors are to the second decimal for all scales, which is slightly higher than the estimate of average uncertainty of measurements.

	H	Response	n	Min	Q25			Q50			Q75			Max	IQR		
					Q	Δ	$\frac{\lvert\Delta\rvert}{Q}$	Q	Δ	$\frac{\lvert\Delta\rvert}{Q}$	Q	Δ	$\frac{\lvert\Delta\rvert}{Q}$		Q	Δ	$\frac{\lvert\Delta\rvert}{Q}$
El Centro	5 M1	Laboratory	50	0.128	0.23			0.52			0.77			1.00	0.55		
		$c_{Housner}$	61	0.116	0.31	0.08	34%	0.46	-0.06	12%	0.64	-0.13	17%	1.02	0.34	-0.21	39%
		c_{Exp}	60	0.152	0.39	0.16	72%	0.52	0	0%	0.68	-0.09	12%	0.98	0.29	-0.26	47%
	5 M2	Laboratory	66	0.000	0.29			0.46			0.65			1.03	0.36		
		$c_{Housner}$	55	0.006	0.23	-0.06	19%	0.42	-0.04	10%	0.63	-0.02	3%	1.03	0.40	0.04	10%
		c_{Exp}	63	0.015	0.36	0.07	26%	0.52	0.06	13%	0.68	0.03	5%	1.01	0.32	-0.04	11%
	10	Laboratory	92	0.000	0.17			0.25			0.42			0.80	0.25		
		$c_{Housner}$	95	0.049	0.16	-0.01	5%	0.28	0.03	12%	0.40	-0.02	4%	0.81	0.24	-0.01	3%
		c_{Exp}	94	0.036	0.18	0	3%	0.29	0.04	17%	0.40	-0.02	4%	0.92	0.22	-0.02	9%
	20	Laboratory	100	0.005	0.02			0.03			0.10			0.46	0.08		
		$c_{Housner}$	100	0.000	0.01	-0.01	71%	0.02	-0.01	42%	0.05	-0.04	45%	0.44	0.05	-0.03	40%
		c_{Exp}	100	0.000	0.01	-0.01	66%	0.02	-0.01	39%	0.05	-0.04	45%	0.46	0.05	-0.03	40%
Lefkada	5	Laboratory	51	0.271	0.45			0.55			0.70			0.98	0.25		
		$c_{Housner}$	60	0.220	0.43	-0.01	3%	0.57	0.02	4%	0.71	0.01	2%	0.96	0.28	0.03	11%
		c_{Exp}	52	0.240	0.48	0.04	8%	0.61	0.06	11%	0.72	0.02	3%	0.94	0.24	-0.02	7%
	10	Laboratory	93	0.033	0.25			0.36			0.51			1.02	0.26		
		$c_{Housner}$	91	0.033	0.22	-0.03	11%	0.33	-0.03	8%	0.43	-0.07	14%	0.82	0.22	-0.04	17%
		c_{Exp}	92	0.041	0.22	-0.03	11%	0.35	-0.01	3%	0.50	-0.01	1%	0.83	0.28	0.02	8%
	20	Laboratory	100	0.014	0.03			0.08			0.19			0.54	0.15		
		$c_{Housner}$	100	0.019	0.04	0.01	34%	0.11	0.03	39%	0.19	0.01	3%	0.49	0.15	-0.01	4%
		c_{Exp}	100	0.011	0.06	0.03	80%	0.12	0.04	44%	0.21	0.02	12%	0.51	0.15	0	3%

Table 8.2: Comparison of probability of overturning for different offset correction methods: first 100 and detrend. The accelerations are offset corrected with either first 100 or detrend method. Laboratory values for overturning are not affected by the offset method. Average values are calculated based on the four combinations of predicted P-values within each ensemble. Green values denote relative error less than 10 %, orange values between 10 % and 20 % and red values larger than 20 %. First 100 values are comparable to the all CDF and box plots in part III if not stated otherwise.
The results show significant differences on probability of overturning for slight changes in either accelerations or coefficient of restitution. Notice how the influence of coefficient of restitution is reversed for El Centro H5m by changing the accelerations. The overturning values for prototype scale H10m show large relative errors, even though the nominal errors are small. Probabilities lower than 10 % can hardly be accurately determined by a set of only 100 values.
For the average values the predictions are based on a set of 400 and the results are closer. For Lefkada the probabilities are predicted with 7 % error, especially for Lefkada H10m the error is reduced significantly. The probability for El Centro H10m is still notably underestimated.

			Overturning P(OT)								
			First 100			**Detrend**			**Average**		
	H	**Response**	P [%]	Δ [%]	$\frac{\lvert\Delta\rvert}{P}$	P [%]	Δ [%]	$\frac{\lvert\Delta\rvert}{P}$	P [%]	Δ [%]	$\frac{\lvert\Delta\rvert}{P}$
El Centro	5	Laboratory	34			34			34		
		$c_{Housner}$	45	11	32 %	35	1	3 %	39.8	5.8	17%
		c_{Exp}	37	3	9 %	42	8	24 %			
	10	Laboratory	8			8			8		
		$c_{Housner}$	5	-3	38 %	4	-4	50 %	4.5	-3.5	44 %
		c_{Exp}	6	-2	25 %	3	-5	63 %			
	20	Laboratory	0			0			0		
		$c_{Housner}$	0	0	-	0	0	-	0	0	-
		c_{Exp}	0	0	-	0	0	-			
Lefkada	5	Laboratory	49			49			49		
		$c_{Housner}$	40	-9	18 %	47	-2	4 %	45.5	-3.5	7 %
		c_{Exp}	48	-1	2 %	47	-2	4 %			
	10	Laboratory	7			7			7		
		$c_{Housner}$	9	2	29 %	3	-4	57 %	6.5	-0.5	7 %
		c_{Exp}	8	1	14 %	6	-1	14 %			
	20	Laboratory	0			0			0		
		$c_{Housner}$	0	0	-	0	0	-	0	0	-
		c_{Exp}	0	0	-	0	0	-			

Table 8.3: Comparison of mean and median values for different offset correction method, values of overturns are *excluded*. *Both* accelerations *and* maximum rocking angle are offset corrected with either first 100 or detrend method. Green values denote relative error less than 10 %, orange values between 10 % and 20 % and red values larger than 20 %. First 100 values are comparable to the all CDF and box plots in part III if not stated otherwise.
The mean values show small relative errors for prototype scales H5m and H10m. For all scales the mean is better predicted than the median. The mean values are either higher than or almost equal to the median values for all results. For the detrend method some of the medians are slightly higher. For scale H20m there are notable relative errors on predictions of both mean and median, but the nominal differences are in the range of the uncertainty in measurements.

			Mean μ [-]						**Median Q50 [-]**					
			First 100			**Detrend**			**First 100**			**Detrend**		
	H	**Response**	μ	Δ	$\frac{\lvert\Delta\rvert}{\mu}$	μ	Δ	$\frac{\lvert\Delta\rvert}{\mu}$	Q	Δ	$\frac{\lvert\Delta\rvert}{Q}$	Q	Δ	$\frac{\lvert\Delta\rvert}{Q}$
El Centro	5	Laboratory	0.46			0.46			0.46			0.46		
		$c_{Housner}$	0.45	-0.01	3 %	0.47	0.02	3 %	0.42	-0.04	10 %	0.49	0.03	7 %
		c_{Exp}	0.51	0.05	10 %	0.48	0.02	4 %	0.52	0.06	13 %	0.48	0.02	4 %
	10	Laboratory	0.31			0.31			0.25			0.25		
		$c_{Housner}$	0.31	0.00	1 %	0.31	0.00	1 %	0.28	0.03	12 %	0.27	0.02	9 %
		c_{Exp}	0.31	0.00	0 %	0.33	0.02	5 %	0.29	0.04	17 %	0.30	0.05	19 %
	20	Laboratory	0.08			0.08			0.03			0.03		
		$c_{Housner}$	0.06	-0.02	28 %	0.06	-0.02	28 %	0.02	-0.01	42 %	0.02	-0.01	37 %
		c_{Exp}	0.07	-0.01	17 %	0.06	-0.01	18 %	0.02	-0.01	39 %	0.02	-0.01	40 %
Lefkada	5	Laboratory	0.58			0.57			0.55			0.55		
		$c_{Housner}$	0.58	0.00	0 %	0.59	0.02	3 %	0.57	0.02	4 %	0.60	0.05	9 %
		c_{Exp}	0.61	0.04	6 %	0.61	0.04	7 %	0.61	0.06	11 %	0.62	0.08	14 %
	10	Laboratory	0.38			0.38			0.36			0.36		
		$c_{Housner}$	0.33	-0.05	13 %	0.37	-0.01	2 %	0.33	-0.03	8 %	0.34	-0.02	5 %
		c_{Exp}	0.37	-0.02	4 %	0.38	0.00	0 %	0.35	-0.01	3 %	0.35	-0.01	1 %
	20	Laboratory	0.12			0.12			0.08			0.08		
		$c_{Housner}$	0.14	0.02	13 %	0.14	0.02	14 %	0.11	0.03	39 %	0.11	0.03	39 %
		c_{Exp}	0.14	0.02	18 %	0.16	0.03	28 %	0.12	0.04	44 %	0.13	0.05	57 %

8.10 Comparison of Offset Methods

Both measured accelerations and measured rocking angle signals are given with offset values that are assumed to be constant. For the results in all plots in part III the values are based on signals that are offset corrected by subtracting the mean value of the first 100 data points, see chapter 5. Thereafter the acceleration signals are further manipulated by calculation of main component and cutting. The post processed acceleration signal is used as input for the numeric rocking response model, which is known to be sensitive to all parameters. All these steps of numeric manipulation of the signal are associated with uncertainty and possible propagation of error. Additionally the accuracy of the accelerometers and of the discretization of the acceleration signal is not determined.

A second offset correction method is applied on both rocking angle and acceleration signals to compare how the results are affected. The second method is based on the built-in MATLAB function `detrend` [10]. This method computes the least-squares fit of a straight line, which might have a slope, and subtracts it from the the original signal. The detrend function bases thus the offset on all data points in the signal, while the first 100 method only bases the offset on the first 100 data points.

Comparison of Overturning In table 8.2 the probability of overturning is compared for offset correction by the methods first 100 and `detrend`. The laboratory values for number of overturns are equal for both methods since this is based on a count of discrete cases: either does it overturn or not. There is no uncertainty in measuring this quantity. On the other hand, are the numbers of overturns definitely not equal for the predictions based on different methods. By comparing the values for El Centro H5m predictions based on c_{Housner} it is observed that the number of overturning is reduced from 45 to 35 only by correcting the offset of the acceleration signals. For El Centro H5m predictions based on c_{Exp} the opposite effect is observed: the number of overturning is increased from 37 to 42. Also for the three other ensembles where overturning were observed, a similar, unpredictable effect is seen. See also CDF plots in figure 8.24 and 8.25.

Figure 8.20 to 8.23 show two examples of how the predicted rocking response is significantly changed by input accelerations calculated with different offset correction method. All other parameters are identical. The maximum and minimum accelerations differ only to the third decimal when comparing the offset methods. In figure 8.21 the lower response show

overturning after short time, where the upper response at same time shows low amplitude rocking and do not overturn at all. In figure 8.23 the predicted responses are similar for the first 6 seconds, but the lower overturns while the upper remains rocking.

The probability of overturning could also be estimated based on an average of all predictions. The predicted results from the four combinations of c_{Housner}, c_{Exp}, first 100 and detrend method lead to a set of 400 results. The uncertainty of the calculated probability deceases by increased size of the set of values. The average results are presented in table 8.2. For both prototype scales for Lefkada the error is reduced to 7 %. Especially for Lefkada H10m is the reduction notable, from errors between 14 % and 57 % down to 7 %. The four original predictions were both larger and smaller than the laboratory value, thus the obtained error is smaller than all previous errors. For the three other ensembles the obtained errors are smaller than the original maximum errors, but here two or three of the original predicted errors are smaller. Nevertheless, the probability based on average of a larger set of results, lead in general to better predictions and smaller errors.

Comparison of Maximum Rocking Angle Table 8.3 shows mean and median values for the maximum rocking angle calculated with different offset correction methods. Here *both* accelerations *and* maximum rocking angle are offset corrected with either first 100 or detrend method.

Consider first the measured laboratory values. When all laboratory mean and median values are compared, they are equal to the second decimal, except for Lefkada H5m where the mean differ with 0.005 and the highest value is rounded up. When comparing each of the 700 measured results with each other, the maximum difference is $5.3 \cdot 10^{-2}$ and the average difference is $2.2 \cdot 10^{-3}$. Thus there is at least an uncertainty of measurement of rocking angle in the third decimal.

Consider now the predicted median and mean values. Even though a change in the measured accelerations can lead to significant differences regarding overturning, the same significance is not observed for mean and median values. In fact, all values are equal to the first decimal or have a difference lower than 0.07. The errors on predictions on mean and median values are in general small for H5m and H10m. Especially the mean is good predicted with errors less than 13 %. For H20m the relative error on predictions are larger, but because of the uncertainty of angle measurements on the second or third decimal, the predictions are hard to fit to the laboratory tests. As seen in figure 8.24 and 8.25, the rest of the distributions

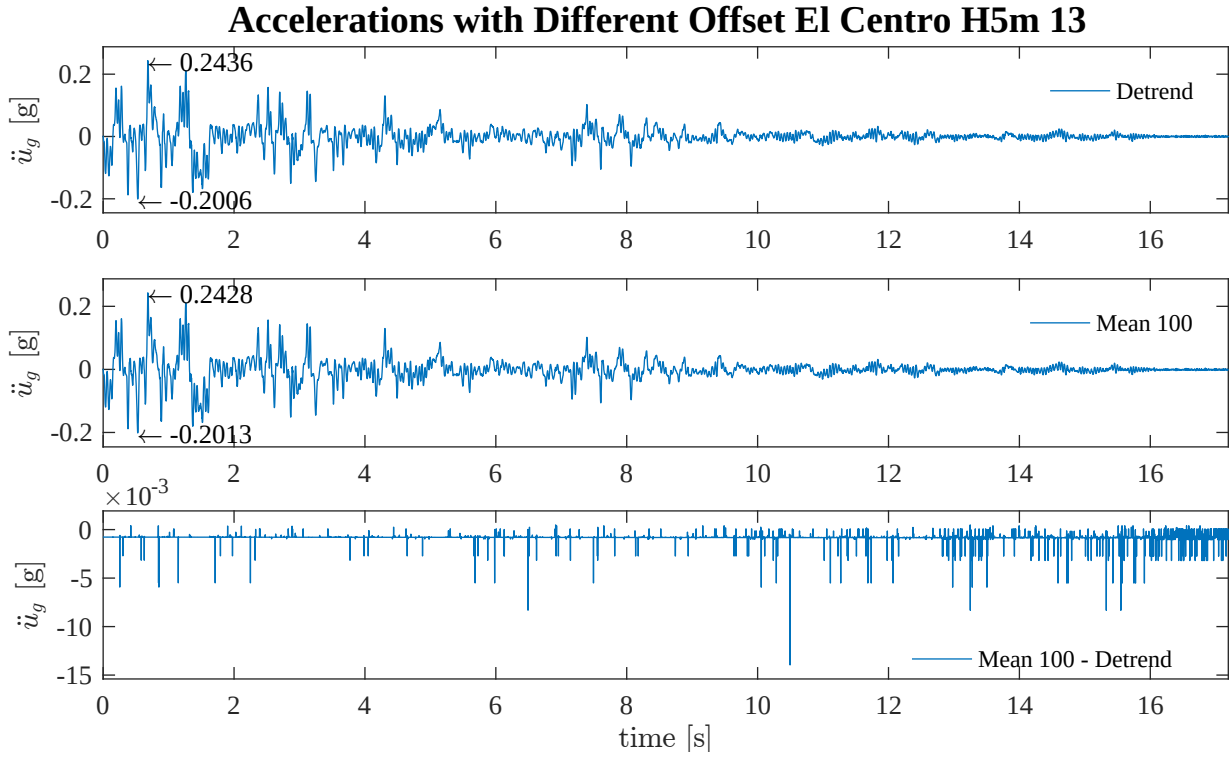

Figure 8.20: Different method of offset correction of accelerations leads to slightly different accelerations, which in turn leads to significantly changed rocking response.

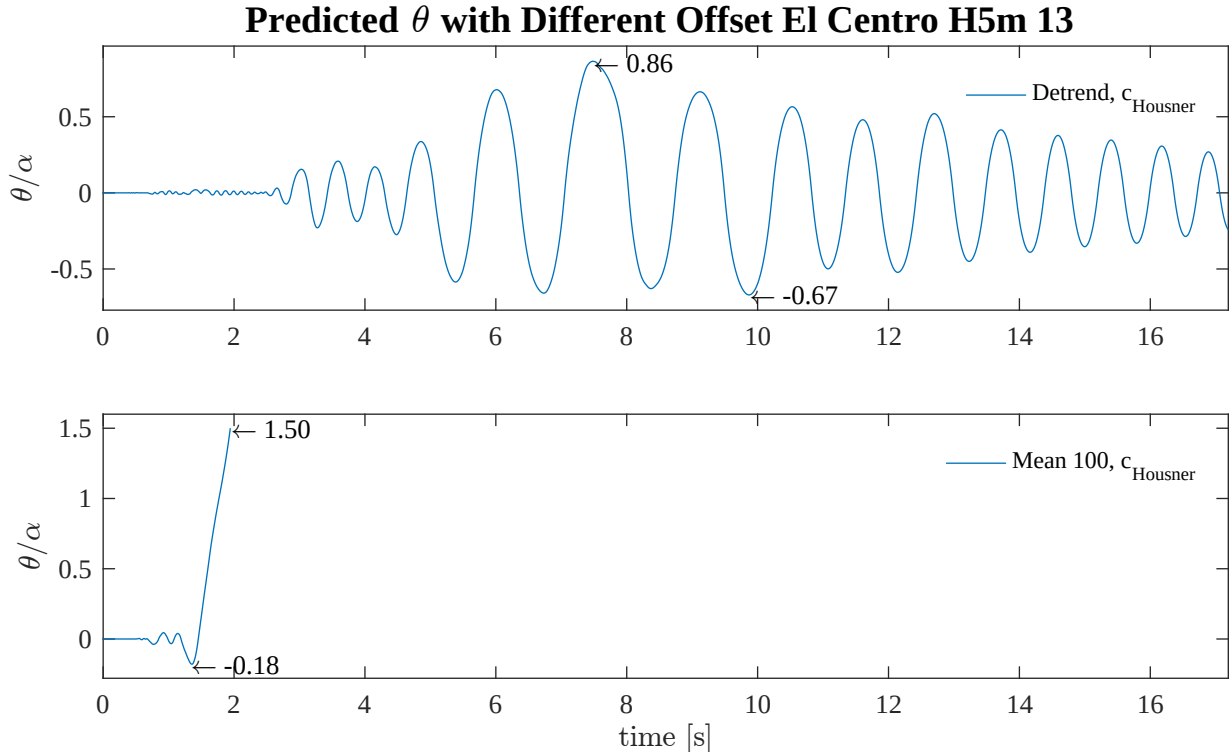

Figure 8.21: Different response for changed method of acceleration offset correction. The upper plot shows almost no rocking for $t < 3$ seconds, while the lower plot shows overturning after less than 2 seconds.

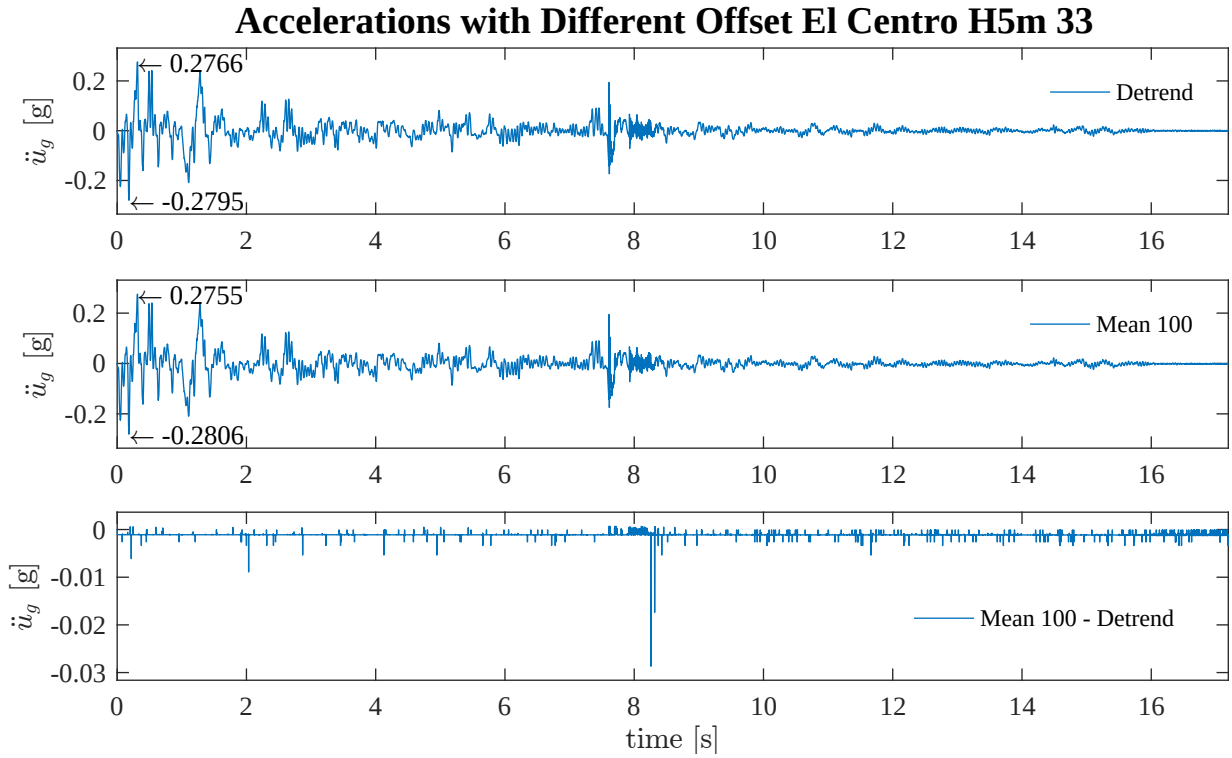

Figure 8.22: Different method of offset correction of accelerations leads to slightly different accelerations, which in turn leads to significantly changed rocking response.

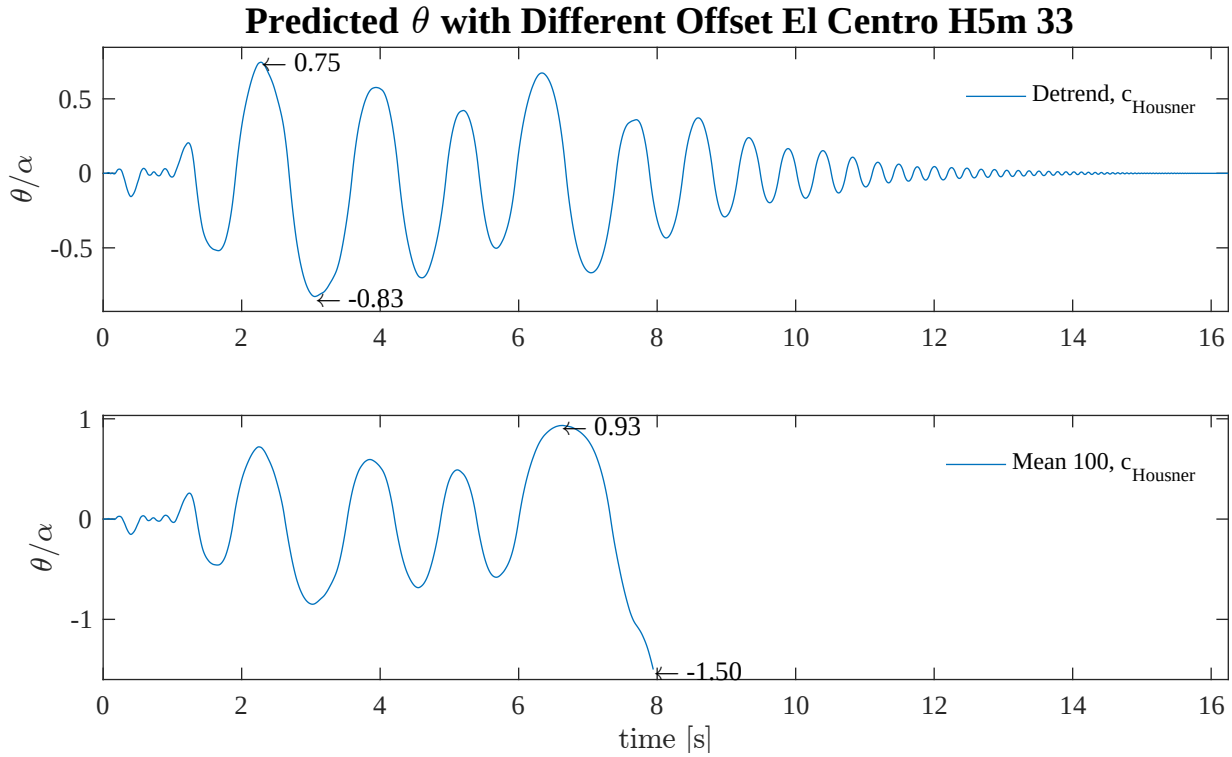

Figure 8.23: Different response for changed method of acceleration offset correction. The two plots show similar responses for 6 seconds, then they diverge.

are well fitted and comparable to the distributions obtained with first 100 offset correction.

Conclusions As seen on the moment diagram in figure 2.2, the seismic resistance is very low for rocking angles close to the critical slenderness angle α. Due to the negative stiffness, a higher angle will lead to even lower resistance. Thus only slight differences in any parameter determining the rocking motion, can affect the response to either overturn or not overturn. Thus rocking motions that attain rocking angles close to α, are much more sensitive to any changes of parameters than for lower rocking angles.

Based on the values and observations that are presented, there is no clear trend regarding which offset correction method that is more correct. However, it is observed that numbers of overturning are notably sensitive to small changes in accelerations. The median and mean values are on the other hand only slightly affected by changes in accelerations. The differences in predicted mean and median values are in the same range as the uncertainty in measurements of rocking angle.

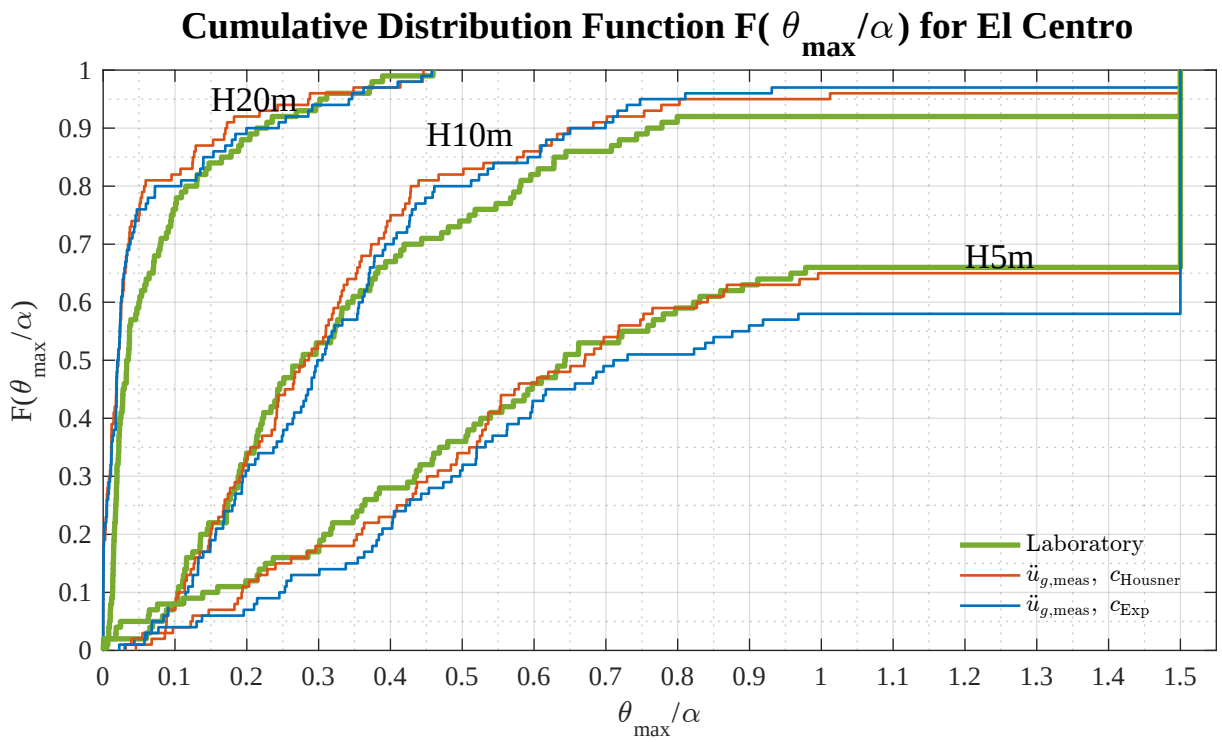

Figure 8.24: Empirical CDF for El Centro with *detrend* offset correction method on both accelerations and rocking angle. There is a close fit for all prototype scales and no significant differences on the distribution of maximum response compared with figure 8.1(b). Notice the difference of predictions of overturning for changed offset method: for H5m the blue line is lower and predicts with most error. In figure 8.1(b) the red line shows similar error.

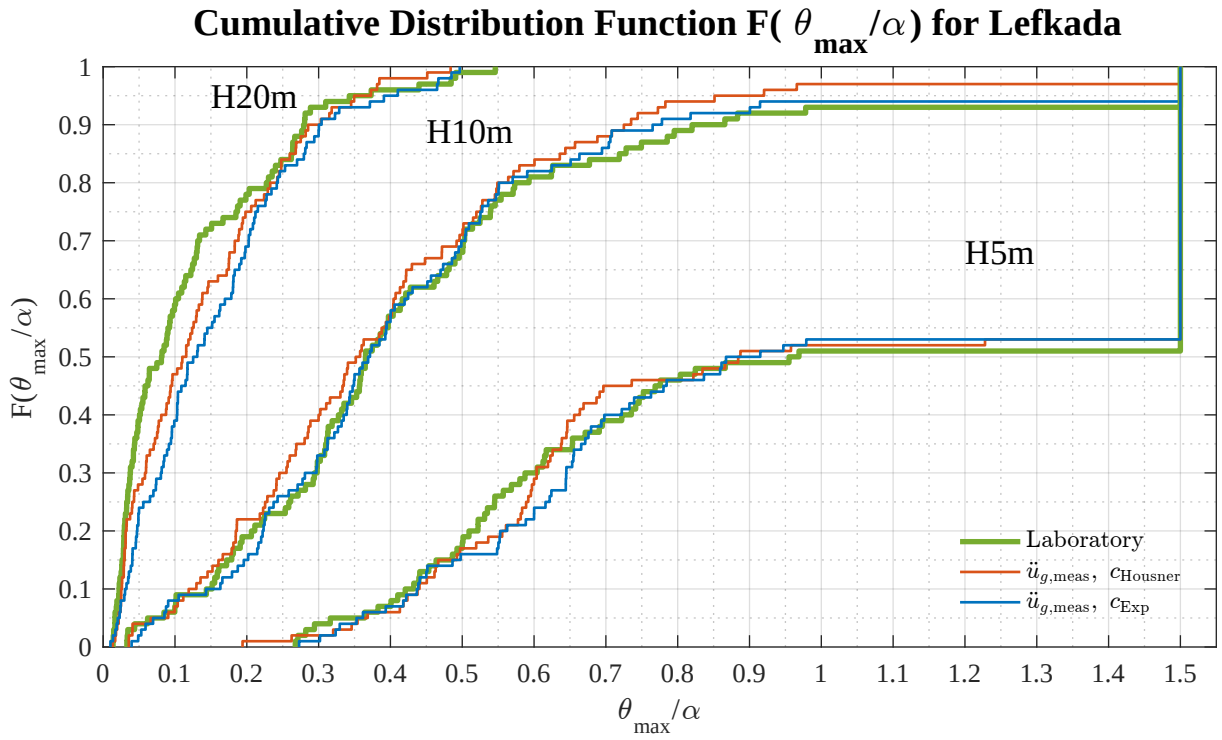

Figure 8.25: Empirical CDF for Lefkada with *detrend* offset correction method on both accelerations and rocking angle. There is a close fit for all prototype scales and no significant differences on the distribution of maximum response compared with figure 8.2(b). An exception is the red line of H5m for $0.5 < \theta_{max}/\alpha < 0.8$. Notice also the difference of predictions of overturning for changed offset method: for H5m the blue and red line line predicts the overturning with small errors. In figure 8.2(b) the red line shows a significantly larger value and error.

Chapter 9

Discussion of Results

9.1 Could the Maximum Rocking Response Be Predicted?

In the presented results there is a significant correlation between the distribution of maximum rocking response for predicted and laboratory results. The ensembles that are used as input for the numerical predictions, are shown to share the same statistical properties by studying energy distributions and elastic response spectra. As seen on the CDF plots, the graphs are similar and have similar variations of slopes and thus similar variations of probability density. As seen on the box plots the distribution represented by quartile values are similar and given with nominal errors less than 0.07α. The means are even better predicted with nominal error less than 0.05α.

El Centro H20m are not so well predicted considering relative errors. On the other hand when nominal errors are considered, these small differences of less than 0.04α on quartile values, might be explained by inaccuracies in measurements, elastic vibrations or inaccuracies in the uplift criterion. About 2×19 of the lowest predicted values are so small that the measurements of a similar physical rocking response, would be dominated by noise.

The ensemble El Centro H5m was tested two times. First with a test specimen that did not have a stable foundation. This unstable foundation lead to that assumptions about initial conditions and uplift criterion in the numeric model, did not represent those of the motion that was measured. If only the median and mean values were compared, the prediction errors were comparable to those results based on test specimens with stable foundations. By studying CDF and box plots, the differences in the rest of the distribution become more evident. Consequently, the central tendency could be well fitted by coincidence. The rest

of the distribution should be investigated to validate the correlation of the predictions with the laboratory results. When the ensemble was retested with the second test specimen, the predicted distributions were closely fitted.

Variation of the damping parameter, coefficient of restitution, is also explored. c_{Housner} implies that around 0.7 % more energy is lost on each impact compared with c_{Exp}. On the CDF plots the red line of c_{Housner} is in general to the left of the blue line for predictions with c_{Exp}. The same effect is seen on the box plots where the box of c_{Housner} in most cases have smaller quartile values than that of c_{Exp}. These observations imply smaller, non-conservative results for higher damping. When the response to only one acceleration signal is tested, increasing the damping might lead to both higher and lower maximum response, thus the effect seems unpredictable. Nonetheless, from these statistical observations there is a clear trend that higher damping, given by lower coefficient of restitution, leads to smaller maximum rocking responses for the whole ensemble of ground motions. Moreover the distribution of maximum response is predicted to shift to smaller values when the damping is increased.

The measured accelerations that are used as input for the numerical model, are numerically manipulated by discretization, offset correction, calculation of main component and cutting. By changing the method of offset correction of the acceleration signals, the final accelerations that were used as input were only slightly changed. Nevertheless, the effect of this change could be significant for each time history. When the effect of an entire ensemble is compared, the difference in the predicted distributions are observable, but not significant. If only means and medians are compared, there are observed slight differences to the second decimal, but the error is in the same range for both offset methods. The offset correction of the rocking angle is compared with the same methods, and the difference for the measurements are only observable to the third decimal. To conclude, small differences in the input acceleration signal could affect each time history response drastically. When the distribution of maximum rocking response is considered, a small difference in accelerations does not affect the distribution significantly. Also for changes of accelerations: the effect that is unpredictable on the individual level, is more predictable on the distribution of maximum response.

Conclusions

Could the mean of maximum rocking response of a rigid rocking oscillator be predicted when subjected to an ensemble of ground motions with similar statistical properties?

Based on the results here presented, there is a clear trend substantiating that the distribution of maximum rocking response, excluding overturn values, could be predicted. For the lowest prototypes, H5m and H10m, the mean and median values are predicted with low errors for both ground motions. The nominal errors are in the range of $\pm 0.08\alpha$, while the relative errors are in the range of $\pm 19\,\%$. The mean values are in general found to be higher than the median values, and are thus conservative predictions of the central tendency. Both when nominal and relative errors are considered, the mean values are best fitted.

For the highest prototype, H20m, the maximum rocking angles are small, 75 % of the values are lower than 0.10α for El Centro and 0.19α for Lefkada (measured values). Thus disturbances or errors from measurements, elastic vibrations or other flawed assumptions are more dominant in the measured value that is interpreted as maximum rocking angle. Even though the relative errors on quartile and mean values are as high as 80 %, the nominal errors are in the range of $\pm 0.05\alpha$, which is comparable to the other prototype scales.

Small changes of the input parameters coefficient of restitution and acceleration are shown to potentially change each time history significantly. But when the response on a whole ensemble is considered, the distributions are only affected to a low degree. The effect of a parameter change that is unpredictable on the individual level, is shown to be more predictable on the distribution of maximum response. These findings support the view that maximum rocking response could be predicted in a statistical manner.

Further Studies

The largest relative errors are experienced for the prototype scales H20m. The different possible error sources should be further explored. First of all the uncertainty of the optical measurements and acceleration recordings should be more accurately determined. Secondly the offset correction methods should be further investigated to obtain the most correct results. An experimental value for the uplift criterion could also be determined to possibly improve the numerical predictions for input accelerations with low peak values. If the test specimen is subjected to various ground motions with peak accelerations lower than the experimental uplift criterion, it could be verified whether there are elastic vibrations in the column that

could be measured by the NDI system or not.

9.2 Could the Probability of Overturning Be Predicted?

In the results presented in this project, the probability of overturning is predicted with significant discrepancy. For El Centro H5m the laboratory probability of 34 % was predicted with values varying from 35 % to 45 %, which equals a relative error up to 32 %. The values for Lefkada H5m were closer fitted. The probability of 49 % in the laboratory was predicted with values between 40 % and 48 %, which equals a relative error up to 18 %. For the prototype scale H10m for El Centro and Lefkada the laboratory values are 8 % and 7 % and the predictions are calculated with nominal errors up to 5 % and 4 %, which leads to relative errors up to 63 %. When an average value is calculated based on the 400 predictions, the estimate of probability of overturning is better predicted.

When the coefficient of restitution is slightly changed, the probability of overturning is drastically changed with an ensemble size of 100. For H5m for both El Centro and Lefkada the number of overturns was changed by 8 by increased damping. The changes were however in different directions: more overturns for El Centro and less for Lefkada. With changed method of offset correction there was observed large changes in the number of overturns, but for El Centro H5m the effect of changed damping was reversed compared to the predictions with first 100 offset correction. The effect of changed parameters on overturning is observed to be highly unpredictable with the limited number of tests.

The effect of changed damping on maximum rocking response was investigated by comparing distributions of a continuous variable. For the overturning phenomenon the effect is studied by comparing the count of a final, binary outcome only. This method is comparable to draw conclusions on maximum rocking response considering mean values only, which could lead to flawed conclusions. The overturning phenomenon could be better understood by comparing more variables, as proposed later.

Conclusions

Could the probability of overturning of a rigid rocking oscillator be predicted when subjected to an ensemble of ground motions with similar statistical properties?

Based on the observations that are presented, we can conclude that overturning is very

sensitive to small changes in the parameters determining the rocking motion. The predictions of probability of overturning that are obtained, are inaccurate and associated with large uncertainty. When only an ensemble of 100 ground motions are used as basis for comparison, small variations of coefficient of restitution or accelerations lead to significant changes on the number of overturns. There is observed no clear trend to substantiate which effect increased damping has on overturning. On the contrary, when only numbers of overturning are compared, the effect thereof seems highly unpredictable.

The obtained prediction of overturning is shown to be uncertain and highly sensitive to small changes in coefficient of restitution or accelerations. Based on a limited number of 100 predictions, the probability of overturning is not well estimated. The results that are observed, call in to question whether the probability of overturning could be predicted with the limited number of 100 tests. The estimates on overturning could presumably be improved by increasing the number of test or by studying overturning with more than one variable.

Further Studies

So far the probability of overturning is determined by a discrete variable with only two outcomes: either overturning or sustained and transient rocking. This is a crude approach of quantifying the overturning phenomenon. By the limited number of 100 predictions, the accuracy of the predictions was poor and the uncertainty was large. By increasing the number of predicted results to 400, the predictions became better. By increasing the number of predicted results even more, the estimated probability will most likely converge to the probability observed in the laboratory. This approach is then based on the assumption that the numerical model is able to predict the overturning phenomenon accurately. Even though the maximum response that do not lead to overturning, is well predicted by the numerical model, it might be that the instability leading to overturn is not well implemented by the numerical model.

A possible approach to increase the numbers of predictions is to increase the amount of accelerations that the numerical predictions are based on. Every measured acceleration signal of an ensemble could be used as a basis to generate e.g. 9 new artificial accelerations. Thus an original ensemble of 100 ground motions is increased to 1000 ground motions. If we assume that these 1000 ground motions share the same statistical properties, they could be used to predict the probability of overturning with possibly increased accuracy and reduced

uncertainty.

Angular Velocity For rocking angles close to the critical angle α, the seismic resistance is very low. For $\theta = \alpha$ the seismic resistance is zero and for $\theta > \alpha$ gravity increases the rocking angle until the column falls to the ground, see the moment diagram in figure 2.2. Due to the low or possibly no resistance only a slight change of a parameter that determine the motion, might drastically change the outcome. For lower rocking angles the seismic resistance is higher, and the effect of a little parameter difference is not critical to the same extent. If the angular velocity $\dot{\theta}$ is large when the rocking angle approaches α, the response will for most cases lead to overturning. In such a case one might assume that a slight change in a parameter will not change the outcome and the column overturns anyhow because of a large angular momentum. On the other hand if the angular velocity is small when the rocking angle approaches α, the outcome will be less predictable. If the column is at the verge of overturning and the angular velocity is approximately zero, even an infinitesimal change of acceleration would determine whether the column overturns or not.

Parameter Studies If the rocking phenomenon rather would be statistically analyzed with a second, continuous variable $\dot{\theta}$, more conclusions could be drawn. Then the distribution of the angular velocity of the response that overturned, could be determined and compared with results from numerical predictions. With this approach the effect of increased or decreased coefficient of restitution on overturning could be investigated by studying the distribution of angular velocity. Will an increased damping lead to lower angular velocities at the instant of overturning in an average sense? The conditional probability of overturning could be investigated considering the angular velocity. In the same manner the effect of slightly different input accelerations could be studied.

Until now the numerical values for R, λ and α have been deterministic. By applying structural reliability analysis, by e.g. Monte Carlo simulations, the parameters $\ddot{u}_g(t), R, \alpha, \lambda, c$ could be given as stochastic variables. In such a way could the overturning phenomenon be studied further in a stochastic manner. Also sensitivity analysis could be performed to determine which parameter that the overturning phenomenon is most sensitive to.

Chapter 10

Summary and Conclusions

10.1 Summary

In this master thesis statistical validation of a rigid body rocking response model is explored. Laboratory tests are performed on a shaking table, and the associated rocking response and accelerations are measured. The measured accelerations are used as input for the numerical predictions, and the results thereof are compared with the laboratory results.

Problem Description The problem description is based on the fact that the rocking response model in question is not able to predict the entire time history with sufficient accuracy. Moreover the response is very sensitive to all parameters that determine the motion. The main goal of this project is to explore whether the response of a rigid rocking oscillator to an ensemble of ground motions with the same statistical properties can be predicted by the numerical model in terms of average quantities.

A rigid rocking column has only one degree of freedom: the rocking angle θ. The motion could either be unstable and overturn, or secondly the rocking column could exhibit stable and transient rocking. In the former case the number of overturns is counted to calculate the probability of overturning. In the latter case the maximum, absolute rocking angle $|\theta_{\max}|$ is determined. Instead of predicting the response of the rigid rocking column subjected to one ground motion, the column is subjected to an ensemble of ground motions that have the same statistical properties. Could the probability of overturning and the average maximum rocking response be predicted in this case?

Rocking Motion The motion of a rocking oscillator differs substantially from the motion of a more common elastic oscillator. First of all the stiffness is negative. This means that by increasing the deformation, the restoring force decreases. Moreover, for large angles there is almost no resistance, which makes the response very sensitive in the large angle range. Secondly, while elastic oscillator restores the motion by elastic forces, the rocking oscillator restores by gravity. Thirdly, the taller the structure, the more stable it is, given same slenderness. This third fact is caused by that the rocking structure mobilizes rotational inertia, which increases proportionally to the square of the height. The seismic demand, on the other hand, increases by the first order of the height. The rocking response model to be tested, predicts the motion by solving a nonlinear differential equation. The parameters for the equation are based on size, slenderness, damping and distribution of mass of the rigid column. The load is given as ground accelerations. In this project overturning is defined as maximum rocking angle larger than 1.5 times the critical angle α.

Ground Motions The two earthquake ground motions El Centro and Lefkada are used as a basis for generation of two ensembles of 100 artificial ground motions. Each ensemble is generated by random Fourier series such that the time variation of the frequency content and the intensity is similar within the ensemble, and such statistically similar. The physical column that is tested in the lab has a height of $H_{\text{experimental}} = 0.5$ m. We want to experimentally test the response of prototypes with heights $H = H_{\text{prototype}}$ of 5, 10 and 20 meters. By dimensionless analysis the time vector could be downscaled by a factor $\sqrt{0.5/H}$ such that the same simulations could be used for each prototype.

Experiments The test specimen consists of two hollow aluminum columns that are connected at the top and bottom. The test specimen is placed onto the shaking table without any connection or attachment to the foundation. The 2×100 simulations to three different prototype scales are set into motion on the shaking table, in total 600 tests as a basis for comparison with numerical predictions. One ensemble of ground motions, El Centro H5m, was tested twice because of instability of the column foundation. Two optical markers are connected to the shaking table making a near-horizontal line, and two other optical markers are connected to the rocking column making a near-vertical line. An optical sensor measures the variation of the angle between the two marker lines. This variation is the rocking angle $\theta(t)$. The actual acceleration of the shaking table, $u_{g,\text{meas}}(t)$, is measured by accelerometers

and used as input for the numerical prediction.

Post Processing Both measured accelerations and rocking angles are given with a offset that needs to be estimated and subtracted to obtain physical values. The calculation of this offset is associated with uncertainty that affects the numerical predictions and the accuracy of the laboratory results. The numerical predictions are calculated with two different coefficients of restitution: one analytical Housner value and one experimental value. The experimental value for coefficient of restitution and an inertia factor are determined by fitting the numeric prediction to a measured free vibration response.

Same Statistical Properties of Accelerations The measured accelerations are analyzed by comparing distribution of energy and calculating elastic response spectra. There is an apparent correlation between the accelerations within each ensemble both in time and frequency domain. The accelerations are thus considered to share the same statistical properties within each ensemble. The elastic spectra of the accelerations that lead to overturning show no significant difference compared to the spectra of those accelerations that did not lead to overturning.

Results There is observed a clear correlation between the distributions of the predicted and measured maximum response. When only values excluding overturns are considered, the median and mean are well predicted for prototype scales H5m and H10m for both El Centro and Lefkada. The mean values are predicted with error less than 13 % and the medians with error less than 19 %. The error on the mean is in general smaller than for the median, and the mean values are in most cases larger than the median.

When the maximum response for prototype scale H20m is considered, the nominal errors are in the same range as for the other results. The relative errors are on the other hand high because the rocking angles are small. For El Centro is there observed a significant discrepancy for the 20 % lowest values. Possible error sources for these low values are uncertainty in optical measurements of rocking angle, inaccurate uplift condition or elastic vibrations of the test specimen. These errors might dominate the laboratory results leading to a poor correlation between the measured results and the numerical predictions for low values.

Small changes in the damping parameter or accelerations are shown to lead to small changes in the distribution of maximum response. Increased or decreased damping showed

additionally a predictable direction of the change of distribution.

Overturning was only observed for the prototype scales H5m and H20m. The probabilities of overturning was inaccurately predicted and associated with large uncertainty. Small changes of damping or acceleration signal lead to drastic, but highly unpredictable, changes of the estimated overturning probability.

10.2 Conclusions

Based on a limited number of 100 predictions, the maximum response of a rigid rocking oscillator could be well estimated by mean and median values for the prototype scales H5m and H10m. The mean and median values for the scale H20m show nominal prediction errors in the same range, but the predicted values are numerically small and prone to be dominated by numerical and physical disturbance. The mean values are in general found to be higher than the median values, and are thus conservative predictions of the central tendency. Both when nominal and relative errors are considered, the mean values are best fitted.

The effect of a parameter change that is unpredictable on the individual level, is shown to be more predictable on the distribution of maximum response. These findings support the view that maximum rocking response could be predicted in a statistical manner. The obtained prediction of overturning is uncertain and highly sensitive to small changes in coefficient of restitution or accelerations.

The obtained prediction of overturning is shown to be uncertain and highly sensitive to small changes in coefficient of restitution or accelerations. Based on a limited number of 100 predictions, the probability of overturning is not well estimated. The results that are observed, call in to question whether the probability of overturning could be predicted with the limited number of 100 tests. The estimates on overturning could presumably be improved by increasing the number of test or by studying overturning with more than one variable.

Appendix A

All Box Plots Gathered

All seven box plots are shown together in figure A.1 and A.2.

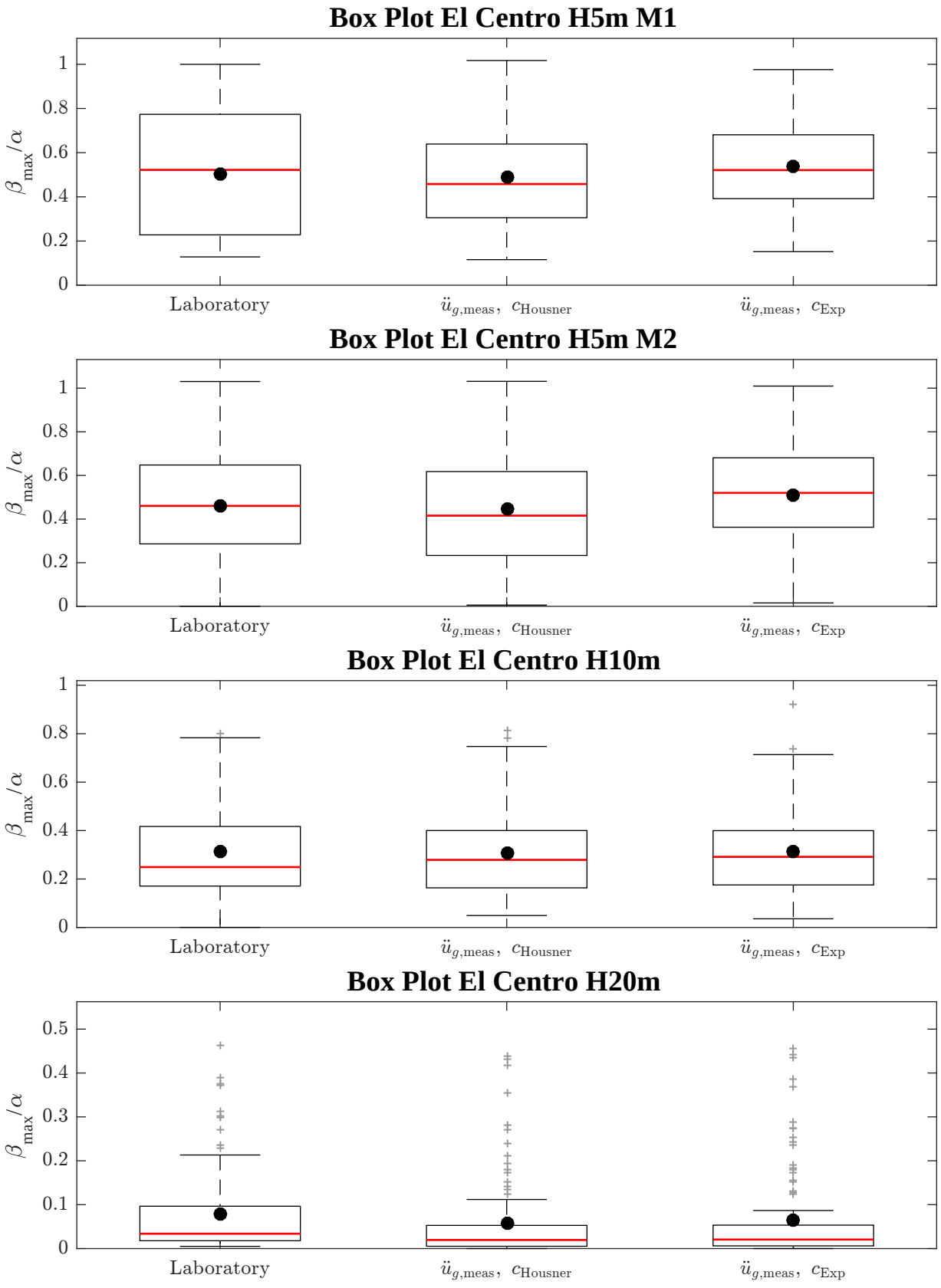

Figure A.1: All box plots for El Centro.

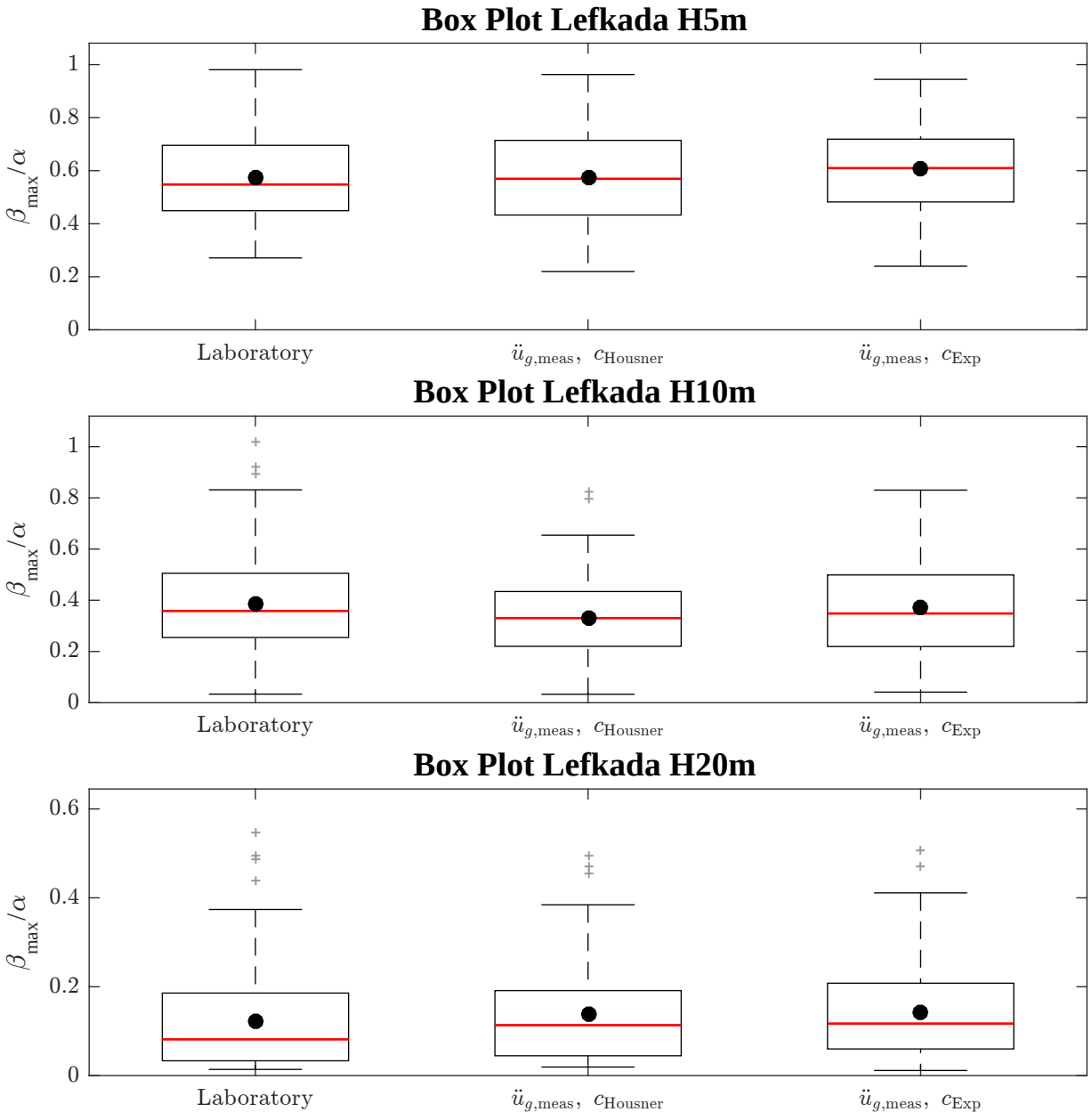

Figure A.2: All box plots for Lefkada.

Appendix B

CDF Plots Including Response to Simulated Accelerations

CDF plots for the seven different test groups are shown in figure B.1 to B.7 based on both measured and simulated accelerations and experimental and Housner coefficient of restitution. The predicted lines based on simulated accelerations do in general neither fit well to the laboratory lines nor to the lines based on measured accelerations.

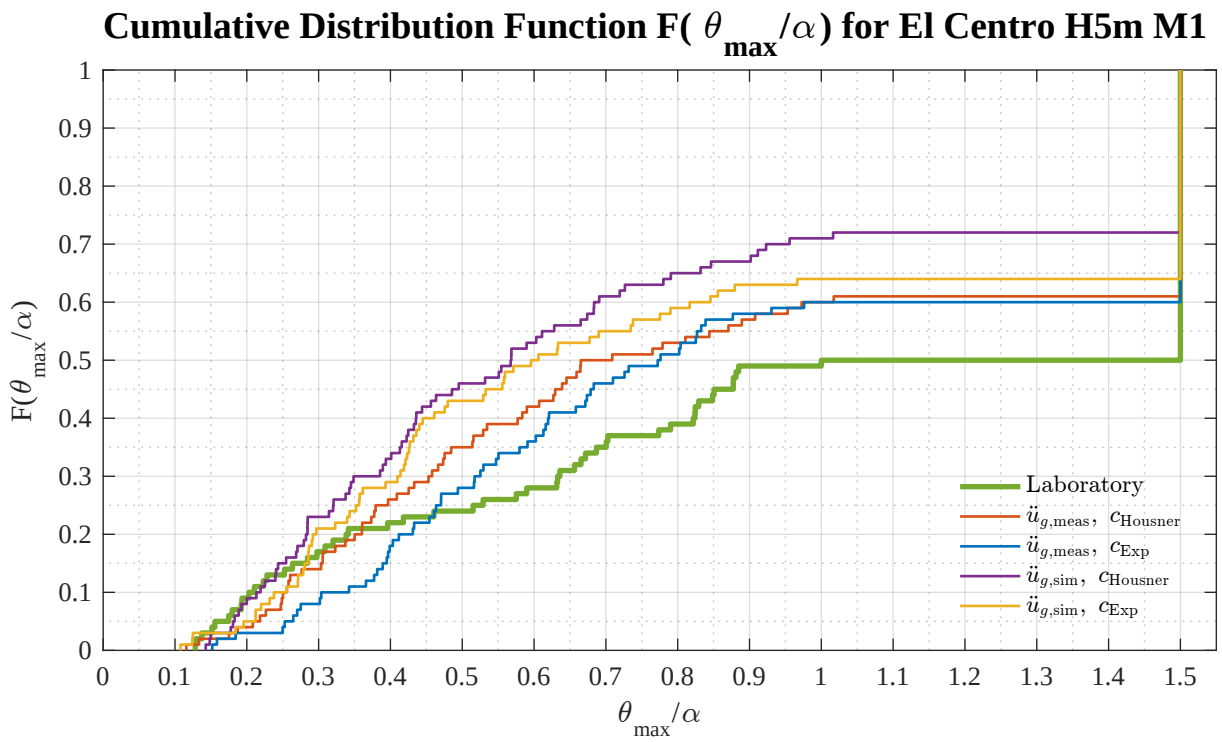

Figure B.1: Empirical CDF for El Centro H5m M1

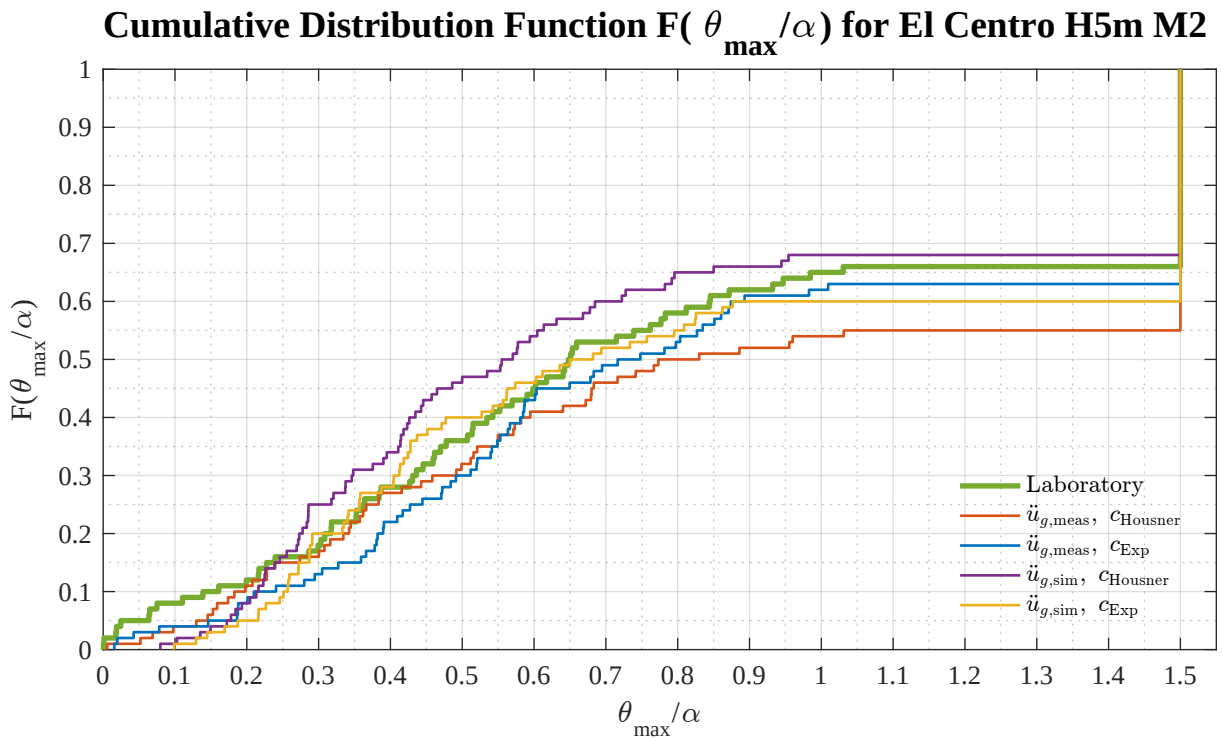

Figure B.2: CDF El Centro H5m M2

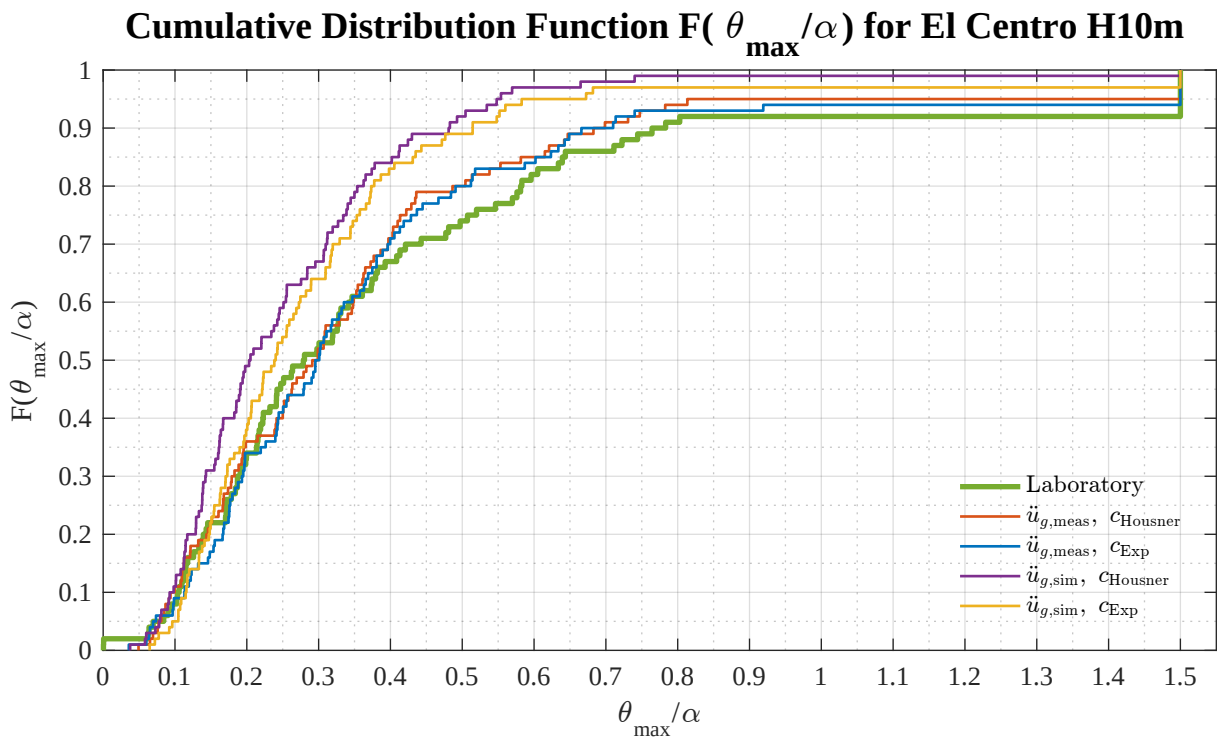

Figure B.3: Empirical CDF for El Centro H10m

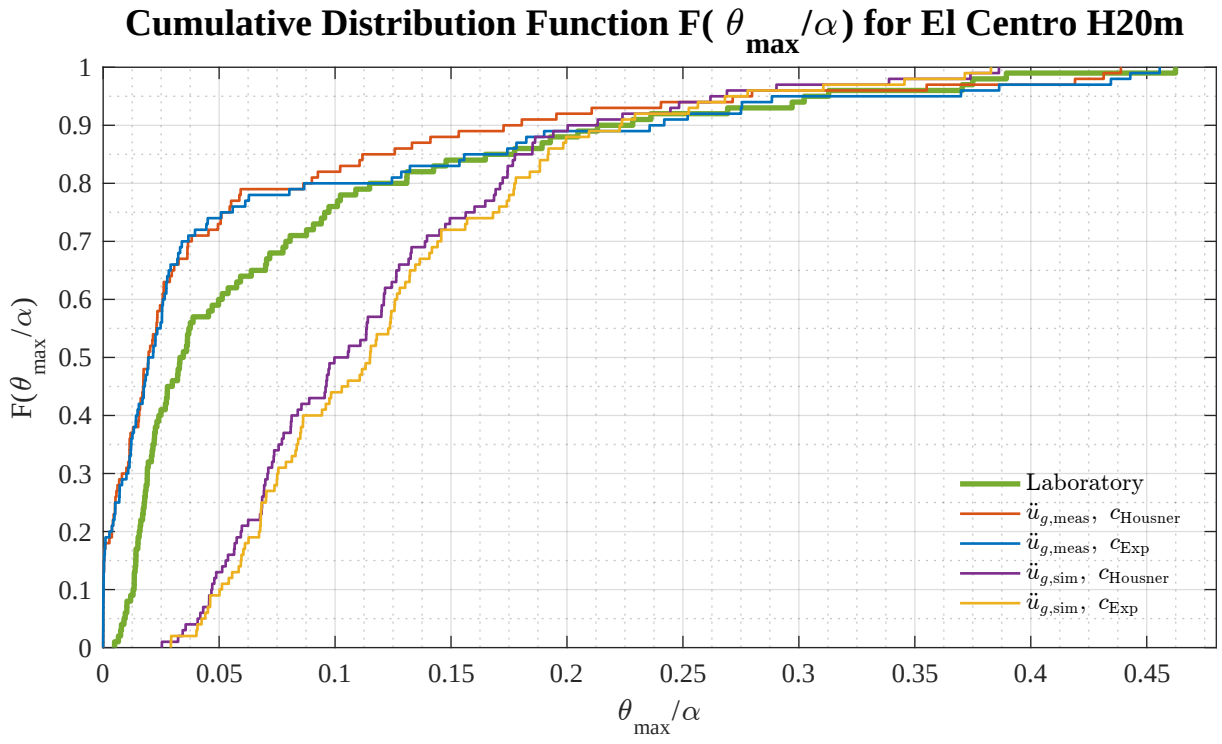

Figure B.4: Empirical CDF for El Centro H20m

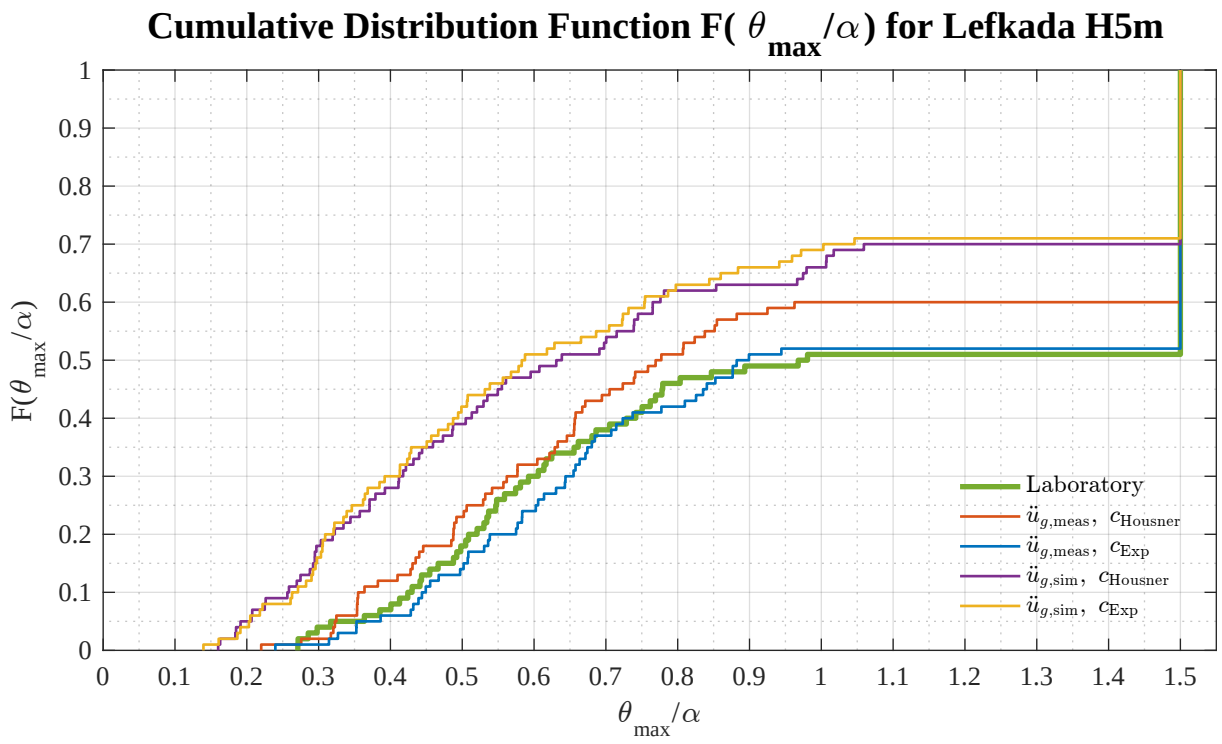

Figure B.5: Empirical CDF for Lefkada H5m

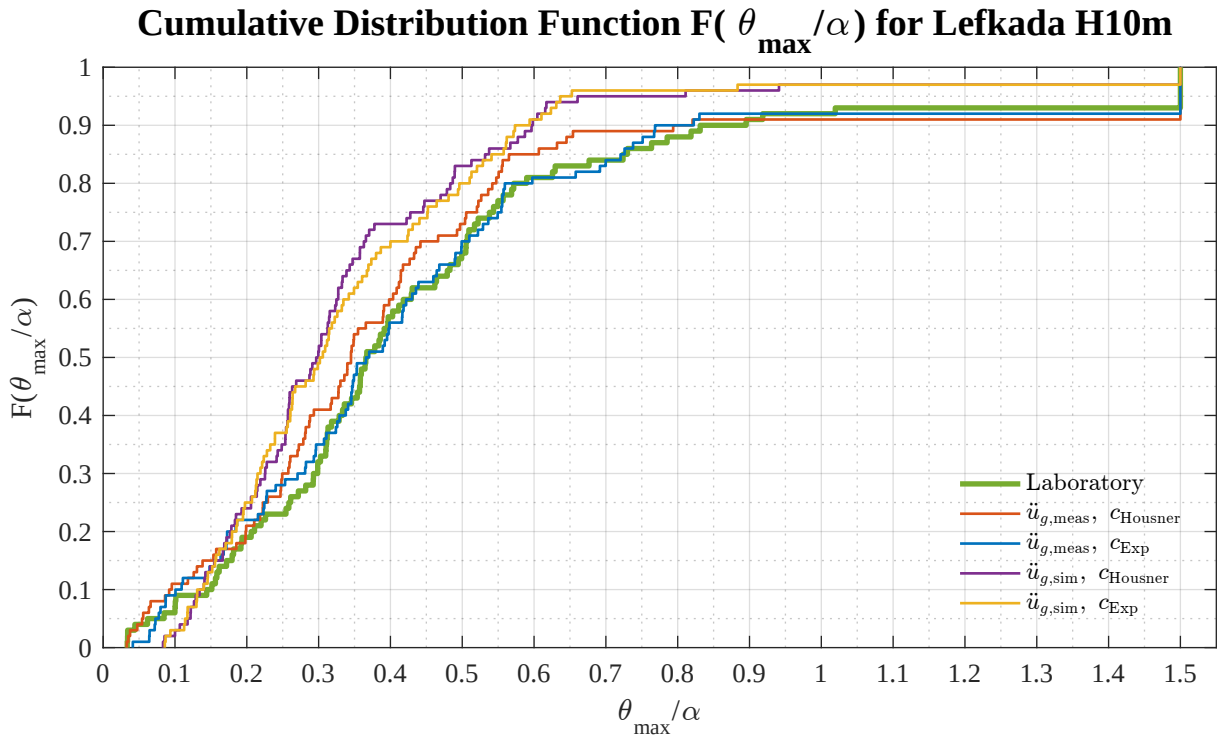

Figure B.6: Empirical CDF for Lefkada H10m

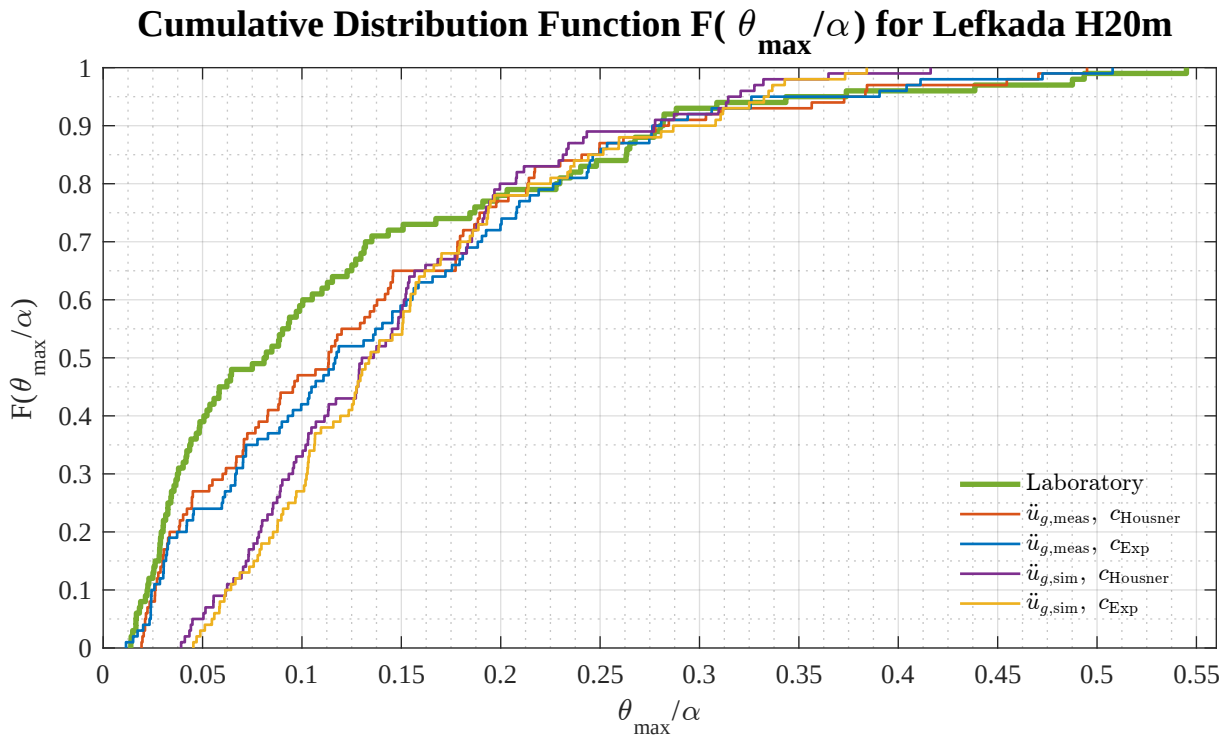

Figure B.7: Empirical CDF for Lefkada H20m

Appendix C

Numerical Response to Varying α-Values

The following CDF plots are calculated based on measured accelerations and Housner value for coefficient of restitution. The slenderness angle α attains three different values as $\alpha = \tan^{-1}[0.10 \quad 0.15 \quad 0.20]$ while all other parameters are as before.

As expected a more slender column exhibits a higher possibility of overturning and a larger maximum rocking angle and vice versa.

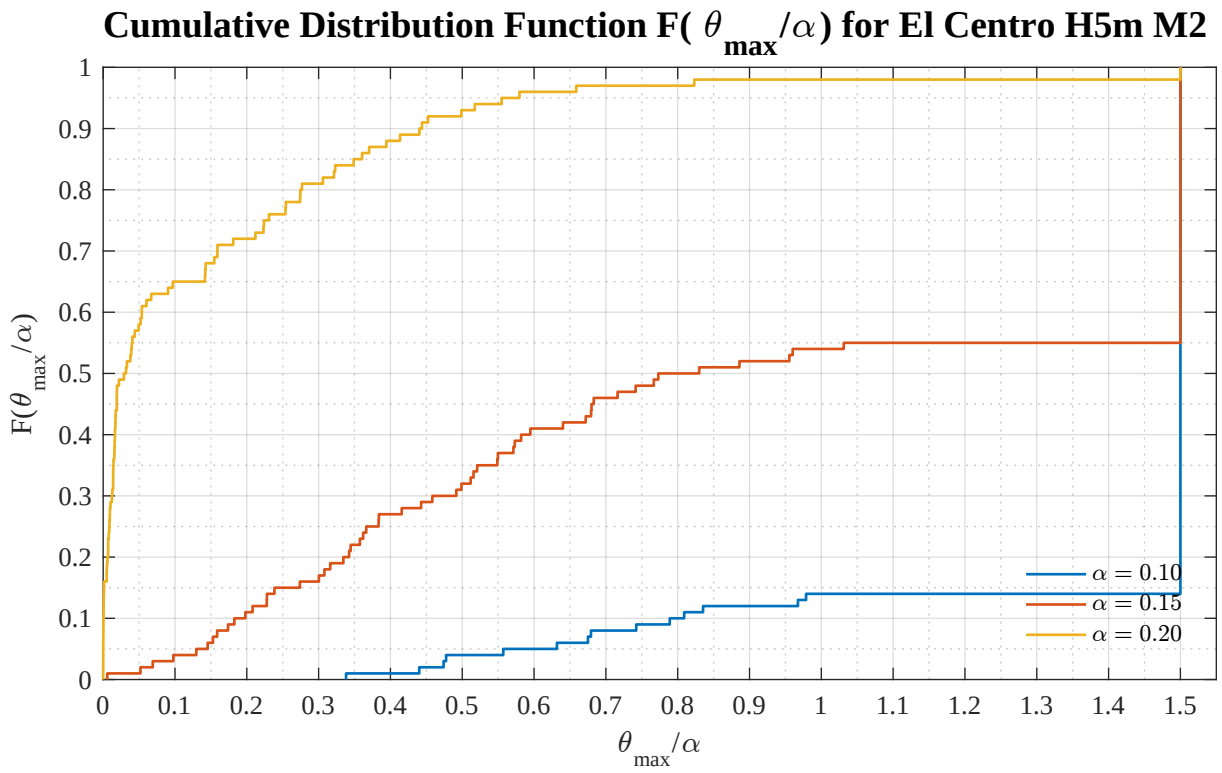

Figure C.1: Empirical CDF for varying α-Values El Centro H5m M2

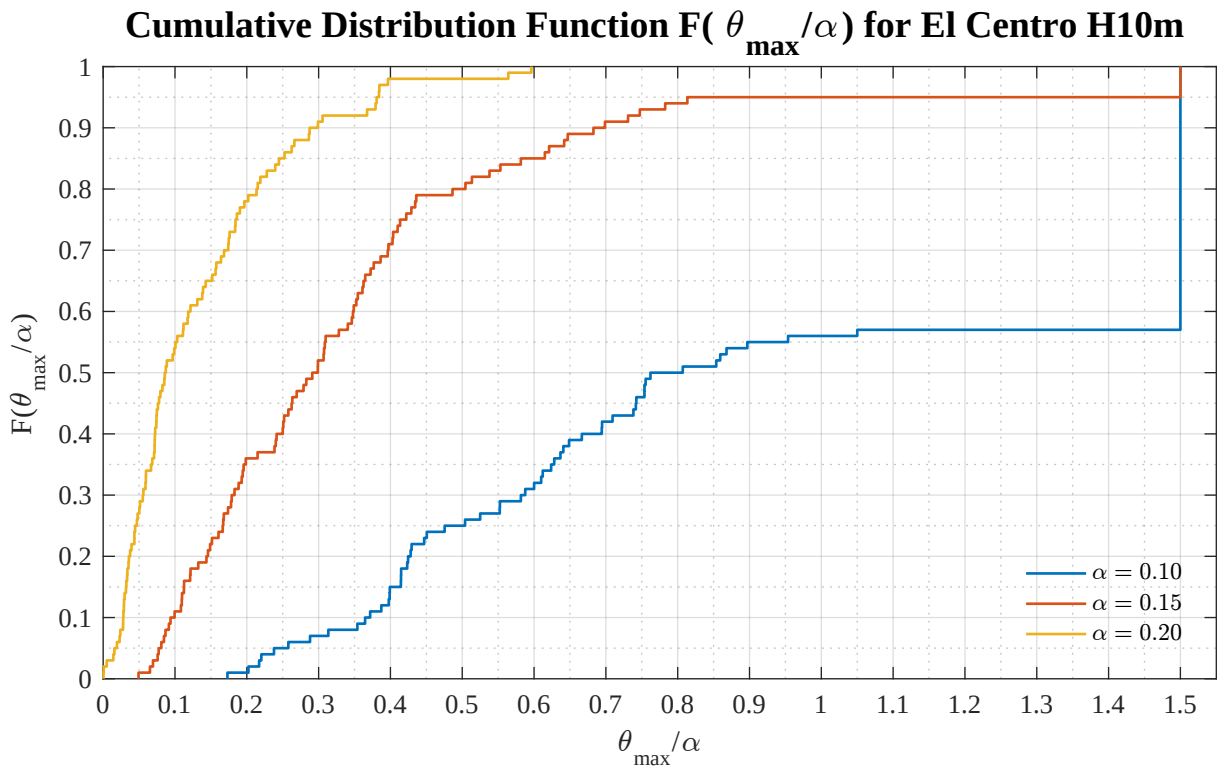

Figure C.2: Empirical CDF for varying α-Values El Centro H10m

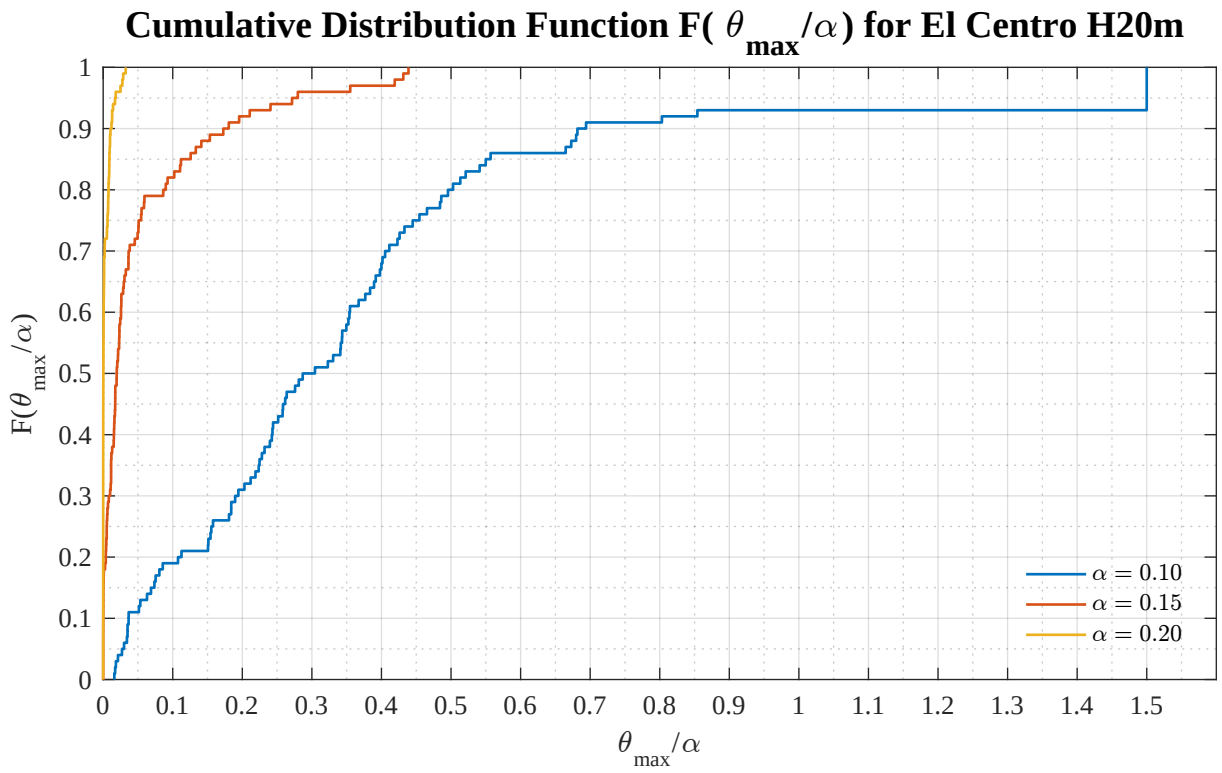

Figure C.3: Empirical CDF for varying α-Values El Centro H20m

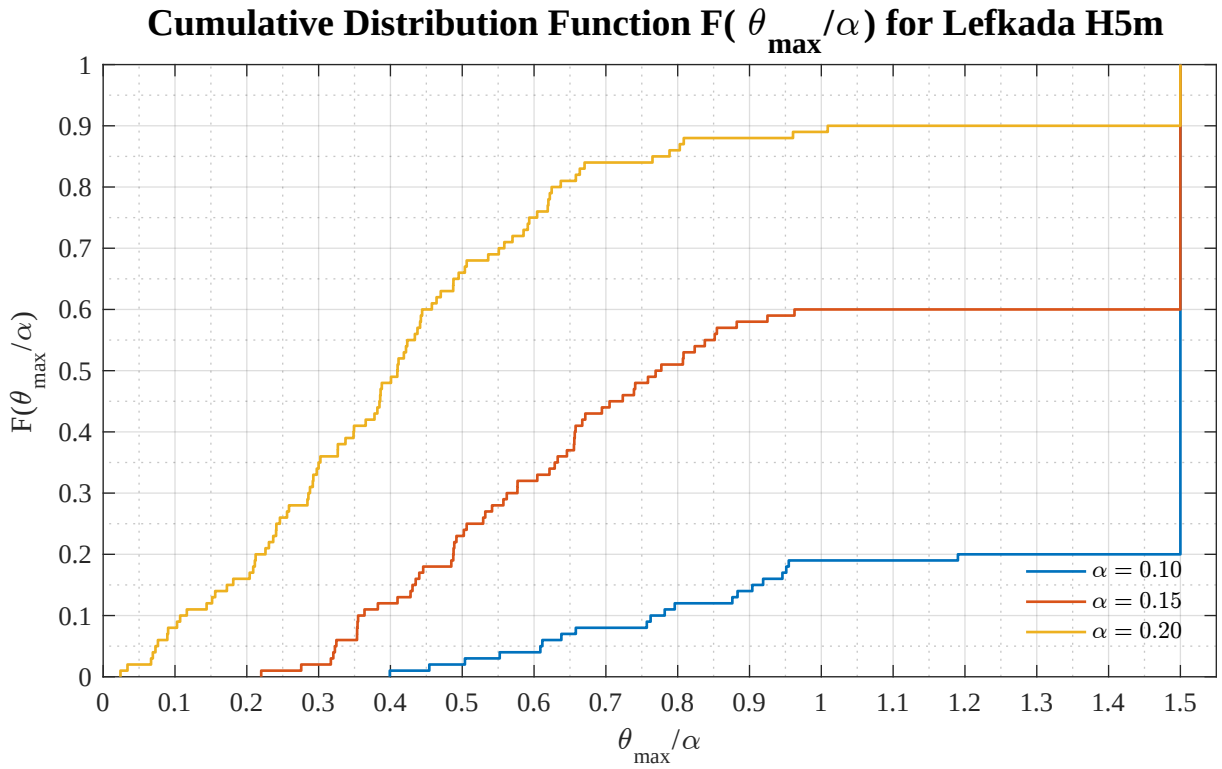

Figure C.4: Empirical CDF for varying α-Values Lefkada H5m

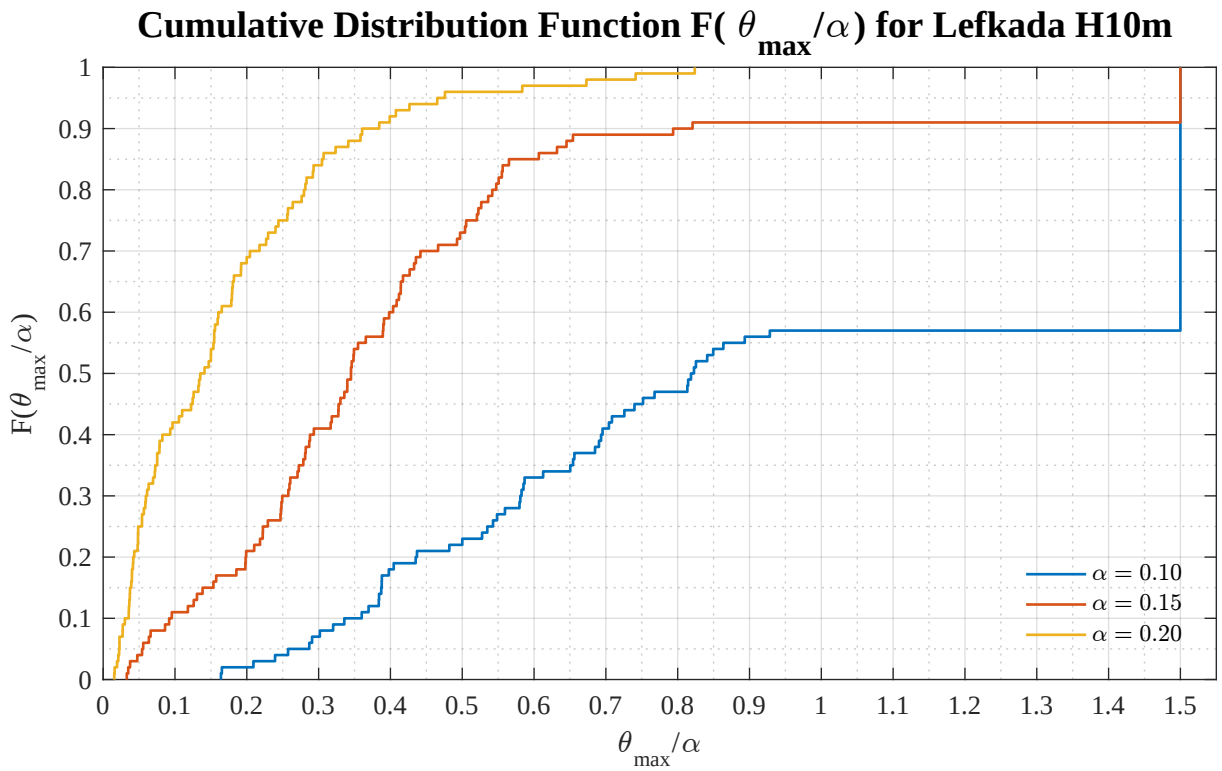

Figure C.5: Empirical CDF for varying α-Values Lefkada H10m

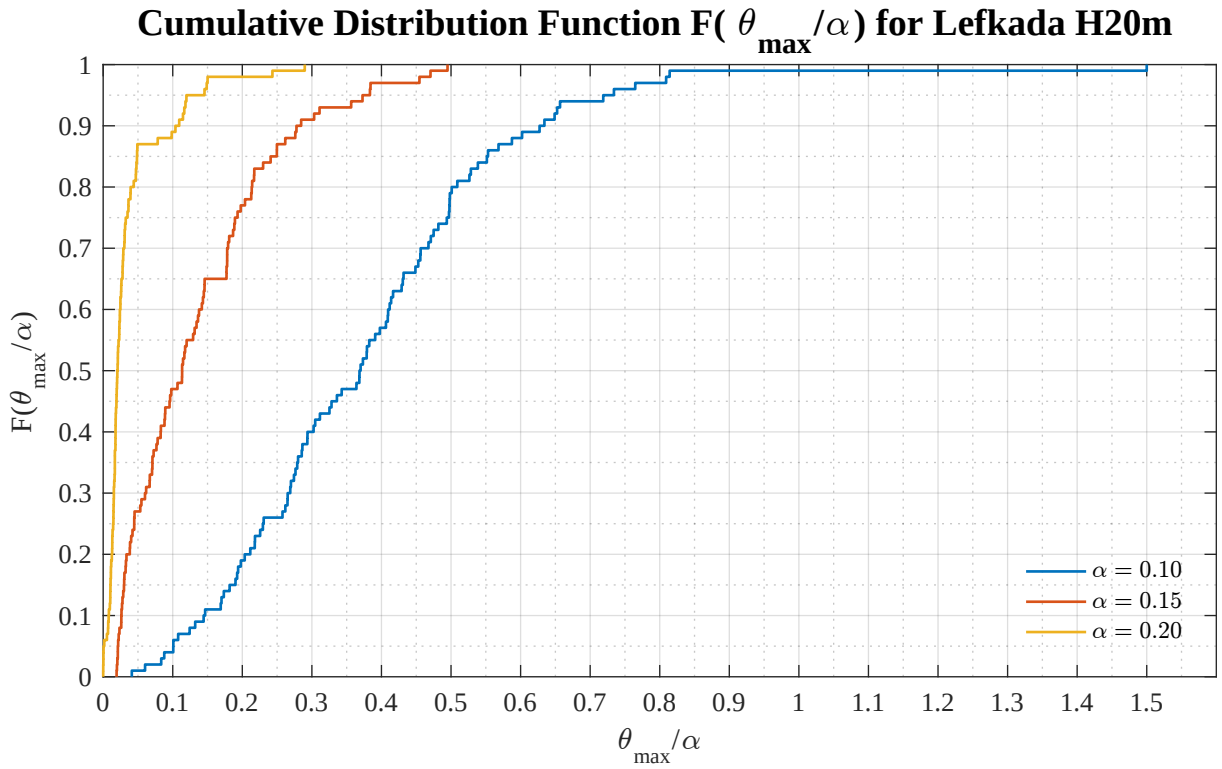

Figure C.6: Empirical CDF for varying α-Values Lefkada H20m

Bibliography

[1] Aslam, M., Godden, W. G., and Scalise, D. T. (1980). Earthquake Rocking Response of Rigid Bodies. *Journal of the Structural Division*, 106(2):377–392.

[2] Broccardo, M. and Dabaghi, M. (2017). A spectral-based stochastic ground motion model with a non-parametric time-modulating function. *12th International conference on Structural Safety and Reliability, Wien 2017*.

[3] Broccardo, M. and Der Kiureghian, A. (2014). Simulation of near-fault ground motions using frequency-domain discretization. *Tenth U.S. National Conference on Earthquake Engineering Frontiers of Earthquake Engineering. Anchorage, Alaska*, (January).

[4] Chopra, A. K. (2012). *Dynamics of Structures*. Prentice Hall, 4 edition.

[5] Conte, J. P. and Peng, B. F. (1997). Fully Nonstationary Analytical Earthquake Ground-Motion Model. *Journal of Engineering Mechanics*, 123(1):15–24.

[6] Housner, G. W. (1963). The behavior of inverted pendulum structures during earthquakes. *Bulletin of the Seismological Society of America*, 53(2):403–417.

[7] Makris, N. (2014). A half-century of rocking isolation. *Earthquake and Structures*, 7(6):1187–1221.

[8] Makris, N. and Konstantinidis, D. (2001). The rocking spectrum and the shortcomings of design guidelines. *Pacific Earthquake Engineering Research Center Research Reports*, (2001/07).

[9] Rezaeian, S. and Der Kiureghian, A. (2008). A stochastic ground motion model with separable temporal and spectral nonstationarities. *Earthquake Engineering and Structural Dynamics*, 37(13):1565–1584.

[10] The MathWorks, Inc., Natick, Massachusetts, United States (2016). MATLAB Release 2016b.

[11] Zhang, J. and Makris, N. (2001). Rocking Response of Free-Standing Blocks Under Cycloidal Pulses. *Journal of Engineering Mechanics*, 127(May):473–483.